AN EXPERIMENTAL AND ANALYTICAL STUDY OF VARIOUS SOIL SLOPES IN LABORATORY CONDITIONS

A Thesis Submitted to
the Graduate School of Engineering and Science of
İzmir Institute of Technology
in Partial Fulfillment of the Requirements for the Degree of

MASTER OF SCIENCE

in Civil Engineering

by
Hasan Fırat PULAT

November 2009
İZMİR

We approve the thesis of **Hasan Fırat PULAT**

Assoc. Prof. İsfendiyar EGELİ
Supervisor

Assist. Prof. Yusuf ERZİN
Committee Member

Assist. Prof. Nurhan ECEMİŞ
Committee Member

9 November 2009

Prof. Gökmen TAYFUR
Head of the Department of Civil Engineering

Assoc. Prof. Talat YALÇIN
Dean of the Graduate School of Engineering and Sciences

ACKNOWLEDGMENTS

I would like to express my great gratitude and sincere thanks to my supervisor, Assoc. Prof. Dr. İsfendiyar EGELİ, for his continued inspiration, support and invaluable guidance during my study. Without his endless efforts and experienced guidance, it would not have been possible to complete this work.

I thank the members of the thesis defense committee Assist. Prof. Dr. Yusuf ERZİN and Assist. Prof. Dr. Nurhan ECEMİŞ for their assistance in reviewing and editing my manuscript. My special thanks go to Assist. Prof. Dr. Tahir Kemal ERDEM for his inspiring discussions and comments. I also would like to thank to my research assistant colleagues Can Ali GÜVEN and Başak DOĞAN for their dedicated support during my experimental studies.

I am grateful to my parents and my sister for their constant support and endless encouragement. Lastly, my gratitude also due to my fiancee Pelin TUAÇ, whose love, patience and continuous support helped me to finish this thesis. Thanks to all.

ABSTRACT

AN EXPERIMENTAL AND ANALYTICAL STUDY OF VARIOUS SOIL SLOPES IN LABORATORY CONDITIONS

Slope stability is a significant subject of geotechnical engineering. Slope failures triggered by rainfall are causing considerable damage and loss of life every year throughout the world. Especially at dry seasons when the rainfall is scarce, the ground can develop considerable amount of suction and this improves the shear strength of the soil. In rainy season, when rainfall infiltrates into ground, suction decreases, while the shear strength also reduces, which may lead to slope instability. One of the principle objectives of this study is to represent the development of soil-water interaction modeling system (SWIMS) at IYTE. Using this system; effects of 3 different parameters, such as: initial water content, soil density, slope angle on modelling unsaturated slope stability were studied. Moreover, effects of infiltration on slope stability in shallow landslides, where it is assumed that the ground water tables are located at significant depths, were examined.

In this thesis study, 12 main slope model experiments were completed in laboratory conditions, using Soil-Water Interaction Modelling System (SWIMS) by varying 3 different parameters. Result of studies shows that slope angle is the most important parameter affecting slope stability. Furthermore, parameters such as; soil density, degree of relative compaction of soil and initial water content affects slope stability, while these parameters also affect slope surface erosion and infiltration depths.

In addition to experimental studies conducted in laboratory conditions with the 12 main slope model experiments, slope stability analyses to find FOS were performed by using Plaxis V9 (2D) finite element program (FEM), which uses shear strength reduction (SSR) technique and infiltration analyses using the Plaxflow module to model the rainwater infiltration into slope soil were performed. The FEM analyses show conforming results with the actual observations made using the tested soil model in laboratory conditions.

ÖZET

ÇEŞİTLİ ZEMİN ŞEVLERİNİN DURAYLILIĞININ LABORATUAR ŞARTLARINDA DENEYSEL İNCELENMESİ VE ANALİZİ

Şev duraylılığı geoteknik mühendisliğinin önemli bir konusudur. Yağmur suyunun tetiklediği şev göçmeleri tüm dünyada her sene önemli miktarda can ve mal kaybına sebep olmaktadır. Özellikle yağmurun az olduğu kurak mevsimlerde, zemin yüksek emme gösterebilmekte ve bu zeminin kayma mukavemetini arttırmaktadır. Yağmur sezonunda ise zemine infiltre olan yağmur suyu, zeminin emmesini ve kayma mukavemetini azaltmakta, bu durum zeminin göçmesine sebep olabilmektedir. Bu çalışmanın temel amaçlarından biri İYTE'de geliştirilen Zemin-Su Etkileşim Modelleme Sistemi'nin (SWIMS) tanımlanmasıdır. Bu sistemi kullanarak; zeminin başlangıç su içeriği, zeminin sıkılığı ve şev açısı gibi üç farklı parametrenin doymamış şev zemininin duraylılığına etkisinin modellenmesidir. Ayrıca, yeraltı su seviyesinin derinde olduğu şevlerdeki sığ toprak kaymalarında yağmur suyu infiltrasyonunun şev duraylılığına etkisinin incelenmesidir.

Bu tez çalışmasında 12 ana şev modeli deneyi, 3 değişik parametre ile Zemin-Su Etkileşim Modelleme Sistemi (SWIMS) kullanılarak, laboratuvar koşularında tamamlanmıştır. Yapılan çalışmalar sonucunda; şev açısının, duraylılığı etkileyen en önemli parametre olduğu belirlenmiştir. Ayrıca zeminin yoğunluğu, rölatif sıkılığı, başlangıçtaki su muhtevası gibi parametrelerin şev duraylılığını etkilemesinin yanısıra, bu parametreler şev yüzeyi erozyon ve infiltrasyon derinliklerini de etkilemektedir.

Deneysel çalışmalara ek olarak; laboratuvar koşullarında gerçekleştirilen 12 şev modeline ait güvenlik katsayısı duraylılık analizleri için kayma mukavemetini azaltma (SSR) tekniğini kullanan Plaxis V9 (2D) ve yağmur suyunun şev zeminine infiltrasyon koşullarını modelleyen Plaxflow modüllü sonlu elemanlar programı kullanılmıştır. Yapılan analizler ve laboratuvarda gerçekleştirilen deneysel şev modeli neticeleri birbirine uyumlu sonuçlar vermiştir.

TABLE OF CONTENTS

LIST OF FIGURES

Figure **Page**

LIST OF TABLES

LIST OF SYMBOLS

ν	Poisson ratio
β	Anglee of soil slope
ϕ	Angle of friction
ϕ'	Effective angle of internal friction
ϕ^b	Angle indicating the contribution of matric suction to shear strength
α	Inclination of slice base from horizontal
γ	Unit weight of soil
γ_w	Unit weight of water
γ_n	Natural unit weight of the soil
τ	Shear stress
τ_f	Shear Strength
$\tau_{\max}$	Maximum shear stress
σ	Normal stress
σ'	Effective normal stress
σ_x	Standart deviation of X
σ_v	Total stress in the vertical direction
σ_h	Total stress in the horizontal direction
η	Viscosity
λ	Constant evaluate in solving the factor of safety
θ	Angle of the resultant interslice force from the horizontal
ρ	Density of the soil
ρ_d	Dry density of the soil
u	Pore pressure
u_a	Pore air pressure
u_w	Pore water pressure
u_e	Excess pore water pressure
z	Depth of soil

X	Interslice shear force
W	Weight of slice
X	Angle between the tangent to the centre of the base of each slice and the horizontal
G_S	Specific gravity of solid particle
K_0	Coefficient of earth pressure at rest
LL	Liquid limit
PL	Plastic limit
PI	Plasticity Index
CU	Consolidated Undrained triaxial compression test
CD	Consolidated Drained triaxial compression test
UU	Unconsolidated Undrained triaxial compression test
S_r	Degree of saturation
c	Cohesion of the soil
c’	Effective cohesion
c_m	Mobilized cohesion
q	Deviator stress
dq	Increment of deviator stress
ds	Increment of soil suction
$d\varepsilon$	Total strain increment
$d\varepsilon^e$	Elastic strain increment
$d\varepsilon^p$	Plastic strain increment
$d\varepsilon_v$	Increment of volumetric strain
e	Void ratio
t	time
s	matric suction
δx	Increment of horizontal displacement
δy	Increment of vertical displacement
FOS	Factor of safety
F_S	Factor of safety
F_C	Corrected factor of safety
δ	Horrizontal displacement
I	Rainfall intensity

k	Water coefficient of permeability
k_{sat}	Saturated permeability
L_f	Wetting front depth
m_w	Slope of soil water characteristic curve (SWCC)
ψ	Matric suction
t_p	Time when surface runoff start to occur
A_{ev}	Air entry value
h	depth of water table
U	Pore water load acting on base of slice
N	Normal stress acting at the base of slice
S	Mobilized dhear force at the base of slice
Q	Rainfall total flux
w_c	Water (Moisture) content
w_{ci}	Initial moisture content
w_{cn}	Natural moisture content

CHAPTER 1

INTRODUCTION

1.1. Overview

A slope is a ground surface that stands at an angle to the horizontal plane. Slopes may be natural or man made. Each slope possesses unique soil characteristics and geometric features, which either will resist gravity or collapse. Slope failure causes soil mass to slide downward and outward occurring slowly or suddenly. Slides usually begin from hairline tension cracks, which propagate through the soil layers (Das 1994).

Slope stability problems are among the most commonly encountered problems in geotechnical engineering. Due to practical importance of the subject of slope stability, assessing stability of a natural or man-made slope has received wide attention across the geotechnical community for long decades. The first question that must be clarified is why a natural slope moves suddenly after long period of its existence. Rainfall effect is the one of the most effective factors in this question. Slope failure has a close relationship with rainfall. A number of studied have been conducted to improve the climatic and geomorphic processes that trigger slope failures. These studies have investigated the physical properties of the failed slopes, effect of the slope angle, moisture content and pore water pressure variation, mechanism of the debris avalanche movement and properties of the resulting deposits (Fisher 1971, Hutchinson and Bhandari 1971, Scott 1972, Williams and Guy 1973, Swanston 1974, Campbell 1975, Hollingsworth and Kovacs 1981, Istok and Harward 1983).

A number of landslides in unsaturated soils usually occur during wet seasons. In other words, the slope failures are induced by rainfall infiltration. Field studies on the effect of rainfall infiltration on slope instability have been carried out by numerous researchers (Brand, et al. 1984, Johnson and Sitar 1990, Affendi and Faisal 1994, Lim, et al. 1996, Gasmo, et al. 1999, Zhang, et al. 2000, Rahardjo, et al. 2003).

In addition to field studies, a number of researchers exerted numerical studies on the effect of rainfall infiltration on the stability of a slope (Fredlund and Rahardjo 1993,

Alonso, et al. 1995, Ng and Shi 1998, Ng, et al. 1999, Fourie, et al.1999, Leong, et al. 1999, Gasmo, et al. 2000).

During a rainstorm, the negative pore-water pressures in an unsaturated soil slope can be gradually reduced by rainfall infiltration. Consequently, contribution to the strength of a soil strengthens, as the negative pore-water pressures decreases with time, a process which may lead to slope instability. Many researchers (Lumb 1962, Ng and Shi 1998, Sun, at el. 1998, Gasmo, et al. 2000, Tsaparas, et al. 2002, Collins and Znidarcic 2004) have studied infiltration and slope stability in a soil slope during a rainfall event.

Different types of slopes respond differently to rainfall process. For deep seated landslides, the rising of the ground water table and resulting softening of the rock and soil, due to rainfall infiltration, affects the state of slope stability. For shallow landslides, their stability behaviour and occurrence types are dominated by transient pore water pressures, in response to rainfall process, which may be combined with water washing or soil erosion (Lan, et al. 2003).

Blong and Dunkerley (1976) have proposed that it is difficult to illustrate how exactly rainfall affects to produce shallow landslide and debris flow activity. Because rainfall only influences slope stability indirectly, its effect on pore water conditions in the slope material and its influence on pore water conditions in the slope material and because its influence requires an interaction with other characteristics of the slope. Starkel (1979) presented that both the rainfall depth and the intensity define the rainfall threshold, for a catastrophic slope failure to occur.

Tarantino and Bosco (2000) have proposed that the intensity and the duration of the rainfall plays a major role on the occurrence and mode of the slope failure. The slope may be subjected to negative as well as positive pore pressures, whose values are subject to change during rainfall infiltration. They have found that shallow landslides are usually triggered by high intensity rainfalls, whereas low intensity rainfalls also may initiate some deep landslides (Fig. 1.1.)

Tohari, et al. (2000) have proposed that slope failures are initiated by an increase in the moisture content of a soil slope at its toe. Rainfall-induced slope failure is the consequence of instability of the toe of the slope, induced by a saturation process under the drained condition, while the major portion of the sliding mass may still be in an unsaturated condition. The direct measurements of change in the soil moisture contents

could provide important information in predicting the critical timing for the initiation of rainfall induced slope failures.

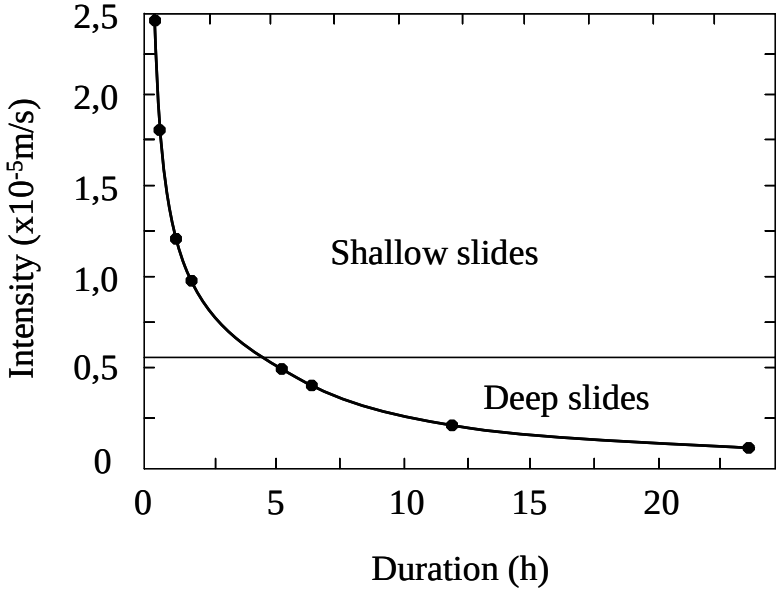

Figure 1.1. Intensity-Duration Threshold Curve
(Source: Tarantino and Bosco 2000)

1.2. Objective and Scope of Study

The principal objective of this research is to investigate the interrelations between slope stability and rainfall infiltration in laboratory conditions. To achieve the objective, this research study is divided into the following steps to be studied in detail:

- Review existing literature of slope stability analysis and procedures,
- Comparison of various developed slope stability analysis methods from past to present.
- Study of rainfall infiltration process and infiltration affecting factors,
- Detailed review of used soil's index parameters, determined in the laboratory by using ASTM-D standards,
- Investigating failure behaviour of the infinite slopes having different slope angles (15°, 25°, 35°), initial moisture contents (%14, %30), degree of compactions (10, 25 blows each layer) and using different soil types (CL-ML-Medium Sand),

- Representation and application of the IYTE-developed Soil Water Interaction Modeling System (SWIMS) to study slope stability during a rainfall event,
- Observation and measurements of infiltration and erosion depths in the conducted experiments,
- Performing the finite element method (FEM) analyses for various experimented slopes by using Plaxis V9 and Plaxflow programs,
- Comparison of the experimented slope stability results with the FEM analysis results,
- Determination of the weak points to avoid slope instability in practice and recommending some precautions for future works.

1.3. Organization of the Thesis

This thesis is composed of seven chapters. The contents of each chapter are summarized as follows:

Chapter 1 consists of three subtitles. The first subtitle is overview of the thesis, which includes definition of a slope, slope instability effecting factors and review of studies that were conducted in relation to this subject.

Chapter 2 starts with the background information study about the slope failure events globally, as well as studying slope failure triggering factors. Slope stability analysis methods are examined comprehensively until present time. Limit equilibrium methods and its subdivisions such infinite slopes, method of slices and limit analysis methods are reviewed. Types of slope movements and their characteristics are also studied.

Chapter 3 gives brief description about the infiltration process, including infiltration affecting factors. Further, differences between saturated and unsaturated soil properties, their shear strength characteristics are reviewed. Additionally, shallow-depth slope failures, wetting band theory and soil-water characteristics curve (SWCC) subjects are studied.

Chapter 4 is devoted to detailed 13 different laboratory experiments to determine the properties of the used soil. Firstly, short descriptions are given about the soil tests. Then, explanations are provided at the end of the chapter for summarizing the experiments.

Secondly, slope model test preparation procedures are explained, including compaction process and undisturbed soil sampling.

Chapter 5 contains a presentation of the IYTE-developed slope-water-interaction modeling system (SWIMS). Firstly, components of the system are defined. Secondly, details of the conducted twelve main experiments (including variations of the slope geometry, soil characteristics and types) are explained. Thirdly, collected experimental data and analysis of results are given in a number of tables. Finally, observations made on the experimental and analytical results obtained are commented.

Chapter 6 includes slope stability analysis methods, general finite element method (FEM) and Plaxis-V9 type finite element program used, is defined comprehensively. This included providing information about which slope stability techniques can be used (Shear Strength Reduction Method, SSR) with the Plaxis V9 (PV9) and which types of soil models can be defined in the PV9 for the used soil and infiltration analyses using the Plaxflow module to model the rainwater infiltration into slope soil were performed. Conducted experimental model slope results are compared with the PV9 results.

Chapter 7 is the final part of the thesis, which includes a summary and conclusion parts. Recommendations are given in this section on better practices to avoid slope instability problems, on correcting some experimental deficiencies and on the way forward for the future studies.

CHAPTER 2

BACKGROUND OF SLOPE STABILITY ANALYSES METHODS AND MASS MOVEMENTS TYPES

2.1. Introduction

Slope failures occur globally very frequently resulting in great loss of lives and properties. Behaviour of slopes may vary depending on different slope angles, heights and soil properties. In this study, a modeling facility was used to study slope behaviour under laboratory conditions, where a total of 12 tests were conducted using 2 kinds of soils having different soil characteristics.

Slope failures are common in many areas throughout the world. The failures become a problem, especially if they interfere with human activity so that they cause disasters with damages to properties and loss of lives. In China and Peru, thousands of people are killed each year by slope failures. Tens of thousands of deaths have resulted from landslides. For example, on May 31st 1970, a single landslide of rock debris from Mt. Huascarán, Peru, killed over 18.000 people in the town of Yungay (Plafker and Ericksen 1978). Annual property damage from landslides worldwide is estimated in tens of billions of dollars, with more than 2 billion dollars in the USA, more than 1,5 billion dollars in Japan and more than 1 billion dollars in Italy (Pickering and Cwen 1997). Damage to ecosystems has not been well documented, but generally landslides may destroy habitats, such as; by blocking streams and denuding slopes.

There are many ways in which slopes may fail, depending on the angle of slope, the water content of soil, the type of earth material and many other factors. Slope failure may take place suddenly and catastrophically, resulting in debris flows, rock falls and slides. It may occur gradually, resulting in slides (of earth/rock debris, blocks) or may cause topples (for rocks), slumps (for rock/earth), complex landslides and creep.

Slope failure is a natural process which can be induced, accelerated or retarded by human actions. It's often resulted from processes that increase shear stresses or

decrease shear strength of the soil mass. Processes that most commonly cause an increase in the shear stresses acting on slopes include; removal of support (by erosion or excavation), overloading (rain, snow, or man-made construction), earthquakes, and increase in lateral pressure (by expansion of clays or freezing of the water in the cracks) etc. Processes that most commonly cause a decrease in the shear strength of slope materials include; stratification, hydration of minerals and effect of pore pressure due to rainfall event or melting snow, etc (Abramson, et al. 2002).

Slope failures can be triggered by atmospheric processes, geologic processes, human modifications of the landscape or most commonly, some interaction of all of the above. Therefore, failures occur nearly everywhere slopes exist. Generally, areas which receive abundant precipitation and have moderate to steep slopes have the highest risk to fail. As a result, rainfall is the most common triggering factor in slope stability. Both shallow and deep slope failures can be triggered by rainfall having different intensity, duration and other effects caused by different types of storms. For example; in shallow landslides, soil slips and debris flows in mountainous area are triggered by intense rainfall, whereas, shallow landslides in clayey soils are more sensitive to events of long and moderate rainfall intensity. As a consequence, rainfall analysis is the most frequently adopted approach for forecasting the occurrence of slope failures.

Slope stability problems have been faced throughout history when the balance between human and natural soil slope has been disrupted. Moreover, increased demand for the engineered cut and fill slopes on construction projects has in turn increased the need to understand analytical methods, investigate tools and stabilization methods to overcome potential slope instability problems.

2.2. Factors Causing Instability

Factors leading to instability can be classified as: (1) Those causing increased stress, (2) Those causing a reduction in strength.

Factors causing stress include; increased unit weight of soil by wetting, added external loads such as building, traffic loads on embankments, steepened slopes either by natural erosion or by excavation. Loss of strength may occur by absorption of water, increased pore pressures, freezing and thawing action, loss of cementing materials and weathering processes.

Presence of water is a factor of the most slope failures, since it causes both of increased stresses and reduced strength. Rate of slide movement in a slope failure may vary from a few millimeters per hour to very rapid slides in which large movements have taken place in a few seconds. Slow slides occur in soils having a plastic stress-strain characteristic, where there is no loss of strength with increased strain. Rapid slides occur in situations, where there is an abrupt loss of strength, as in liquefaction of fine sand or sensitive clay.

These several factors produce shear stresses through the soil mass, and a movement will occur, unless the shearing resistance on every possible failure surface throughout the mass is sufficiently larger than the shearing stresses.

2.3. Slope Stability Analysis Methods

Slope stability problems, as one of the prime concerns of the geotechnical engineering field, deal with the condition of ultimate failure of a soil or rock mass. Analyses of slope stability, bearing capacity and earth pressure, in general, fall into this area. Stability of a slope can be analyzed by a number of methods, which comprise limit equilibrium method, limit analysis method, variational calculus method, strength reduction method, rigid element method and others. In the following sections, commonly used plain strain (2D) stability methods will be shortly summarized.

2.3.1. Limit Equilibrium Methods

The principle of limit equilibrium methods can be found in any standard Soil Mechanics text book (e.g., Das 1990). The common basis of numerous limit equilibrium methods can be concisely summarized as follows; Firstly, at any local point in a slope, available shear strength of the material can be expressed in terms of the Mohr-Coulomb criterion:

$$\tau_f = c' + \sigma' \tan \phi' \tag{2.1}$$

Where,

τ_f indicates shear strength, c' denotes effective cohesion, ϕ' represents effective angle of internal friction and σ' shows effective normal stress.

Secondly and as a common practice, is to assume the same degree of mobilization for the soil's cohesion and friction components at all points in the considered soil mass by expressing the shear stress as:

$$\tau = \frac{c'}{F} + \frac{(\sigma' \tan \phi')}{F} \tag{2.2}$$

where;

σ' and τ represent the applied normal and shear stresses on any section of the potential failure surface, respectively and, F is the factor of safety.

Equation (2.2) thus represents both the presumed local stress condition and the local expression of the factor of safety against slope instability due to shear stress failure.

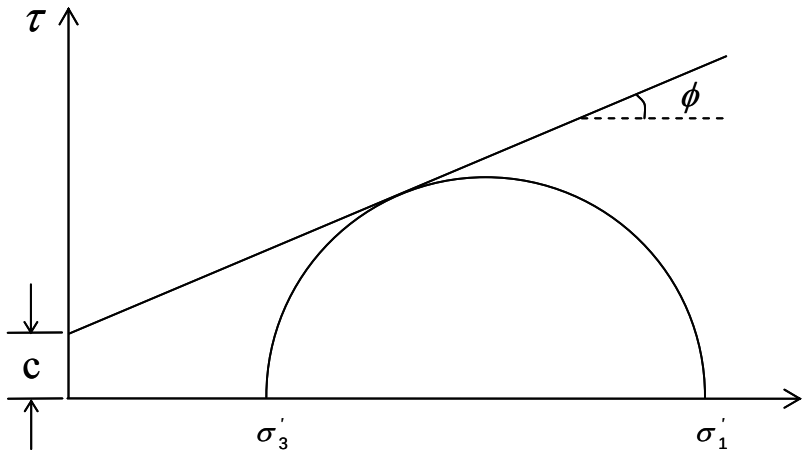

Figure 2.1. Mohr-Cycle Diagram

The integration of the local factors of safety to obtain an estimate of the overall stability is done by writing the factor of safety in terms of the overall equilibrium of the considered soil mass, i.e.,

$$F = \frac{Resisting\ \ force\ of\ \ moment}{Disturbing\ \ force\ of\ \ moment} \tag{2.3}$$

The procedure of method is as follows; Firstly, a potential failure surface is selected, which is then considered as a discontinuity between a rigid sliding mass and a rigid stable base. Secondly, the equation of global equilibrium of the mass is written in terms of either a sum of moments (for circular surfaces) or forces (for non-circular surfaces) or both. The active forces are the weight of the sliding mass and any surface loads, while the reacting forces are the resisting forces along the failure surface. Thirdly, the equation for the equilibrium of the vertical forces in a vertical slice of sliding mass is derived. Since the complete state of stresses is normally unknown, simplifying assumptions have to be made concerning the type and magnitude of the internal and external forces acting on the slice. Fourthly, the equations for the normal stress and shear stress along the base of the slice are derived. Lastly, the equations of the normal stress and the shear stress are substituted into the global equilibrium equation obtained in the second step to obtain the expression of the type:

$$F = f(F) \tag{2.4}$$

which is solved by iteration. Numerous limit equilibrium methods for slope stability analysis have been proposed by several investigators, including the celebrated pioneers Fellenius (1936), Bishop (1955), Janbu (1954), Morgenstern and Price (1965), Spencer (1967), and Sarma (1973).

2.3.1.1. Infinite Slope Stability

The nature of the slide is controlled by geological features such as soil properties, bedrock, rock layer, geometry of slide etc. Most of the slide normally can be defined as circular slide, if the length of the slide is short relative to its depth. But if the slide is very long relative to its depth, then the soil resistance contributed by the slip surface may be minor (Cornforth 2005) and the slip surface is approximately parallel to the ground surface. In infinite slope, the method of slices can be applied with assumption that the slide does not occur in circular slides, but occurs parallel to the

ground surface, which is called transitional failure. Figure 2.2 (a) shows an example of infinite slope modeling and Figure 2.2 (b) shows how the method of slices was applied on an infinite slope.

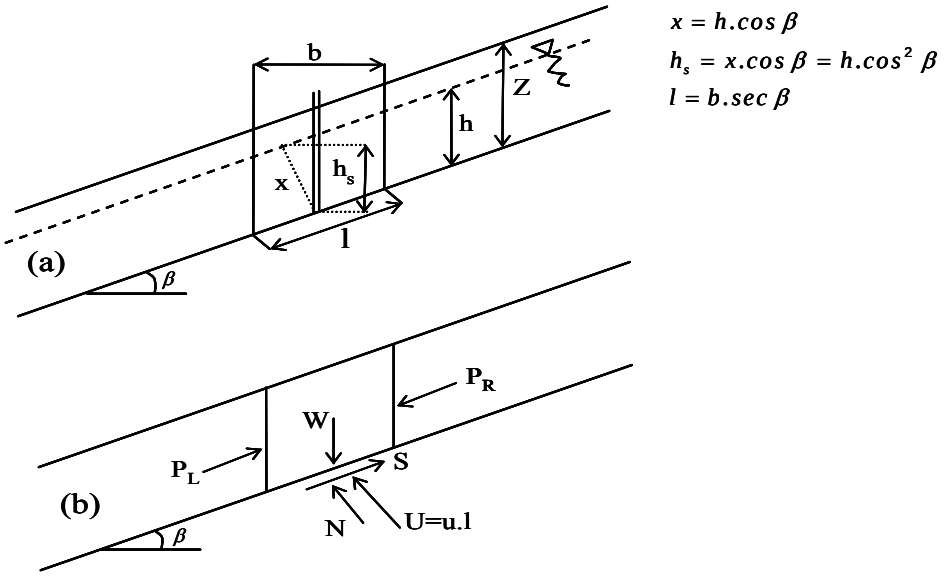

Figure 2.2. Infinite Slope a) vertical head on base of slice, b) forces acting on a slice (Source: Cornforth 2005)

In Figure 2.2(a), a slip failure is expected to occur at a depth z from the ground surface with the groundwater existing at a height h above the slip surface. Both slip surface and groundwater are parallel to the ground surface and are inclined at an angle β to the horizontal. The equipotential lines are perpendicular to the flow lines also at an angle β to the vertical. The *x* in Figure 2.2(a) indicates the equipotential line at the centre of the slice. Interslice forces P_L and P_R are equal in infinite slope and can be cancelled out.

Other variables are described as follows:

i. Weight of soil slice, $W = \gamma.z.b$, (2.5)

ii. Pore-water pressure acting at the centre of slice base, $u = \gamma.w.h.cos2\beta$ (2.6)

iii. Water force, $U = u.l = \gamma.w.b.h.cos\beta$ (2.7)

iv. Total normal force, $N = W.cos\beta$ (2.8)

v. Resistance shear force, $S = c'l + N'tan\phi'$ *whereas* $N' = (\gamma.z - \gamma.w.h)b.cos\beta$ (2.9)

vi. Force that causing failure = W.sinβ (2.10)

Therefore, the FS for an infinite slope can be derived by using the equations above.

$$FS = \frac{c'l + N'\tan\phi'}{W\sin\beta} \tag{2.11}$$

$$FS = \frac{c'\sec\beta + (\gamma z - \gamma_w h)\cos\beta.\tan\phi'}{\gamma z\sin\beta} \tag{2.12}$$

$$FS = \frac{c'\sec^2\beta + (\gamma z - \gamma_w h)\tan\phi'}{\gamma z\sin\beta} \tag{2.13}$$

2.3.1.2. Method of Slices

A variety of analytical techniques for the method of slices have been developed. The primary difference between these methods is the expression used to satisfy the static equations, the interslice normal and shear forces and the assumed relationship between the interslice forces (Krahn 2003). Figure 2.3 illustrates a typical slice in a potential sliding mass with the forces acting on the slice. Normal and shear forces act on the slice base, as well as on the left and right sides of the slice.

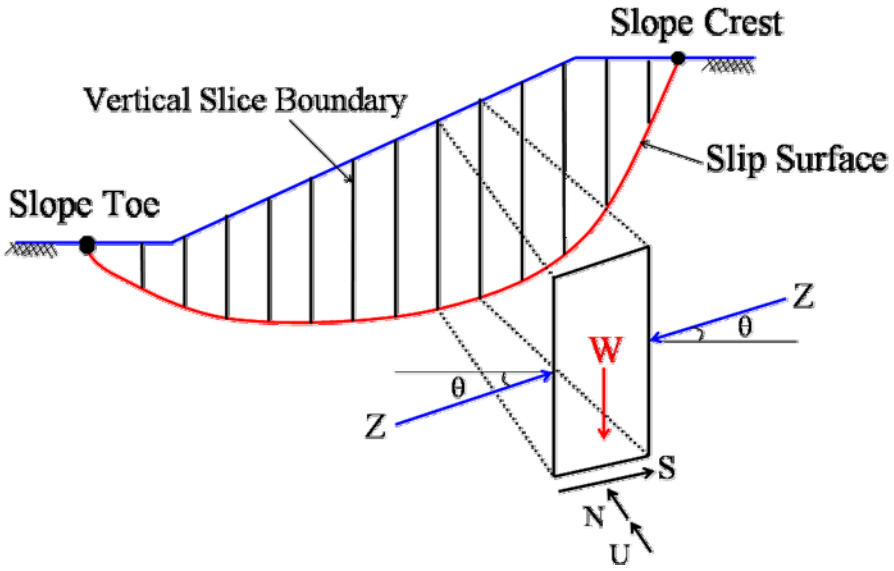

Figure 2.3. Slices and Forces in a Sliding Mass
(Source: Krahn 2003)

The static equilibrium of forces in two directions and also the movements in two directions are used to determine the factor of safety of a particular slope. However, these relationships are insufficient to make the problem a determinate one. Therefore, more information is required about either the normal force distribution or the interslice force distribution (Fredlund and Krahn 1976). Therefore, additional elements of physics or an assumption should also be applied. Based on different assumptions, various methods of analysis have been developed.

The general limit equilibrium formulation is based on two factors of safety expressions and can incorporate a variety of interslice shear-normal force conditions. One expression provides a factor of safety satisfying moment equilibrium and the other satisfies horizontal force equilibrium. These equations are all expressed in terms of effective stresses.

The general limit equilibrium equation for the factor of safety, considering moment equilibrium is;

$$Fs_m = \frac{\sum \{c' lR + (N - ul) R \tan\phi'\}}{\sum Wx - \sum Nf} \tag{2.14}$$

and the factor of safety equation, considering horizontal force equilibrium is;

$$Fs_f = \frac{\sum \{c' l \cos\beta + (N - ul) \tan\phi' \cos\beta\}}{\sum N \sin\beta} \tag{2.15}$$

where;

W is the total weight of the slice of width b and height h, N is the total normal force on the base of the slice over a length l, R is the radius or the moment-arm associated with the mobilized shear force, u is the pore water pressure, f is the perpendicular offset of the normal force from the centre of rotation, x is the horizontal distance from the slice to the centre of rotation and, β is the inclination of the slice base.

2.3.1.2.1. Ordinary Method of Slices or the Fellenius Method

This method is also sometimes referred to as the Swedish Method of Slices (SMS). This is the first method of slices developed and presented in the literature. The simplicity of the method made it possible to compute factors of safety using hand calculations.

In this method, all interslice forces are ignored. The slice weight is resolved into forces parallel and perpendicular to the slice base. The force perpendicular to the slice base is the normal force, which is used to compute all the available shear strength. The weight component parallel to the slice base is the gravitational driving force. Summation of moments about a point used to describe the trial slip surface is also used to compute the factor of safety. The factor of safety is the total available shear strength along the slip surface divided by the summation of the gravitational driving forces (mobilized shear). The simplest form of the factor of safety equation in the absence of any pore-water pressures for a circular slip surface in this method is:

$$F_S = \frac{\sum (c'l + (W\cos\alpha - ul).\tan\phi')}{\sum W\sin\alpha} = \frac{\sum S_{resistance}}{\sum S_{mobilized}} \qquad (2.16)$$

where;

c’ cohesion (effective cohesion)
l slice base length
N base normal (W cosα)
ϕ’ friction angle (effective internal friction angle)
W slice weight, and
α slice base inclination angle

The most noteworthy aspects of this method are the slice forces and force polygons. First of all, it’s noted that there are no interslice shear forces and no interslice normal forces. Secondly, force polygon closure is extremely poor or non-existent. This indicates that all slices are not in force equilibrium condition. With no interslice normal forces, there is nothing available to counterbalance the lateral components of the base

shear and normal forces, particularly when the slice base is close to being horizontal.

When interpreting the free body diagram and force polygons, it is important to note that the shear at the slice base is the mobilized shear, not the available shear strength resistance. The available shear resistance is equal to the mobilized shear times the factor of safety. The available shear resistance, which has to be divided by the factor of safety in order to match the base shear values, is shown on the slice free bodies. Due to the poor force polygon closure, the Ordinary method can give unrealistic factors of safety and consequently should not be used in practice.

2.3.1.2.2. Bishop's Simplified Method

In the 1950's, Professor Bishop at the Imperial College (University of London) has devised a method, which included to consider interslice normal forces, but ignored the interslice shear forces. Bishop developed an equation for the normal forces at the slice base by summing all slice forces in the vertical direction. The consequence of this is that the base normal forces become a function of the factor of safety. This in turn makes the factor of safety equation nonlinear (that is, FS appears on both sides of the equation) and an iterative procedure is consequently required to compute the factor of safety.

A simple form of the Bishop's Simplified Method's factor of safety equation in the absence of any pore-water pressure is:

$$FS = \frac{1}{\sum W \sin\alpha} \sum \left[\frac{c\beta + W \tan\phi - \frac{c\beta}{FS} \sin\alpha \tan\phi}{m_a} \right] \tag{2.17}$$

Note that FS is on both sides of the equation as mentioned earlier. The equation is not unlike the Ordinary factor of safety equation, except for the m_a term, which is defined as:

$$m_a = \cos\alpha + \frac{\sin\alpha \tan\phi}{FS} \tag{2.18}$$

To solve for the Bishop's Simplified Method's factor of safety, it is necessary to start with a guess number for the FS. This initial guess number for the FS is used to compute m_a and then a new FS is computed. Next, the new FS is used to compute m_a and then another new FS is computed. The procedure is repeated, until the last computed FS is within a specified tolerance of the previous FS.

The force polygon closure is now fairly good with the addition of the interslice normal forces. There are no interslice shear forces, as assumed by Bishop, but the interslice normal forces are only included.

In summary, the Bishop's Simplified method,

(1) Considers normal interslice forces, but ignores interslice shear forces and,

(2) Satisfies the overall moment equilibrium, but not overall horizontal force equilibrium.

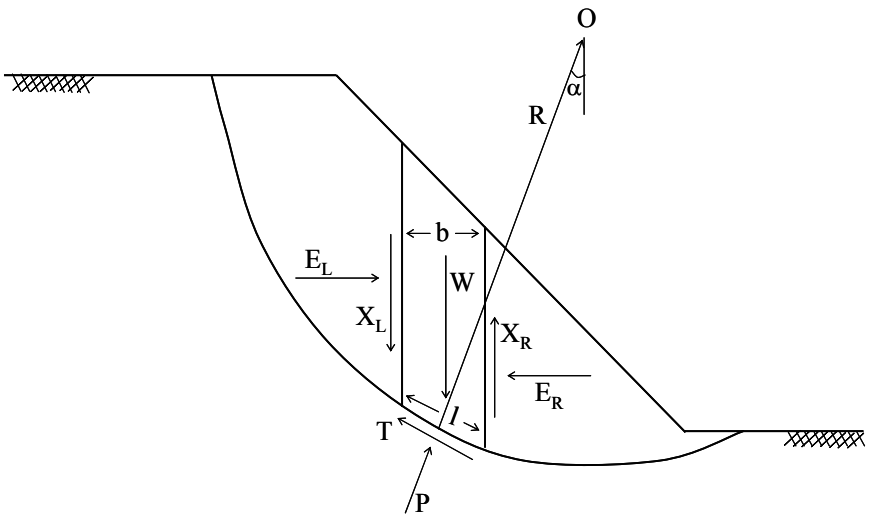

Figure 2.4. Bishop's Simplified Method
(Source: Anderson and Richards 1987)

2.3.1.2.3. Janbu's Simplified Method

The Janbu's Simplified Method is similar to the Bishop's Simplified Method, except that the Janbu's Method satisfies only overall horizontal force-equilibrium, but not overall moment-equilibrium. The slice force polygon closure is actually better than that for the Bishop's Simplified Method. Since force equilibrium is sensitive to the assumed interslice shear, ignoring the interslice shear, as in the Janbu's Simplified Method, makes the resulting factor of safety too low for circular slip surfaces.

Janbu's Simplified Method of Slices derives the factor of safety by utilizing horizontal-force equilibrium only. The factor of safety, Fs_f as expressed in Equation 2.15, is used to designate the factor of safety uncorrected for interslice shear forces. The corrected factor of safety is then;

$$Fs = f_0 Fs_f \tag{2.19}$$

In summary, the Janbu's Simplified Method;

(1) Considers normal interslice forces, but ignores interslice shear forces and,

(2) Satisfies overall horizontal force equilibrium, but not overall moment equilibrium.

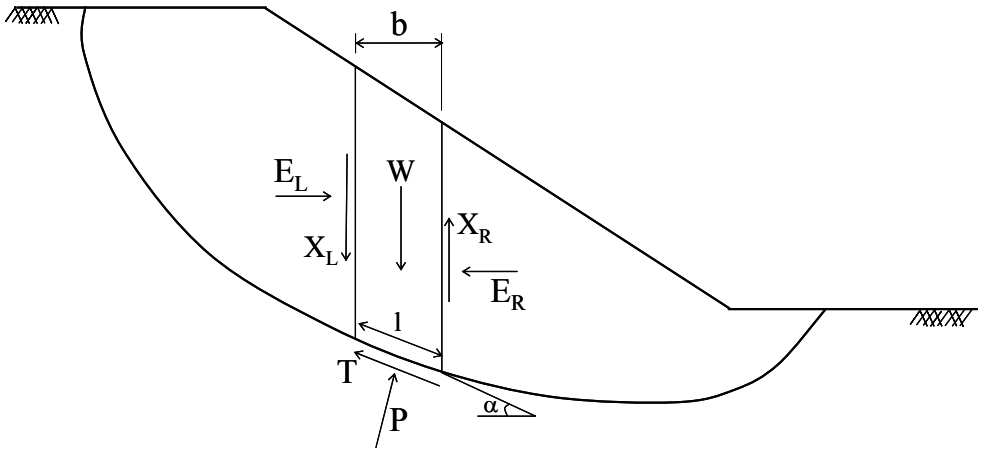

Figure 2.5. Janbu's Simplified Method
(Source: Anderson and Richards 1987)

2.3.1.2.4. Spencer Method

Spencer (1967) developed two factor of safety equations; one with respect to moment-equilibrium and another with respect to horizontal force-equilibrium. He adopted a constant relationship between the interslice shear and normal forces and used an iterative procedure by altering the interslice shear to normal force ratio, until the two factors of safety were the same.

This relationship can be expressed as;

$$tan\theta = \frac{X_L}{E_L} = \frac{X_R}{E_R} \tag{2.20}$$

where;

θ is the angle of the resultant interslice force from the horizontal.

Finding the shear to normal force ratio that makes the two factors of safety equal, means that both moment and force-equilibrium conditions are satisfied.

The following equation relates the interslice shear (*X*) and normal (*E*) forces;

$$X = E\lambda f(x) \tag{2.21}$$

In the Spencer Method, the function *f(x)* is a constant and λ is the percentage of function used. This means that the interslice shear to normal force ratio is the same between all the slices.

It should be noted that when both interslice shear and normal forces are included, the force polygon closure is very good.

In summary, the Spencer Method of Slices;

(1) Considers both shear and normal interslice forces,

(2) Satisfies both moment and force-equilibriums and,

(3) Assumes a constant interslice force-function.

2.3.1.2.5. Morgenstern-Price Method

Morgenstern and Price (1965) developed a method similar to the Spencer Method, but they allowed for various user-specified interslice force functions to be utilized. As with the Spencer Method, the force polygon closure is very good with the Morgenstern - Price method, since both shear and normal interslice forces are included.

In summary, the Morgenstern-Price Method;

(1) Considers both shear and normal interslice forces,

(2) Satisfies both moment and force equilibrium and,

(3) Allows for a variety of user-selected interslice force functions to be used.

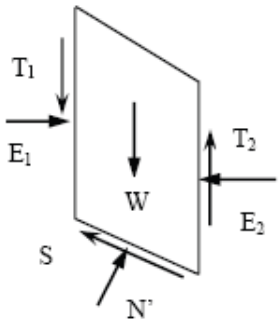

Figure 2.6. Morgenstern-Price Method's Effecting Forces

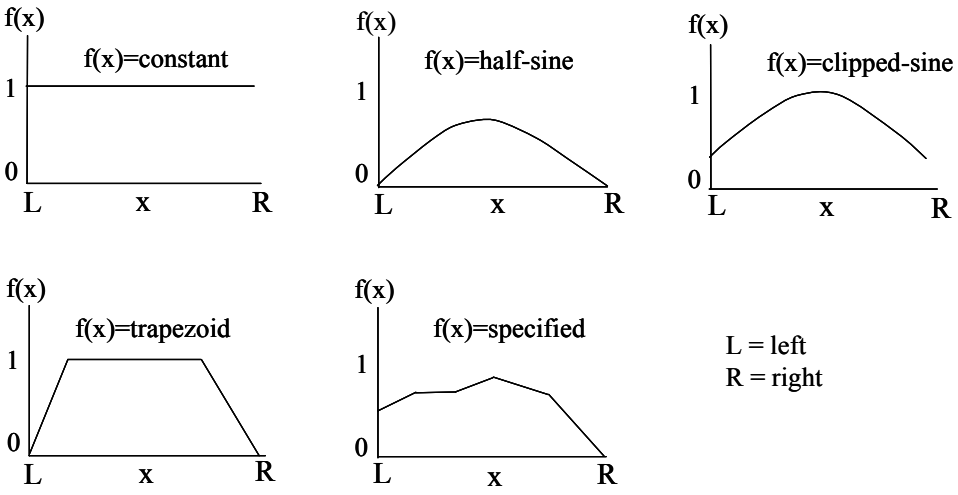

Figure 2.7. Typical functional variations for the direction of the interslice force with respect to (x)

Table 2.1 shows differences between various methods of stability analyses, regarding equilibrium conditions of forces and moments, when factors of safety are calculated.

Table 2.1. Stability Analyses Methods

No	Methods	Moment Equilibrium	Force Equilibrium	Inter Slice Normal Forces	Inter Slice Shear Forces	Moment Factor of Safety	Force Factor of Safety	Inter Slice Force Function
1	Fellenius, Swedish Circle or Ordinary Method (1936)	Yes	No	No	No	Yes	No	No
2	Bishop Simplified (1955)	Yes	No	Yes	No	Yes	No	No
3	Janbu Simplified (1954)	No	Yes	Yes	No	No	Yes	No
4	Spencer Method (1967)	Yes	Yes	Yes	Yes	Yes	Yes	Constant
5	Morgenstern-Price Method (1965)	Yes	Yes	Yes	Yes	Yes	Yes	Constant Half-Sine Clipped-Sine Trapezoidal Specified
6	Lowe-Karafiath Method	No	Yes	Yes	Yes	No	Yes	Yes
7	Sarma Method (1973)	Yes	Yes	Yes	Yes	Yes	Yes	Yes
8	Janbu Generalized Method (1957)	No	Yes	Yes	Yes	No	Yes	Yes

2.3.1.3. Limit Analysis Method

The Limit Analysis Method (LAM) contains both lower-bound and upper-bound approach. General analysis process includes construction of a statically admissible stress field for the lower-bound analysis or a kinematically admissible velocity field for an upper-bound analysis. Optimization analysis of the objective function will then be conducted. The lower- bound approach has been used in 2D slope stability analysis by Chen (1975), Bottero, et al. (1980), Zhang (1999), Kim, et al. (2002), and Loukidis, et

al. (2003). The upper-bound approach was first used in 2D slope stability analysis by Drucker and Prager (1952) to determine the critical height of a slope. Subsequently, Chen and Giger (1971), Chen (1975), Karal (1977a, 1977b), and Izbicki (1981) also applied and extended the upper-bound approaches in 2D slope analysis. Michalowski (1995) proposed an upper-bound approach, based on a translational failure mechanism. The vertical slice techniques, which are often used in traditional limit equilibrium approaches, are employed to satisfy the force equilibrium condition for all individual slices. Two extreme kinematical solutions neglecting the interslice strength or fully utilizing the interslice strength of the soil are then obtained. The traditional limit equilibrium solutions for slices with a proper implicit assumption of failure mechanism can fall into the range of these two extremes. Donald and Chen (1997) presented an upper-bound method on the basis of multi-wedge failure mechanism and the sliding body was divided into a small number of discrete blocks.

2.3.1.4. Variational Calculus Method

Variational Calculus Method (VCM) was first used in 2D slope stability analysis by Baker and Garber (1978). This approach was subsequently employed by Jong (1980) for vertical-cut analysis in cohesive directionless soil. This method does not require an assumption on the internal force distribution, but it is not easy to be used for practical purposes. Cheng, et al. (2008) have developed a numerical algorithm, based on the extremum principle by Pan, and the formulation which relies on the use of a modern try and error optimization method can be viewed as an equivalent form of the variational method in a discretized form, but it is applicable for a complicated real problem.

2.3.1.5. Strength Reduction Method

In the recent decades, there are great developments of strength reduction method (SRM) for slope stability analysis. The general procedure of the SRM analysis is the reduction of the strength parameters by the factor of safety, while the body forces (due to the weight of soil and other external loads) are applied until the system cannot maintain a stable condition. This procedure can determine the safety factor within a single framework, for both two and three dimensional slopes.

The main advantages of the SRM are as follows;

(1) The critical failure surface is found automatically from the application of gravity loads and/or the reduction of shear strength,

(2) It requires no assumption on the interslice shear force distribution,

(3) It is applicable to many complex conditions and,

(4) It can give information such as stresses, movements and pore pressures.

One of the main disadvantages of the SRM is the long solution time required to develop the computer model and to perform the analysis. With the development of computer hardware and software, 2D-SRM can now be performed within a reasonable time span suitable for a routine analysis and design. This technique is also adopted in several well-known commercially available geotechnical finite element or finite difference programs. In strength reduction analysis, the convergence criterion is the most critical factor in the assessment of the factor of safety. Depending on the choice of the program, different criteria for the ultimate state can be used in practice.

With these programs;

(1) The maximum number of iteration can be reached,

(2) The formation of continuous failure mechanism can be applied,

(3) Any sudden change in the displacement for some selected points can be observed.

For simple problems, there are no major differences between these criteria, while major differences can be obtained by applying different convergence criteria for some special cases. Matsui and San (1992) conducted an SRM analysis, in which the slope failure was defined according to the shear strain failure criterion and the hyperbolic nonlinear-elastic soil model was used for practical purposes. Investigation results show that; the factor of safety obtained and the corresponding slip surface determined by the SRM, demonstrate good agreement with the results of the Limit Equilibrium Method (LEM).

2.4. Classification of Mass Movements

Landslides classification is considered as an important first step to scientific investigation of landslides (Crozier 1984, Msilimba 2002). A classification is designed to reduce the multitude of different, but related phenomena to a few easily recognized and meaningful groups on the basis of common attributes (Crozier 1984). A good classification specifies its classificatory parameters in unambiguous and universal terms to allow for standardized application and reproducibility of results. A summary of the criteria for landslide classification is given by Varnes (1978). Landslide classifications are also given by Campbell (1951), Zaruba and Mencel (1969), Crozier (1973), Hutchinson (1978), Coch (1995), and Smith (1996). In the subsections listed below, there is a general landslide classification information and their details.

2.4.1. Topples

Topples involve the outward rotation (or inward buckling and basal collapse) of angular blocks or rock-columns that become detached from cliffs (Crozier 1984, Alexander 1993). These blocks or columns are usually defined by the intersection of joints or other fractures and their basal stability is often disturbed by erosion (Ludman and Koch 1982). Topples have been observed to have occurred on the slopes of Nyambilo Hills in Southern Malawi (Chipili and Mishali 1989). Figure 2.8a shows typical topple movements.

2.4.2. Falls

Falls normally involve the free movement of rock material downwards in steep slopes, with no permanent contact of the moving material to the slope surface (Crozier 1984, Bryant 1991, and Alexander 1993). The movement is turbulent, the reach of the rock fall is in close relation to the angle of internal friction of the moving material and is defined by the energy line (Bryant 1991). Falls are common in Zomba Mountain Area of Southern Malawi (Poschinger, et al. 1998). Figure 2.8b represents typical falls movements.

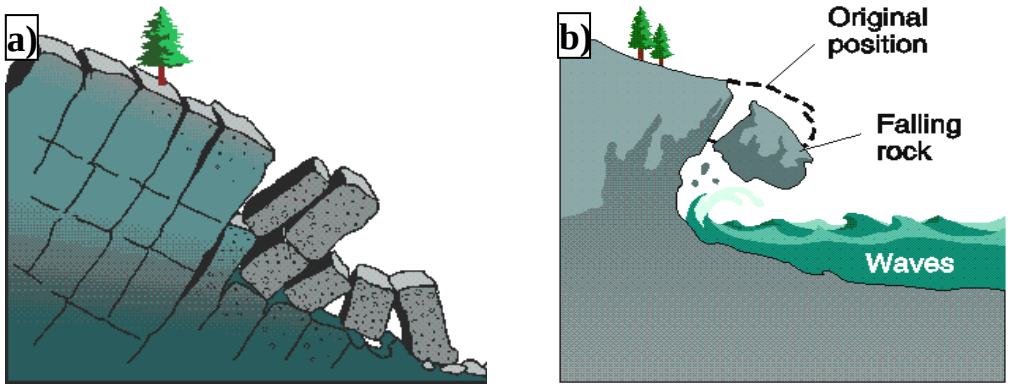

Figure 2.8. Falling Rock Blocks a) Topples and b) Falls

2.4.3. Slides

Slides are the downward slope movements of rock and soil materials along a slip surface and are characterized by almost permanent contact between the moving mass and the slide surface (Crozier 1984, Bryant 1991, Alexander 1993, Smith 1996). The most common sub-groups are "translational" and "rotational" slides. Translational slides are relatively flat, planar movements along surfaces and they generally have pre-existing slide planes that are activated during the slide event. In contrast, rotational slides have a curved surface of rupture and produce slumps by backward slippage (Alexander 1993, Smith 1996). Some rotational slides are multiple-regressive phenomena and are termed as: roto-translation (Alexander 1993). When the slope is almost horizontal, the debris spreads over a wider area. Hence, then the term lateral spread is used (Fig. 2.9). Rotational slides were observed in the Vunguvungu/Banga catchments in Northern Malawi due to deep weathering of the basement (Msilimba 2002, Msilimba and Holmes 2005). They are also common on the slopes of Mount Elgon in Uganda (Knapen, et al. 2006).

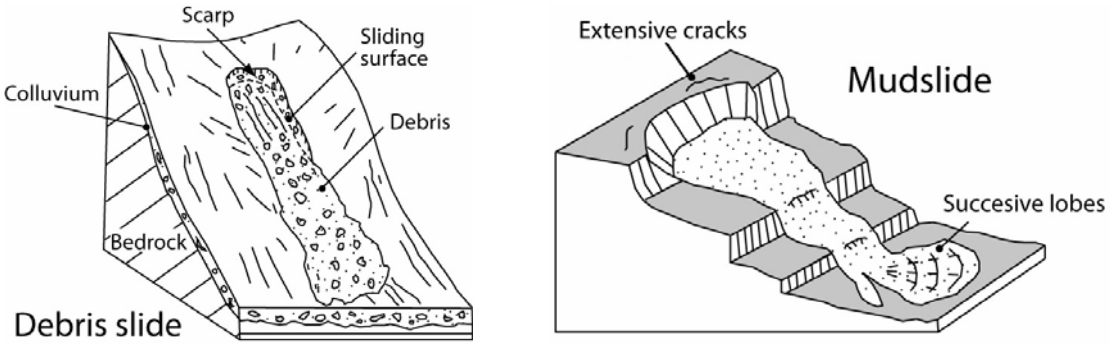

Figure 2.9. a) Debris Slide, b) Mudslide
(Source: University of Caen-Basse-Normandie 2008)

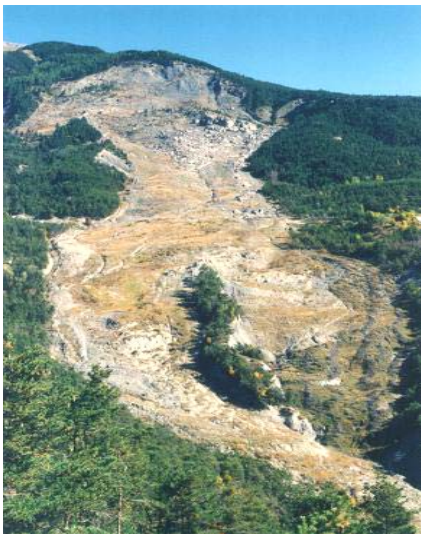

Figure 2.10. La Valette mudslide, Barcelonette Basin, French Alps
(Source: University of Caen-Basse-Normandie 2008**)**

2.4.4. Flows

Flows are downward slope movements of fluidised soil and other materials acting as viscous masses. In a flow, the structure of the material changes into quasi – fluid (Johnson and Rodine 1986, Bryant 1991). The most common type of flow is the debris flow (Corominas, et al. 1996). It is the most dangerous type (Takahashi 1991) due to the fact that debris flows often extend far from their sources and their depositional areas often include inhabited sites. The 1991 Phalombe Landslide (Gondwe

and Govati 1991, Cheyo 1999), and the 1946 Zomba Mountain Landslide (Poschinger, et al. 1998) both in Southern Malawi, are typical examples of debris flows and they were associated with extensive damage to nearby property and life. Other categories include: soilfluction, mudflows and debris avalanches (Coch 1995).

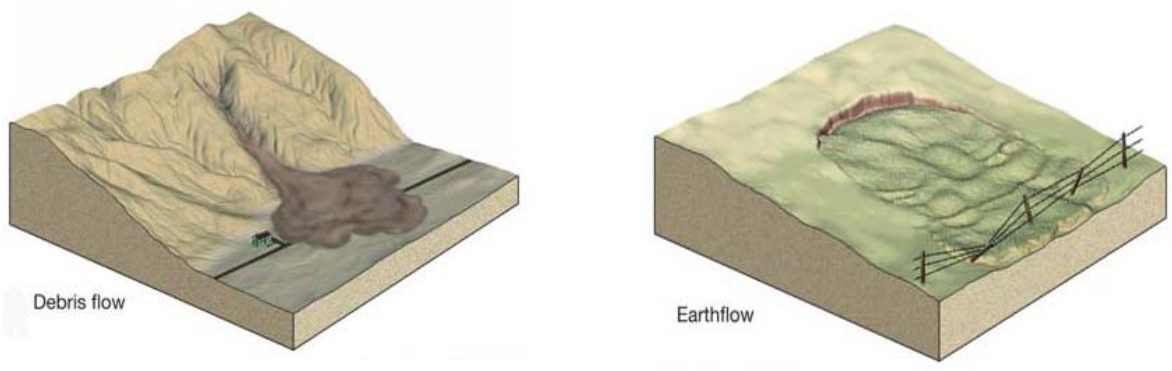

Figure 2.11. Types of flows: a) Debris flow; b) Earth flow

Figure 2.12. Blue Ridge Parkway (Milepost 348) fill-slope failure that initiated Bear Drive Branch National Forest, North Carolina debris flow on Pisgah (Source: Hurricane Frances, September 2004)

2.4.5. Creeping

One of the least destructive mass movement phenomena is soil creeping, which tends to be slow, superficial and predominantly seasonal (Hutchinson 1978, Crozier 1984, Alexander 1993). However, many of the other forms of landslides can undergo creeping and gradually cause serious damage. Soil creeping was observed in Vunguvungu/Banga catchments in Northern Malawi (Msilimba 2002). A summary of landslide classification and material involved in the movement is given in Table 2.2**.** Figure 2.13 shows two examples of creep in nature.

Figure 2.13. Examples of Creep in Nature

Table 2.2. Classification of Mass Movements, (adapted from Varnes 1978)

TYPE OF MOVEMENT			**TYPE OF MATERIAL**		
			Bedrock	**Soil**	
				Predominantly coarse material	**Predominantly fine material**
Falls			Rock Fall	Debris Fall	Earth Fall
Topples			Rock Topple	Debris Topple	Earth Topple
Slides	Rotational	Few Units	Rock Slump	Debris Slump	Earth Slump
	Translational	Few Units	Rock Block Slide	Debris Block Slide	Earth Slide
		Many Units	Rock Slide	Debris Slide	Earth Slide
Lateral Spreads			Rock Spread	Debris Spread	Earth Spread
Flows			Rock Flow	Debris Flow	Earth Flow
			Deep creep	Soil creep	
Complex			Combination of two or more principal types of movements		

CHAPTER 3

LITERATURE REVIEW ON RAINFALL INFILTRATION PARAMETERS AFFECTING SLOPE STABILITY

3.1. Introduction

A number of researchers carried out several numerical studies about the effects of rainfall infiltration on slope stability (Fredlund and Rahardjo 1993, Alanso, et al. 1995, Ng and Shi 1998, Ng, et al. 1999, Fourie, et al. 1999, Leong, et al. 1999, Gasmo et al. 2000). These studies have investigated physical properties of failed slopes, effects of slope angle and pore water pressure, mechanism of debris avalanche movement, properties of deposits resulting from avalanches. Rainfall infiltration into such soil slope leads to increases in pore-water pressures (due to loss of suctions), which may in turn result in soil swelling or changes in its stress state. In contrast, the resultant stress changes and soil swelling may affect the infiltration of rainwater, surface runoff and the evolution of pore-water pressures. (Pierson 1980, Premchitt, et al. 1994, Wilson and Dietrich 1987, Iverson and Major 1986, Iverson 2000, Lan, et al. 2003, Chen 1996 &1997, Du 1991, Xie and Xu 1999, Li, et al. 2001, Huang and Lin 2002).

3.2. Infiltration

Infiltration refers to the movement of liquid from a boundary into a porous medium. It involves a combination of horizontal flow, in which the capillary forces of the soil draw liquid outwards and vertical movement, in which both gravity and capillarity act to pull liquid vertically downwards. The interface between the wetted soil and the drier soil is called the wetting front and this wetting front defines the region of the subsurface containing the mobile liquid.

Infiltration has been studied since the turn of the century because of its relevance to crop irrigation and it continues to be a critical topic because of the need to avoid

contaminant migration to groundwater supplies. Leaks of petroleum products from underground storage tanks and pipelines, potential migration of radionuclides from nuclear waste sites located in the saturated zone and leaching of liquid waste beneath landfills or storage ponds are a few examples of situations in which infiltration is the dominant mechanism of contaminant transport phenomena. Despite the voluminous quantity of research dedicated to the topic, there has been little improvement in accuracy and ease of application for proposed models in the field studies. This is primarily because of the parameters needed in most infiltration models are difficult to measure and are subject to large measurement errors. Also, the nonlinearity of the parameter relationships makes solving the governing equations difficult or computationally intensive. Researchers continue to work with the established models seeking incremental improvements in precision, while in most cases it is the errors in parameter measurements that limit the accuracy of solutions. Because of uncertainties in characterizing subsurface geology and inevitability of unanticipated heterogeneities, investigators can be considered fortunate, if their predictions are within 50 percent of the measured field values, irrespective of the level of sophistication of the used infiltration model. This leads to the idea that simple models may be as accurate and easier to use, compared to complex models, if they rely on the evaluation of fewer parameters.

3.2.1. Infiltration Scenarios

There are three scenarios of infiltration into soil during a rainfall event. If the rainfall intensity (i.e. the rate of rainfall) is less than the infiltration rate (IR), all the water that reaches to a soil surface infiltrates into the subsoil. On the other hand, if the rainfall intensity is greater than the infiltration capacity, the extra water fills the soil surface depressions or flows downwards at the ground surface. If ground is sloping, depression storage may be small and surface runoff begins, soon after depression storage is filled. If the soil profile is already saturated, water fills the depression immediately, when the rainfall intensity exceeds the infiltration capacity.

3.2.2. Factors Affecting Infiltration

Generally, infiltration rate (IR) depends on soil, plant, climatic (Skaggs, 1980), and management factors. Soil factors affecting IR are antecedent to soil moisture content, soil texture, soil aggregation and structure, soil pores, soil surface conditions (crust and compaction) and the presence of impeding layers within the soil profile. A wet soil has a lower IR than a dry one (Haan, et al. 1994). This is attributed to the fact that some of the colloids in the wet soil swell, which results in reducing both the pore space amount and the rate of water movement within the soil (Schwab, et al. 1993). In general course-textured gravels and sands have higher infiltration rates than fine-textured clays. According to Hillel (1980), steady infiltration rates (under saturated conditions or at saturated hydraulic conductivity) for different soil types are as follows; Gravels and sands: > 20 mm/hr, sandy and silty soils: 10-20 mm/hr, loams: 5-10 mm/hr and clay soils: 1-5 mm/hr. D'Andrea (2001) also reported that soil hydraulic conductivity of clean sandy gravel might be 10 or more orders of magnitude higher than that of plastic clay, pretty much in agreement with Hillel's (1980) results.

Soils that have stable and strong aggregates with granular or blocky soil structure have higher infiltration rate than soils that have weak, massive or plate-like structure. Generally soils that have uniform particle sizes (such as: uniform sands) have higher infiltration rates than soils that have well-graded particle sizes. A soil surface with a highly porous structure has a greater initial infiltration rate than that of a uniformly structured soil. In contrast, a compacted soil surface and a profile covered by a surface crust of lower conductivity leads to a lower infiltration rate than that of the uniform (not compacted) soil (Hillel 1982).

Plant factors that affect infiltration include canopy cover and depth of the root zone (Skaggs 1980). Plant canopies intercept energy of raindrops, thereby minimizing their impact on the soil surface. For this reason, there is high infiltration rate and low runoff on a soil with a full and established canopy, compared to low infiltration and high runoff on a bare soil (Haan, et al. 1994).

The climatic factors that affect infiltration are; intensity, duration, time distribution of rainfall, total rainfall, temperature and whether or not the soil is frozen (Skaggs 1980). If rainfall intensity is greater than the infiltration rate, water will accumulate on the surface until impoundment areas are full, and then runoff will occur.

High intensity rainfall also leads to soil surface seal formation, which has low infiltration. However, low intensity rainfall does not cause surface sealing. On the other hand short duration rainfall is associated with high rainfall intensity, which leads to surface sealing and low infiltration. The longer the rainfall duration, the lower the infiltration rate is, because a wet soil swells. This means reducing of both pore space and rate of water movement within soil (Schwab, et al. 1993).

3.3. Influence of Seepage on Slope Instability

Seepage is one of the most prominent factors to cause slope instability in the soil mass. Slope instability in turn may cause landslides. A mass of rock, debris or earth moving as a mass down a slope is defined as a landslide (Cruden 1991). As one of the major hazards, landslides account for significant property damage each year. There are number of factors triggering landslides, which are;

1. Sudden changes in the water table levels, due to rainfall, human drains, earthquakes, ocean waves against a cliff face,
2. Rapid increase in the shear stress or decrease in the shear strength of slope-soil (Dai, et al. 2001).
3. Human activity, such as; deforestation or excavation of slopes for road cuts and building sites.

Just before a slope fails, the driving forces are equal to the resisting forces. Seepage is the main driving force for a slope failure to take place. A reduction of seepage force can be accomplished by redirecting the flow paths of the seepage in the slope, but most of the existing methods to reduce seepage are expensive and are difficult to set up.

Some methods of reducing seepage in the slope are:

- Horizontal drains (for deep seated failures).
- Cutoff trenches (for shallow failures).

Horizontal drains are inserted below the failing soil mass to direct the seepage force vertically down. Cut-off trenches are typically placed parallel to the top (crest) of a slope and remove seepage from the slope, if the water table can be intersected before

groundwater moves into the slope. If the water table cannot be intercepted, before the slope crest, longitudinal trenches parallel to each other and in the direction of maximum slope inclination can be used (Stanic 1984). With the drains installed, a majority of the seepage force is eliminated from the sum of the resisting forces, thereby increasing the factor of safety.

3.4. Rainfall Infiltration and Shallow Landslides

It is widely known that rainfall causes to a rise of the groundwater level and a decrease in matric suctions (negative pore water pressures) that results in slope failures. Shallow landslides are one of the most common types of landslides, occurring frequently in steep landscapes in different climatic zones (e.g. Kirkby 1987, Benda and Cundy 1990, Selby 1993).

Shallow landslides occur in response to heavy rainstorms in steep hillslopes, as dominant erosional processes in especially humid and temperate climatic regions. Landslides remove materials from hillslopes and scour low-order channels, supplying a large quantity of sediment to high-order fluvial systems (Dietrich and Dunne 1978). Denudation by landsliding causes to major sediment yields from drainage basins (Aniya 1985).

Rainfall-induced shallow landslides pose a grave threat to human lives and property, since they occur suddenly and often travel along a distance as a high-speed debris flow. A shallow landslide and subsequent debris flow may cause thousands of deaths and serious economic damage worldwide, especially in mountainous regions subjected to heavy rainfall. Shallow landslides can also be indirectly impacted by climate change, through effects on glaciers, permafrost or forest fires. Glacier retreat and permafrost degradation may lead to large areas of unstable slopes (especially because of cohesion loss, due to the melting of ice particles in these slopes). These voluminous materials could potentially become debris flows at high altitudes, particularly in the case of very steep slopes.

Figure 3.1. Shallow Landslide in Merlas-Isère, South-Eastern France

3.5. Uncertainties in Slope Stability under Rainfall Conditions

Various uncertainties are involved in the stability of slopes affected by rainfall infiltration. First, soil properties that can cause instability of a slope exhibit considerable variation from point to point. The soil properties, e.g. soil permeability, also vary with time because of change of pore-water pressure and stresses. Secondly, when one tries to estimate soil properties from laboratory test results or empirical models, errors in testing and empirical models are introduced into the estimated parameters. Thirdly, one may also apply a prediction model for slope stability analysis. The uncertainties of the estimated soil properties will influence outcome of the analyses. The intensity, duration and pattern of a rainstorm are not definitely known. The initial pore-water pressures cannot be measured exactly at every point in the slope. The boundary conditions used in the analysis are not certain, even with accurate measurements.

Soils are geological materials formed by weathering processes, transported by physical means to their present locations. They have been subject to various stresses, pore fluids, physical and chemical changes. Thus, it is not surprising that the physical properties vary from place to place.

3.6. Saturated and Unsaturated Soils

When the soils encounters with water for a certain time, voids in the soil mass will be filled by water gradually and air in the voids will undergo a gradual transformation process leading to saturation due to the difference in acting pressures in air, water and between air and water. The same process also happens, even if the soil is under the groundwater table (GWT). In this condition, the void ratio (e) is equal to zero and the degree of saturation (S_r) is equal to 1 and the soil is categorized as a 'saturated soil'. Most of the problems in saturated soils (including slope instability) can be analyzed using the effective stress equation (Equation 3.2), requiring pore-water pressure value (u_w) to be us.

The terms 'partly saturated' or 'partially saturated' are usually refer to the condition, where the voids in the soil are filled by both air and water at a certain ratio and the soils are not directly subjected to the groundwater table action. This happening generally occurs in soils that are located above the groundwater level. Figure 3.2 illustrates the soils that are subjected to the different types of pore-water pressures.

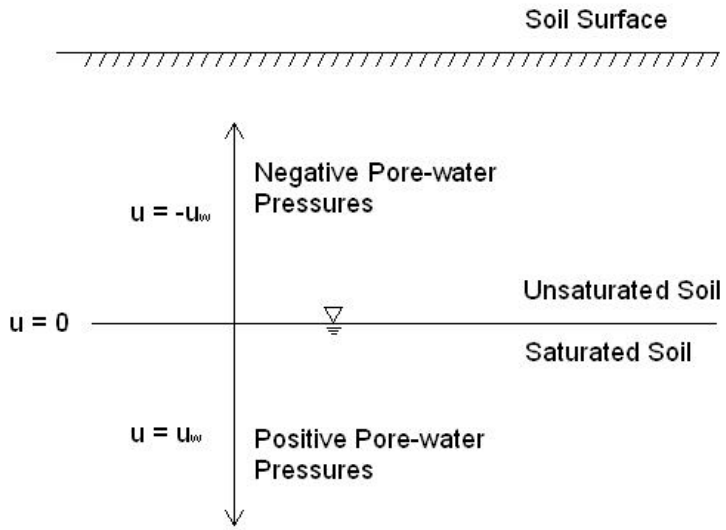

Figure 3.2. Various Soil Conditions Subjected to the Different Types of Pore-Water Pressures

Since soils are subjected to the different types of pore-water pressures, stresses that develop in each particular soil condition are also different. In saturated soils, soil strength is influenced by the effective stress state variables, whereas positive pore-water pressures that developed within soil will reduce the strength, by eliminating the friction between soil particles. In unsaturated soils, because of the effect of contractile skin (menisci with surface tension), soil strength is subjected to two independent stress state variables, which are net normal stress (σ-u_a) and matric suction (u_a-u_w), (Wulfsohn, Adams and Fredlund 1996).

3.6.1. Shear Strength Characteristics for Saturated and Unsaturated Soils

In this thesis geotechnical instability conditions are examined, especially to include shallow (up to 3-4m deep) landslides occurring in fine grained soils. Shallow landslides are directly related to the reduction of shear strength that takes place near the soil surface. The shear strength of a soil in any plane is concerned with the stress-state of soil. The stress-state of soil depends on two stress-state variables net normal stress, (σ-u_a) and matric suction, (u_a-u_w). For the majority of the theoretical principles in soil mechanics, the saturated case is presented first, because of its relative simplicity.

3.6.1.1. Shear Strength Equation for Saturated Soils

Shear strength of a saturated cohesive soil can be defined by the Mohr-Coulomb failure criterion using the effective stress principle mentioned (Equation 3.1). For saturated soils, shear strength of a soil is defined as:

$$\tau = c' + (\sigma - u_w)\tan\phi' \tag{3.1}$$

The Mohr-Coulomb failure criterion assumes that; soil is at failure once the maximum principal stress ratio is reached, for a specific normal stress level. The criterion can be performed even to undecomposed intact rocks (having peak strengths) and to soils (having residual strengths) formed by decomposition of rocks that are now completely remolded. Equation 3.1 defines a straight line, which is referred to as the

Mohr-Coulomb failure envelope (Figure 3.3). Equation 3.1 can be point out graphically through the construction of at least two (or more) Mohr circles presenting different stress conditions that produce failure in a soil. A Mohr circle describes the interaction between the shear stress and normal effective stress on a variety of different orientations at a point within the soil.

With the construction of a few Mohr circles at failure, a straight line can be drawn tangent to the circles defining the failure envelope. The slope of the line represents the internal friction angle, ϕ', and the intercept on the τ-axis represents the effective cohesion, c' (in overconsolidated soils, failure envelopes are generally bi-linear).

The shear strength of a two-phase soil mass depends on the effective stress concept. The effective stress concept for a saturated soil is as follows:

$$\left\{\sigma'\right\} = \left\{\sigma\right\} - u_w \left\{I\right\} \tag{3.2}$$

The effective stress concept is widely accepted and at times regarded as a law (Fredlund and Rahardjo 1993). The effective stress concept is independent of soil properties, meaning it is applicable to all types of soils (sands, silts and clays).

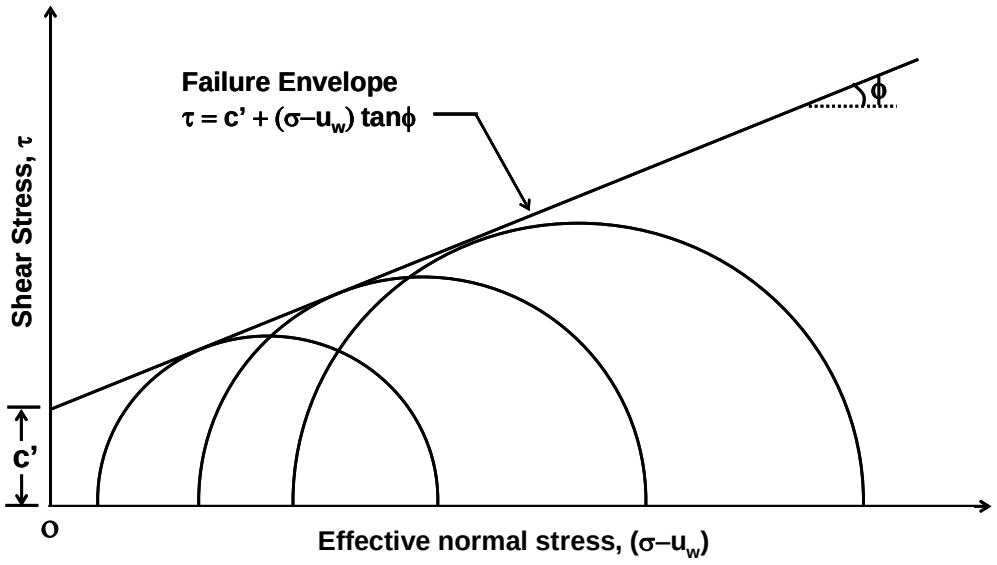

Figure 3.3. Mohr-Coulomb Failure Envelope for a Saturated Soil
(Source: Fredlund and Rahardjo 1993)

3.6.1.2. Shear Strength Equation for Unsaturated Soils

The shear strength of an unsaturated soil utilizes the Mohr-Coulomb failure criterion and the effective stress concept similar to the saturated condition, but with an additional stress-state variable. Fredlund, et al. (1978) presented a shear strength equation for unsaturated soils that has become extensively accepted by the scientific community. The equation is expressed as:

$$\tau = c' + (\sigma - u_a)\tan\phi' + (u_a - u_w)\tan\phi^b \tag{3.3}$$

The shear strength equation for an unsaturated soil is an extension of the saturated case (Equation 3.1) with the addition of the stress-state variable; (u_a-u_w) and the strength parameter; ϕ^b. With these two stress-state variables, the Mohr-Coulomb failure envelope becomes three-dimensional (Figure 3.4). The (u_a-u_w) term defines the third orthogonal axis.

The ϕ^b parameter is the parameter that represents any change in the shear strength associated with any change in the matric suction. This is the most important parameter in unsaturated soil mechanics. The ϕ^b parameter was initially thought to be constant for a specific soil. But recent evidence has shown that; ϕ^b parameter varies with matric suction level up to the air entry value, then it is constant and less than ϕ'. The tan(ϕ^b) function is currently represented by a bi-linear function with the air entry value being the inflection point (Fredlund and Rahardjo 1993). Morris, et al. (1992) has suggested that $\phi^b = \phi' - 4°$, as a global approximation for upto the air entry value, Vanapalli, et al. (1996) has suggested value of $\phi^b = \phi'$.

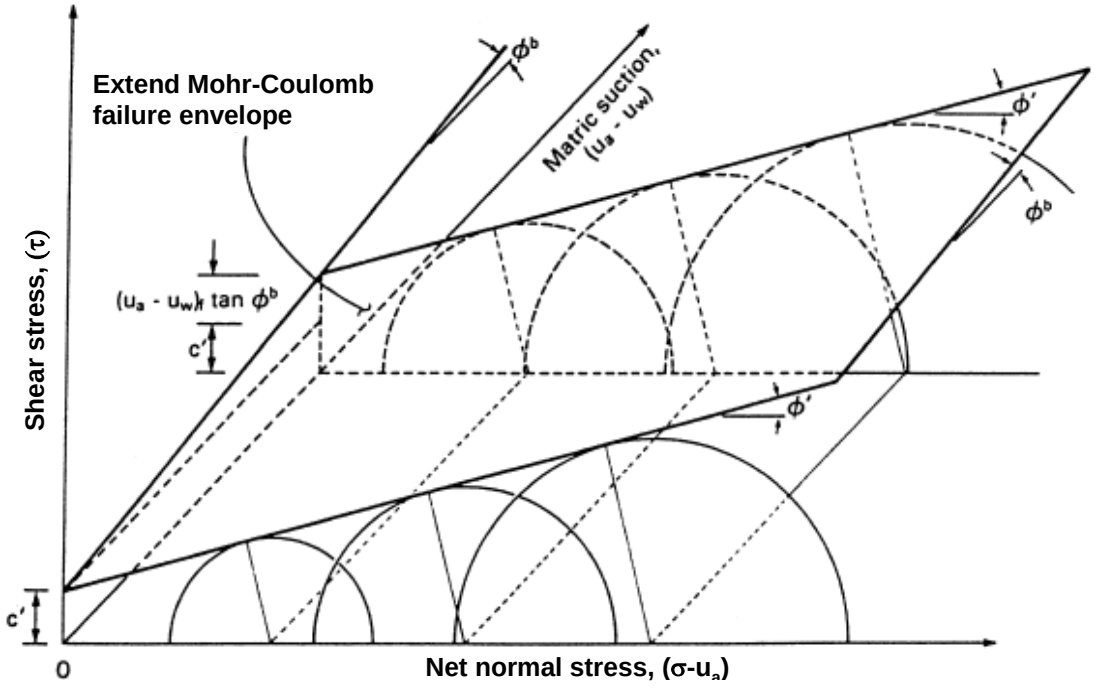

Figure 3.4. Mohr-Coulomb Failure Surface for an Unsaturated Soil
(Source: Fredlund and Rahardjo 1993)

3.7. Stages of Saturation

Unsaturated soils occur within a wide range in degrees of saturation (S_r) varying from 0 to 1. If the soil is saturated, idealization of S_r is a single point and it is equal to 1. Many researchers realized that for research purposes, the unsaturated soils should be divided into several stages (Wroth and Houlsby 1985, Vanapalli 1994, Fredlund 1995, Fleureau, et al. 1995, Bao, et al. 1998, Cho and Santamatina 2000). The reason for the divisions is the pattern of air and water phase with respect to the form and continuity is different in each stage. Hence the movement of air and water in an unsaturated soil can be different, when its boundary conditions are changed (e.g., when a change in soil suction or confining pressure applied to the soil). For a given soil, the hydraulic and mechanical behaviors at different saturation stages can be significantly different. Thus, the research methodologies and experimental techniques may change from one stage to another. For example, in a relatively dry soil, the water phase tends to exist only in small voids (e.g. pore corners) meaning that water phase is discontinuous. The movement of water due to a change in the applied hydraulic gradient takes place via water vapor and hence may not conform to Darcy's law. Consequently, suction equalization (in terms of value) is a distinctly slow process. Although the suction in the

soil is high, the contribution of suction to the shear strength and stiffness is negligible, due to small portion of the wetted area. The humidity control method (rather than axis translation technique) is generally adopted for the control of suction in such a soil.

3.8. Wetting Front and Moisture Redistribution

Wetting front and moisture redistribution are two important phenomena in the saturation profile of an unsaturated soil. As mentioned earlier, the conceptual model based on sharp wetting front approach was first developed by Green and Ampt (1911). The studies in wetting front have been extended by numerous researchers, with the likes of Lumb (1962), Bouwer (1966), Mein and Farrel (1974), Pradel and Raad (1993), Kim, et al. (2006), and Wang, et al. (2003). Recent studies attempted to correlate the wetting front with the redistribution in order to provide a more comprehensive explanation to the soil moisture movement after the infiltration processes (Youngs, 1958, Jury, et al. 2003, Wang, et al. 2003).

As illustrated in Figure 3.5, the wetting front depth (L_f) under uniform amount of rainfall infiltration (P) can be approximated to (Wang, et al. 2003).

$$L_f = \frac{P}{\theta_a - \theta_i} \tag{3.4}$$

Where is θ_a the average moisture content in the wetted zone, and θ_i is the initial moisture content.

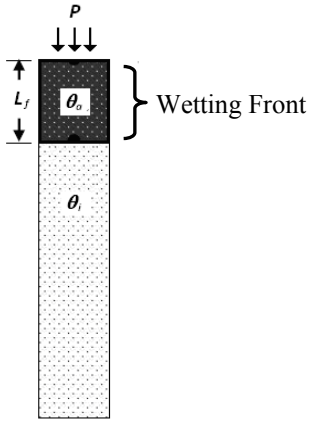

Figure 3.5. Development of Wetting Front
(Source: Wang, et al. 2003)

Wang, et al. (2003) found that the soil below the wetting front, initially takes up moisture following an absorption curve OA, until suction reaches the water entry value (W_{ev}) at the wetting front. Subsequently the volumetric water content increases abruptly to θ'_s. Above the wetting front (soil near the ground surface), water drains-out from the soil following the desorption curve BO. When suction reaches the air-entry value (A_{ev}), the major pores begin to empty. The difference between the W_{ev} and A_{ev} indicates the ability of a porous medium to entrap a zone of higher water content behind the wetting front (Glass, et al. 1989). Considering the inclination angle of slope (β), Wang, et al. (2003) revised this special moisture retention ability and proposed a term known as the critical wetting front depth (L_{cr}):

$$L_{cr} = \frac{W_{ev} - A_{ev}}{\cos\beta} \tag{3.5}$$

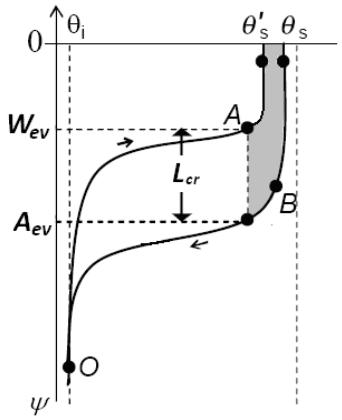

Figure 3.6. Volumetric water content and suction in the development of a wettingfront (Source: Wang, et al. 2003)

The term of critical wetting front depth was given, because it is the limit for suction redistribution and unstable flow to take place. In other words, when $L_f < L_{cr}$, the downward flux is not possible and the corresponding suction redistribution will be as shown in Figure 3.7a. Otherwise (if $L_f > L_{cr}$), downward flow continues, when water input stops, due to excessive amount of infiltration and the corresponding suction redistribution is as illustrated in Figure 3.7b. It can be inferred from some recent studies that; with this type of redistribution pattern, a threshold water-entry pressure at the

wetting front is required for the water to enter the unwetted zone (Liu, et al. 1993, Geiger and Durnford 2000).

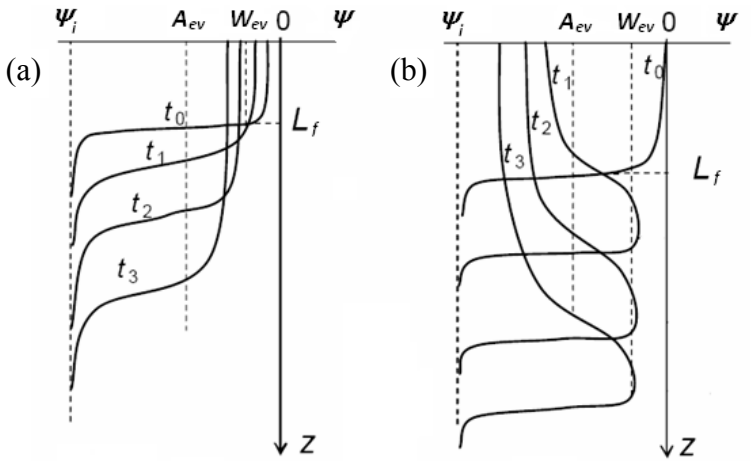

Figure 3.7. Redistribution of Soil Moisture for a) $L_f < L_{cr}$ and b) $L_f > L_{cr}$
(Source: Wang, et al. 2003)

3.9. Wetting Band Theory – Lumb's Equation

During severe and constant intensity rainfall and in the first few-hours of it, slope stability is depended upon; *(i)* the thickness of the saturated soil layer, existing as a result of rainfall infiltration into soil and, *(ii)* ability (capacity) of the soil layer to drain infiltrated rain. Lumb (1975), proposed the following formula to predict the thickness of the water saturated wetting band layer in time (t), caused by an infiltrated rainwater amount exceeding the drain ability capacity of the soil.

Lumb (1975) derived a wetting-band equation for the case of one-dimensional infiltration in the vertical direction. This equation has become the well-known Lumb's wetting-band theory and has been used in addressing the issue of soil moisture and suction development in a soil mass in association with rainfall infiltration.

$$h_w = \frac{k_s t}{n(S_f - S_0)} \tag{3.6}$$

h_w the depth of the unsaturated wetting front

S_0 the initial degree of saturation at time t

S_f the final degree of saturation at time t

k coefficient of permeability

t the rainfall duration

n the porosity

Yet this commonly used Lump's equation (3.6) in practice, though considers soil impermeability to water and duration of the rainfall, it does not consider rainfall intensity and its variability over its duration/time.

3.10. Soil-water Characteristic Curves

The relationship between the water content (the degree of saturation) and soil suction is called the soil-water characteristic curve (SWCC). The water content can either be gravimetric (ratio of weight of water to weight of solids) or volumetric (ratio of volume of water to total volume). Figure 3.8 is an example of a soil water characteristic curve. Through the absorption and desorption processes, Soil Water Characteristic Curve (SWCC) shown in Figure 3.9 is obtained for each type of soil.
Three zones are labeled in the figure (changing from the lowest suction to the highest):

1. Boundary effect zone: Soil in this zone is mostly saturated, as capillary forces in the voids between the soil grains draw water upwards from the groundwater table. The upper bound of this zone is the air entry value (AEV), which is the suction at which air begins to enter the largest of the void spaces.

2. Transition zone: In this zone, air displaces water in the void spaces. With increasing suction, increasingly smaller pores are filled with air, due to their larger capillary potentials. The high-suction bound of this zone is defined by the residual water content, the water content at which the water phase in the soil becomes discontinuous.

3. Residual zone: In this zone, pore water exists in a discontinuous phase (i.e. water exists only in pockets that are isolated from one another). Water moves primarily

through the vapor flow. In this zone, it takes extremely large amount of suction to remove any additional water. The generally recognized suction limit of the SWCC is 10^6 kPa, representing the suction value at which water can no longer exist in the soil (Fredlund and Xing 1994).

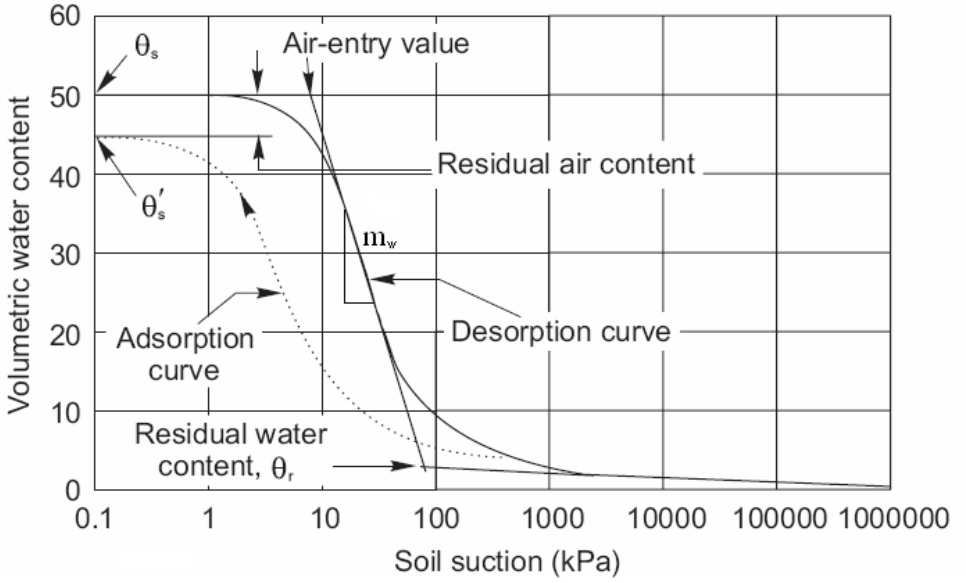

Figure 3.8. Typical Absorption and Desorption Resulted SWCCs
(Source: Zhan and Ng 2004)

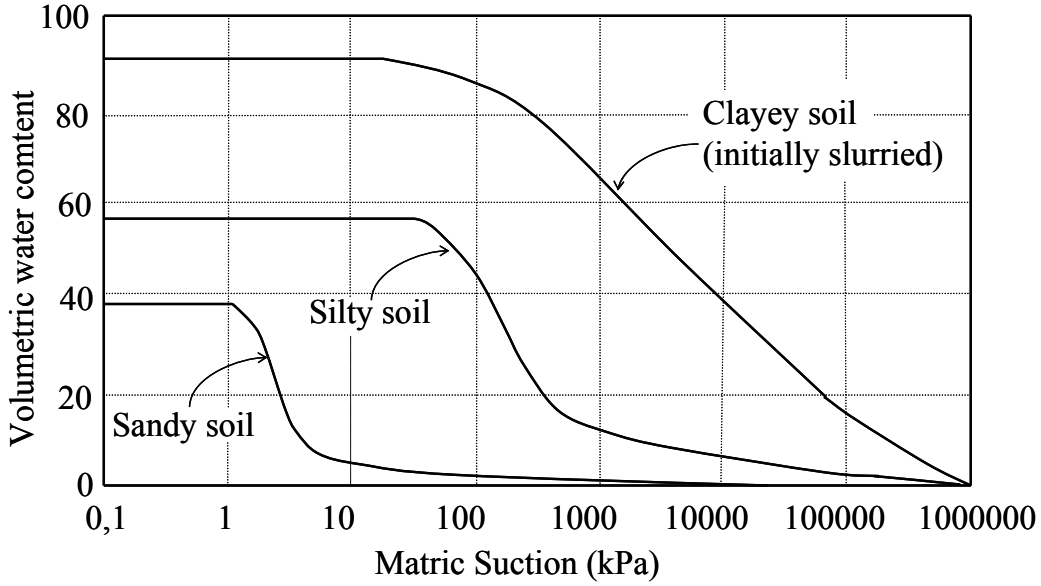

Figure 3.9. SWCCs for Various Soils.
(Source: Fredlund and Xing 1994)

CHAPTER 4

DETERMINATION OF SOIL PROPERTIES AND SLOPE MODEL PREPARATION PROCEDURES

4.1. Introduction

In order to obtain reliable information about any slope soil, first a comprehensive preliminary study should be done. Each soil may have different engineering properties and if these differences are not well-recognized, negligence is likely to create problems in future studies. Therefore from this point of view; physical, mechanical and chemical properties of slope soils should be established.

First of all, the main soil classification tests had to be made (i.e. Particle Size Distribution, Atterberg Limits, Proctor Compaction and Specific Gravity) and then the soil classification symbol was identified, in accordance with the Unified Soil Classification System (USCS).

Mechanical properties of soils depend mainly on the particle size distribution and on the stress state of a soil. Mechanical soil tests provide an opinion about the resistance of a soil under static and dynamic loading conditions, bearing capacity, relative density and settlement etc.

4.2. Soil Classification Tests

4.2.1. Particle Size Distribution

Soil is composed of an gathering of ultimate soil particles (discrete particles) of various shapes and sizes. The purpose of a particle size analysis is to group these particles into separate ranges of sizes and so determine the relative proportions by weight of each size range. The percentage of the samples in each group can be represented graphically in bar charts or histograms (Figure 4.1). Another method for

graphic display is the cumulative curve or cumulative arithmetic curve. Cumulative curves are extremely practical, because many sample curves can be plotted on the same graph and differences are at once apparent.

Several test methods can be used to determine the percentage of the samples in each class. For this project; wet sieve analysis was used for coarse soils in addition to averages of hydrometer and laser diffraction methods were used for the fine fraction. These particle size distribution methods are mostly used because the tested soil in this project was highly composed of fine-grained particles (i.e. 50% or more finer than #200 sieve 0.075mm).

4.2.1.1. Wet Sieve Analysis

This method includes a quantitative determination of the particle size distribution in a soil down to the fine sand size. Application of dry sieve analysis in fine grained soils may encounter some difficulties, for example clay particles may lump together or stick to each other and cannot pass the sieve, but they can easily disintegrate from each other and pass the sieve sizes in wet conditions. So, in practice wet sieve analysis is more preferred, compared to dry sieve analysis.

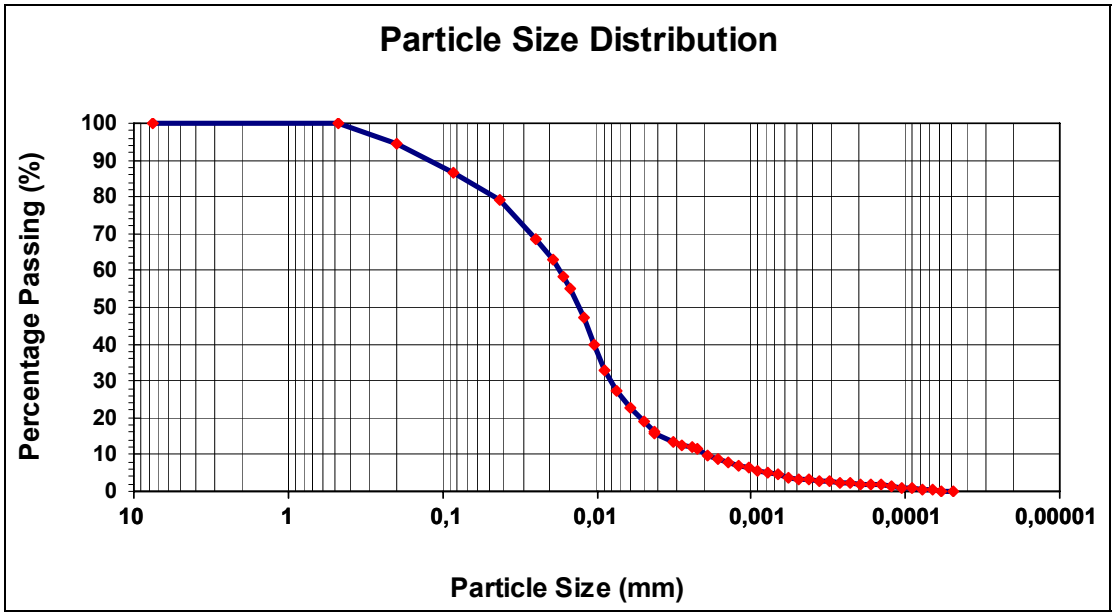

Figure 4.1. Particle Size Distribution (PSD) Graph

4.2.1.2. Hydrometer Test

This test is an application of the Stokes Law, which in essence states that; in a suspending fluid, larger particles fall more quickly, while the finer particles remain in suspension longer. The time at which the hydrometer readings are taken, determines the sizes of the particle remaining in suspension, while the reading on the hydrometer determines the amount of that size (Figure 4.2).

Several assumptions are made about the particles' shape and other test conditions, so the results are somewhat approximate. The sieve portion and hydrometer portion of the test may not exactly conform to each other. The method as presented, assumes a particle specific gravity (G_S) value of 2.65. For most purposes this will be adequate, even though the real G_S may be somewhat lower or higher. If further improvement is required, additional corrections may be found in the references.

Results are used to indicate whether the soil is frost susceptible and for comparing soils from different areas and strata. Because the sample size is small, extra should be taken to obtain a representative material. Considerable care should also be taken in all weighing and liquid volume measurements. The sample must be completely dispersed and remain dispersed throughout the test. Also the dispersing agent should not be more than one month old. Further, the stirring paddle is not badly worn. Some soils (like heavy clays) tend to coagulate and form curds to settle quickly giving false readings. If any evidence of coagulation is seen, then the test must be re-run. Reducing the sample size to 25 g sometimes helps to solve this problem.

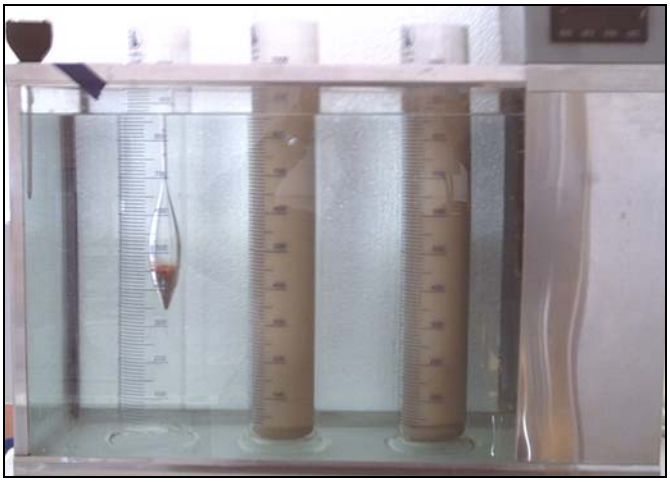

Figure 4.2. Hydrometer Test Equipment

4.2.1.3. Laser Diffraction Method

Laser diffraction is a modern, convenient and the most widely used technique for determining the particle size distribution. In laser diffraction type particle size analysis, a representative cloud or ensemble of particles passes through a broadened beam of laser light which scatters the incident light onto a Fourier lens. Laser diffraction based particle size analysis (Figure 4.3) relies on the fact that particles passing through a laser beam will scatter light beam at an angle that is directly related to their size. As particle size decreases, the observed scattering angle increases logarithmically. Scattering intensity is also dependent on the particle size, which diminishes with increasing particle volume. Large particles will scatter light at narrow angles with high intensity, whereas small particles will scatter light at wider angles with low intensity. In this method the lens focus the scattered light onto a detector array and using an inversion algorithm, a particle size distribution is obtained from the collected diffracted light data. Sizing particles using this technique depends upon availability of accurate, reproducible, high resolution light scatter measurements to ensure a full characterization of the sample to be made.

Laser diffraction is a non-destructive, non-intrusive method that can be used for either dry or wet samples. As it derives particle size data using fundamental scientific principles, there is no need for external calibration, in addition to a wide dynamic measuring range with particles in the size range of 0.02 to 2000 microns. (Source: www.chemie.de/articles/e/61205/)

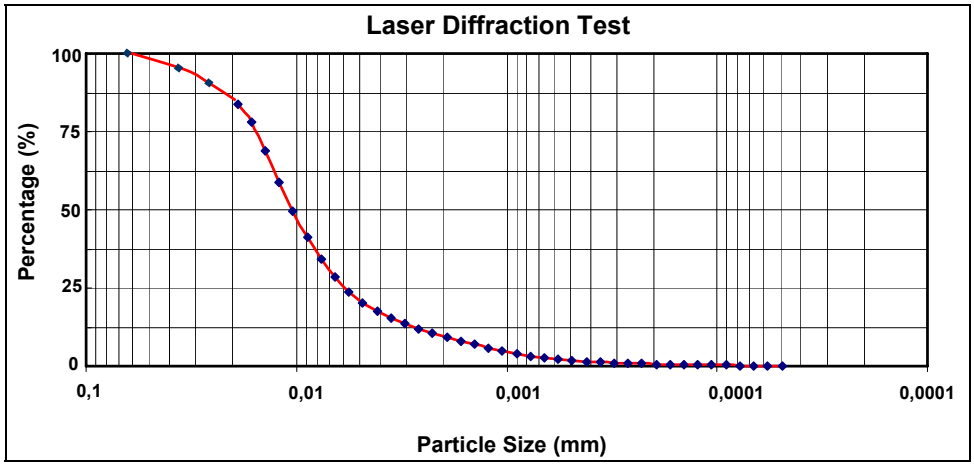

Figure 4.3. Laser Diffraction Test Graph

In general, a softer tip supplies greater pulse duration with low frequency content than a harder tip. However, a harder tip will provide an impulse of larger amplitude with high frequency content to the excitation than a softer tip.

In summarizing: average result of three tests showed that 98% percent of the tested soil (by weight) was finer than (passes/below) the US No.40 sieve. Additionally, 83% percent of the tested soil sample was finer than the US No.200 sieve. On the contrary, 100% passes the US No.10 sieve. In the light of this information, soil is dominantly consisting of the fine grained soil (2%medium sand + 15% fine sand + 83% silt and clay). As the amount of fine-grained soil portion is significant, a more comprehensive classification procedure for fine-grained soils should be done. Few soil samples were taken from the bottom of the US No.200 sieve. Further; laser diffraction method was used and more detailed information was obtained with respect to the fine-grained soil particles.

4.2.2. Atterberg Limits

A fine-gained soil can exist in any of several states, depending upon the amount of water in the soil system. When water is added to a dry soil, each particle is covered with a film of adsorbed water. If water is added to any soil with individual particles, then the thickness of the water film on a particle increases. Increasing the thickness of the water films permits the particles to slide past one another more easily. The frictional behavior of the soil, therefore, is related to the amount of water in the system. Approximately sixty years ago, A. Atterberg defined the boundaries of four states in terms of "limits" as follows:

- Liquid limit (LL): The boundary between the liquid and plastic states;
- Plastic limit (PL): The boundary between the plastic and semi-solid states;
- Shrinkage limit (SL): The boundary between the semi-solid and solid states

These limits have since been more definitely defined by A. Casagrande as the water contents, which exist under the following conditions:

- Liquid limit (LL): The water content at which the soil has such small shear strength that it flows to close a groove of standard width when jarred in a specified manner.
- Plastic limit (PL): The water content at which the soil begins to crumble when rolled into threads of a specified size.
- Shrinkage limit (SL): The water content that is just sufficient to fill the pores, when the soil is at the minimum volume it will attain by drying.

The amount of water which must be added to change a soil from its plastic limit to its liquid limit is an indication of the plasticity of the soil. This plasticity is measured by the "plasticity index", which is equal to the liquid limit minus the plastic limit, (PI=LL - PL).

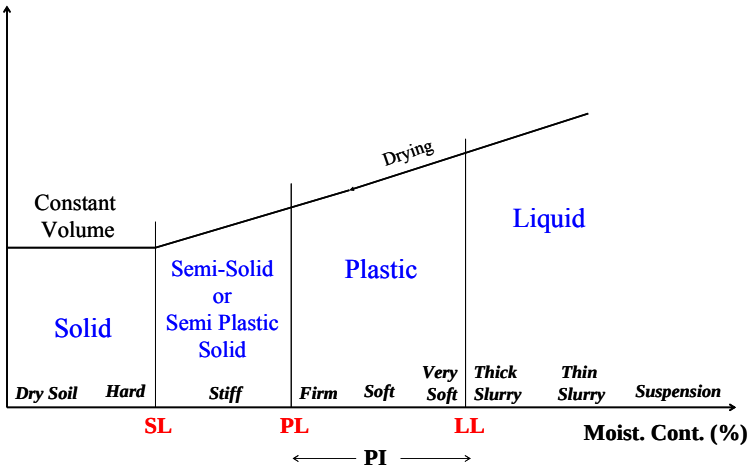

Figure 4.4. Relationship between Volume of Soil and Moisture Content

4.2.2.1. Liquid Limit (LL)

In order to determine the LL of a soil sample two different methods can be used. One of them is the multipoint liquid limit test, as shown in Figure 4.5 using the 'Casagrande Apparatus' (Figure 4.6a) and the other one by using the one-point test set-up. The multipoint liquid limit method is more widely used and is generally more precise than the one-point method. It is recommended that the multipoint method be used in cases, where test results are subject to dispute or where greater precision is required. Figure 4.6b shows the multi-point test process.

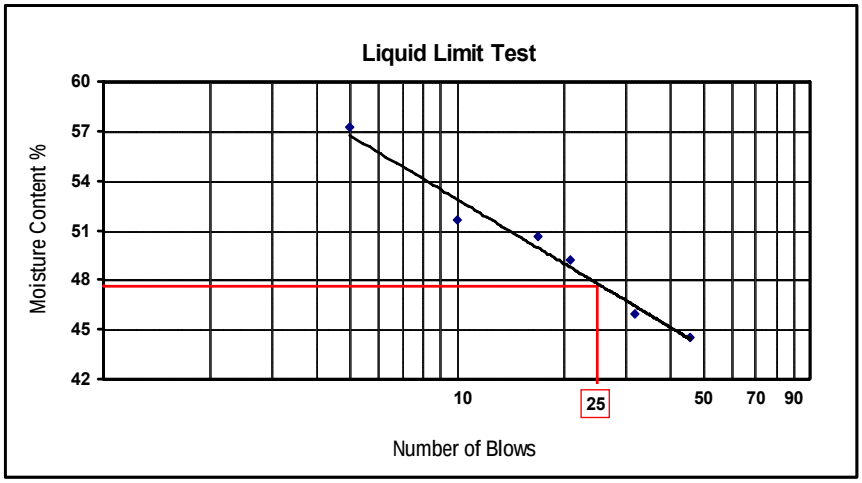

Figure 4.5. Liquid Limit (LL) Test Graph for the Multi-Point Test.

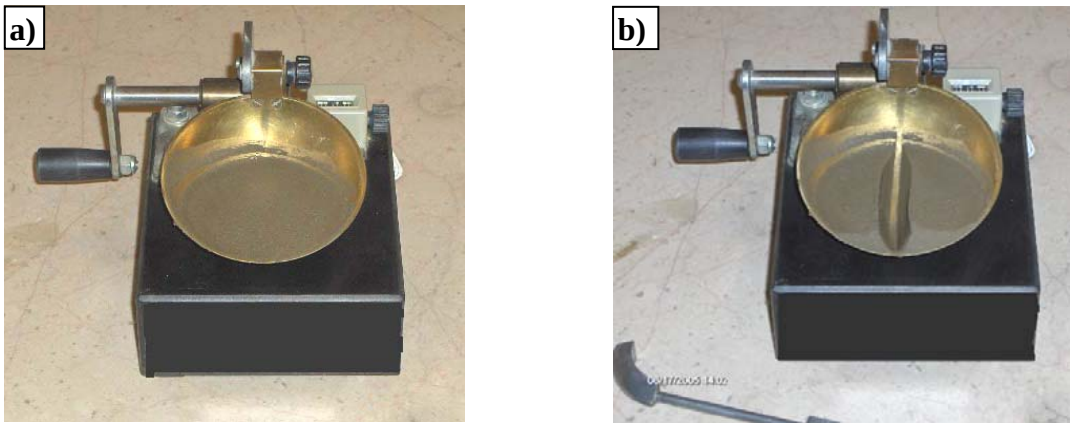

Figure 4.6. Casagrande Apparatus for the Multi-Point Liquid Limit Test (LL)

4.2.2.2. Plastic Limit (PL)

This method is for the determination of the lowest moisture content at which the soil is in plastic state with no hairline cracks. It is preferable to exert this test on remolded materials, prepared from the natural state. For this determination, soil specimen is dried by air drying. Next it's molded into a ball first and then rolled over the surface of a smooth, glass plate beneath the fingers of one hand with backward and forward movements, until it forms thin (about 3mm) diameter threads and without any hairline cracks occurring, between the palms of the hands. The water content at this step is the Plastic Limit of the sample. The difference between the LL and the PL gives

Plasticity Index (PI) of the sample, which widely used in practice to describe/indicate how plastic the soil sample is. Figure 4.7 shows the PL test equipment.

Figure 4.7. Plastic Limit (PL) Test Equipment

In summary: average value of the three tests performed showed that the value of the liquid limit is 47%. Also, six Plastic limit tests were performed and at their average value was 32%. After the particle size analysis and the Atterberg Limit tests were completed, determination of soil classification could have been made, using the Unified Soil Classification System (USCS). When the values of Plasticity Index (PI=LL-PL) and Liquid limit test were intersected in USCS chart below, the classification of the tested soil was determined as a mixture of CL and ML soil types (Figure 4.8).

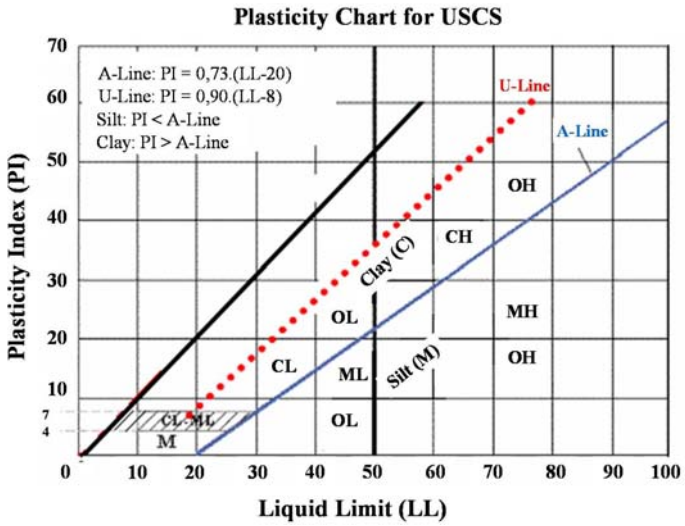

Figure 4.8. Unified Soil Classification Charts

4.2.2.3. Specific Gravity (G_S)

The specific gravity (G_S) of a soil sample is the ratio between the unit masses of soil particles and water. It is just a ratio and has no unit. The method to determine the G_S is defined in the ASTM D 854-02. G_S of soil solids is used to calculate the density of the soil solids. This is done by multiplying its specific gravity by the density of water (at proper temperature).

The test requires the determination of the volume of a mass of dry soil particles. This is obtained by placing the soil particles in a pycnometer, filled completely with air distilled water. To remove all of the air trapped between the soil particles in the pycnometer, its contents are shaken vigorously, if the soil specimen has coarse-grained soils or placed under vacuum for using finer-grained soils. This procedure is the most critical part of the test. The volume of the soil particles is determined from the differences in mass, assuming the G_S of water to be unity, while taking masses in grams (or Mg) and volumes in cm^3 (or m^3).

4.3. Compaction Test

Soil compaction is the process whereby soil particles are more closely packed together (i.e. soil density increased) with the addition of an impact energy provided by certain numbers of hammer blows falling freely from certain heights. This is called Proctor Compaction test (ASTM D 698) and is usually used for fine and cohesive soils. Depending upon the size and weight of the hammer and the compaction mold, the test is called: Standard or Modified Compaction Test. Mechanism of packing (ie. soil density increase) is explained as due to achieving decreases in the air voids volume by mechanical means. The aim of compacting earth fills such as in earth dams and embankments (for highways, railways and canals) is to produce a soil mass that will satisfy the two basic criteria;

- Compaction increases soil's shear strength, which in turn increases the bearing capacity of foundations constructed over them.
- Compaction also decreases the amount of settlement of structures and increases the stability of embankment slopes.

In theory, the most effective compaction process should substantially decrease some free air in the soil pores or bubbled air in the soil's pore fluid by causing them to be dissolved in the pore fluid. However, in practice, compaction cannot completely eliminate the air fraction, but only reduces it to a minimum, provided that it's done properly. In the field several different methods are used to compact the soil such as; tamping, kneading, vibratory and static load compaction.

Compaction test in the laboratory is performed by plotting the relationship between the moisture content and the dry density of a soil specimen using the Standard Proctor Test Procedure (ASTM D 698) as developed by R.R. Proctor in 1933. In the Standard Proctor Test, the soil is compacted by a 2,5 kg hammer falling a distance of 30,5 cm onto a soil filled mold. The mold is filled with three equally thick layers of soil and each layer is subjected to 25 drops of the hammer. The Modified Proctor Test (ASTM D 1557) is identical to the Standard Proctor Test, except that it employs, a 4,5 kg hammer falling a distance of 45,7 cm and uses five equally thick layers of the soil instead of three. There are two types of compaction molds used for the testing. The smaller type is for the Standard Proctor having 4 inches in diameter with a volume of about 1/30 ft^3 (944 cm^3) and the larger type is for the Modified Proctor having 6 inches in diameter with a volume of about 1/13.333 ft^3 (2123 cm^3). Also, if the larger mold is used (of the Modified Proctor Test) each soil layer must receive 56 blows, instead of 25 blows (of the Standard Proctor Test). Figure 4.9 shows Standard Proctor Test Process.

Figure 4.9. Standard Proctor Test Process

As illustrated in the laboratory obtained compaction curve of Figure 4.10, water has a fundamental effect on soil compaction. Even at low water contents, individual soil grains are surrounded by thin films of water. A small increase in w_c may increase the repulsion of particles to facilitate their orderly arrangement. Any addition of water expels air from soils until the optimum w_c is reached and make possible to reach larger dry unit weights. The densest soil state is obtained at the optimum water content, as the w_c exceeds the maximum value and water pushes grains apart. Since water is much more incompressible than the grains themselves and the soil specimen has no time to drain, the dry unit weight (γ_{dry}) starts to decrease.

In summary: the determination of the compaction test (water content-soil density relationship) is obtained by using soil the Standard Proctor Test procedure (ASTM D 698). For each test, set seven points are assigned to drawn the water content-soil density curve and three identical test sets are completed.

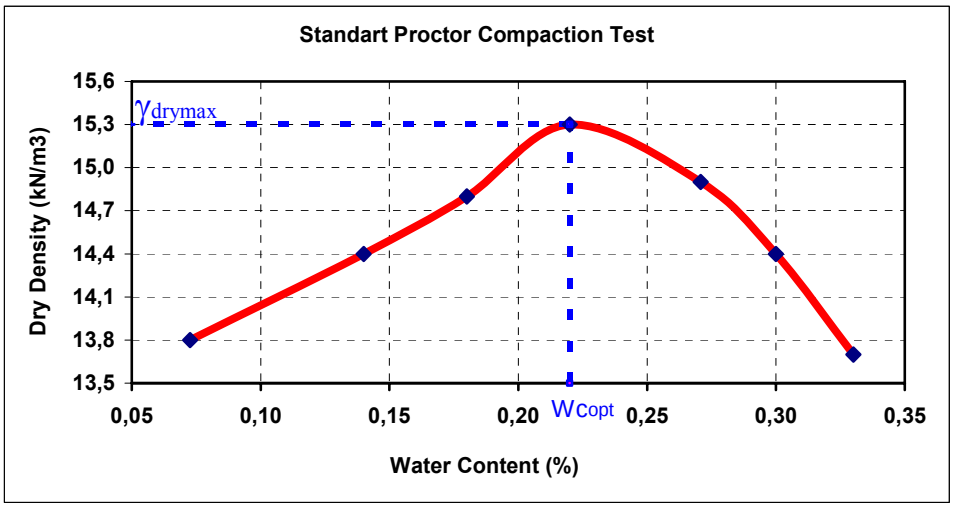

Figure 4.10. Standard Proctor Compaction Test Results

4.4. Shear Strength of Soil

Shear strength parameters are crucial for the slope stability analyses against failures and landslides. When shear stress (τ) in some of the planes exceeds the soil shear strength, the soil cannot resist shear loads greater than its shear strength and fails. Two main shear strength parameters c' and ϕ' generally used to define the failure envelope of a soil sample, which is given by the Mohr-Coulomb equation as;

$$\tau_f = c' + \sigma' \tan \phi' \tag{4.1}$$

This equation can be plotted as shown in Figure 4.11.

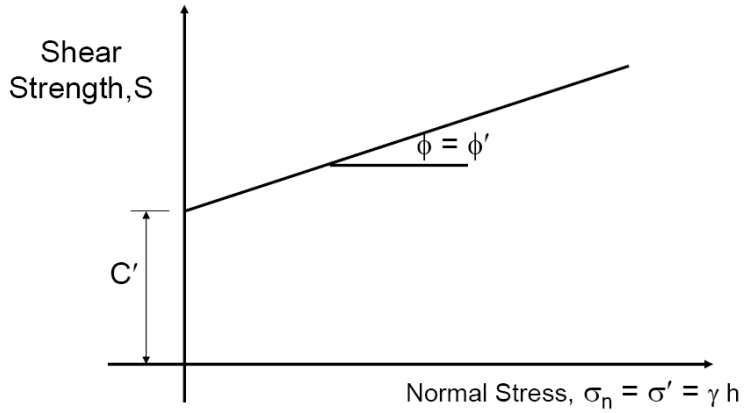

Figure 4.11 Mohr-Coulomb Equation between the Shear Strength and the Normal Stress

Cohesion (in effective stress terms as c') comes from cementation or electrostatic attraction between the soil particles. This component of shear strength is independent of the normal stress on a shear plane. Whereas, Apparent Cohesion comes from the negative pore water pressures or matric suction terms.

Friction is dependent of normal stress on a shear plane. Larger the normal effective stress (σ') larger the shear strength. Cohesionless soils (i.e. sands and gravels) derive their shear strength almost entirely from friction (ϕ). The shear strength of the material can be determined by two tests, direct shear test and triaxial compression test. These two tests are explained below.

4.4.1. Direct Shear Test

The direct shear test (DST) is a strain-controlled test. Strain is the soil sample's unit deformation and the strain rate is the speed of the movement of one part of the soil sample against the other. Strain-controlled means soil sample's allowed deformation (i.e. the total horizontal distance traveled for shearing) is limited. In the DST, a specimen of soil is placed into the 2 halves of a shear box and consolidated in the first stage under an applied normal load is sheared at a certain rate in the second stage

(Figure 4.12). The DST imposes stress conditions on the soil that force the failure plane to occur at a predetermined location (on the plane that separates the two halves of the box). On this plane there are two forces (or stresses) acting to the sample with base area (A). These are; a normal stress (σ_n), due to an applied vertical load P_v and a shearing stress (τ) due to the applied horizontal load P_h. These stresses are simply computed as:

$$\sigma_n = \frac{P_V}{A} \tag{4.2}$$

$$\tau = \frac{P_h}{A} \tag{4.3}$$

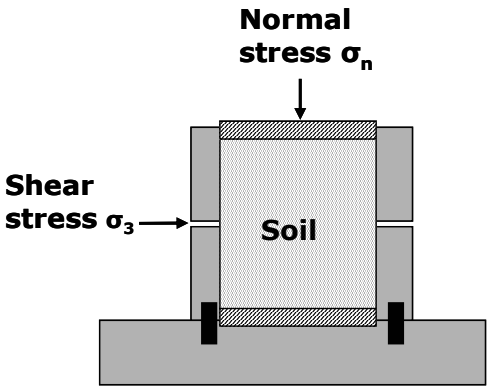

Figure 4.12. Simple Representation of the Direct Shear Test (DST).

The Direct Shear Test (DST) was formerly quite popular, but with the development of the more flexible triaxial test, DST has become less popular in recent years. Its advantages are; inexpensive, fast and simple especially for sands. Figure 4.13 shows laboratory obtained DST results.

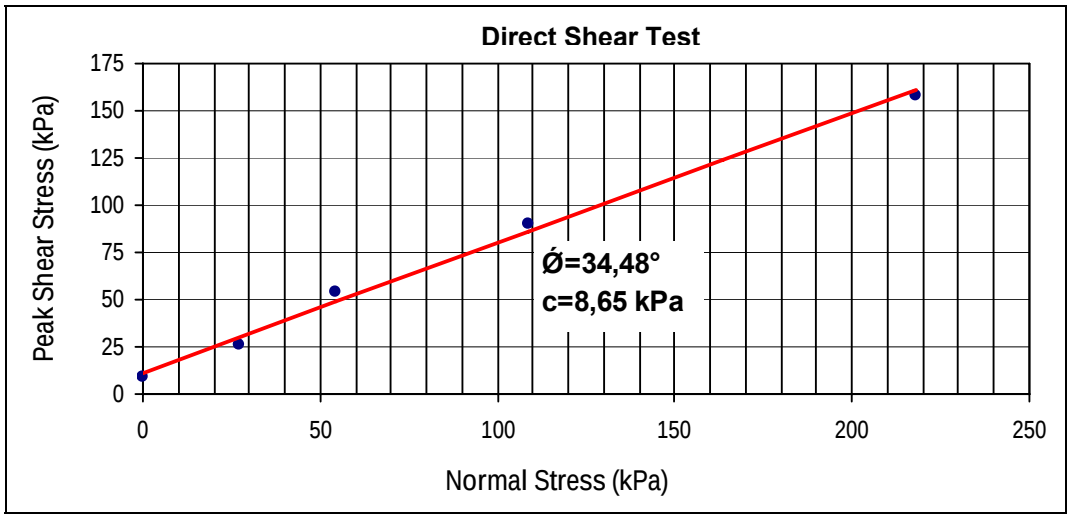

Figure 4.13. Sample Graph of the DST

Figure 4.14. Setting-up the DST

4.4.2. Triaxial Compression Test

During the early history of soil mechanics, the DST was the most popular shear test. Afterwards in 1930, Arthur Casagrande (while at the MIT) began to research on the development of a cylindrical compression test, in an attempt to overcome some of the serious disadvantages of the DST. At the present time this test is commonly called as the triaxial test (Figure 4.15, Figure 4.17).

The triaxial compression test (TCT) is used to measure the shear strength of a soil under controlled drainage conditions. In the conventional triaxial test, a cylindrical specimen of a soil sample encased in a rubber membrane is placed in a triaxial compression chamber (Figure 4.18), which is subjected to a confining fluid pressure and then loaded axially to failure. Connections at the ends of the specimen permit controlled drainage of the pore water from the specimen to occur. The test is called "triaxial" because of the three principal stresses are assumed to be known and are controlled. Prior to shear, the three principal stresses are equal to the chamber fluid pressure. During shear, the major principal stress, σ_1 is equal to the applied axial stress (P/A) plus the chamber pressure, σ_3. The applied axial stress, $\sigma_1' - \sigma_3'$ is termed as the "principal stress difference" or sometimes as the "deviator stress". Obtained TCT (CU) results are given in Figure 4.16.

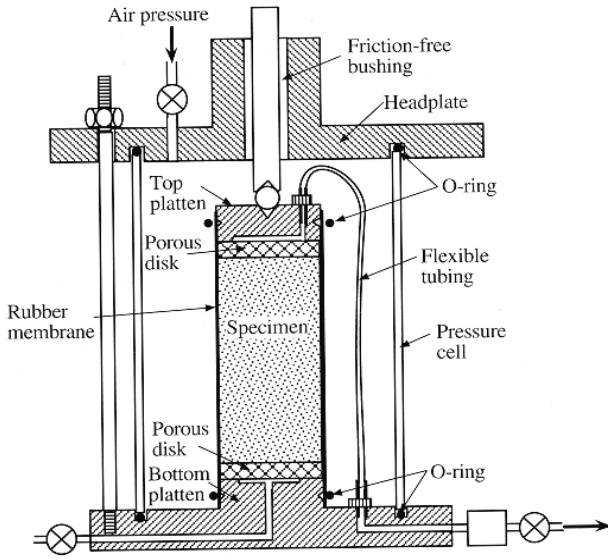

Figure 4.15. Triaxial Compression Test (TCT) Forming Parts

There are 3 types of TCTs:

1. Unconsolidated-Undrained test which is also called the quick test (abbreviations commonly used are UU or Q test). This test is performed with the drain valve closed for all phases of the test. Axial loading is commenced immediately after the chamber pressure σ_3 is stabilized.

2. Consolidated-Undrained test, also termed consolidated-quick test or R test (abbreviated as CU or R). In this test, drainage or consolidation is allowed to take place during the application of the confining pressure σ_3 in the first stage. Loading does not commence, until the sample ceases to drain (or consolidates). The axial load (P) is then applied to the specimen, with no attempt made to control the formation of the excess pore pressures. In this test, the drain valve is closed during the axial loading (shearing) stage and when the excess pore pressures are measured.

3. Consolidated-Drained test, also called as the slow test (abbreviated as CD or S). In this test, the drain valve is left opened during both the consolidation and shearing stages. The load is applied at a slow strain-rate such that particle readjustments in the specimen do not induce any excess pore water pressures (PWP). Since there is no excess PWPs, total stresses will be equal to effective stresses. Provided that the soil sample is saturated after the consolidation stage, the volume change of the sample during the shearing stage can be measured as being equal to the amount of water discharged.

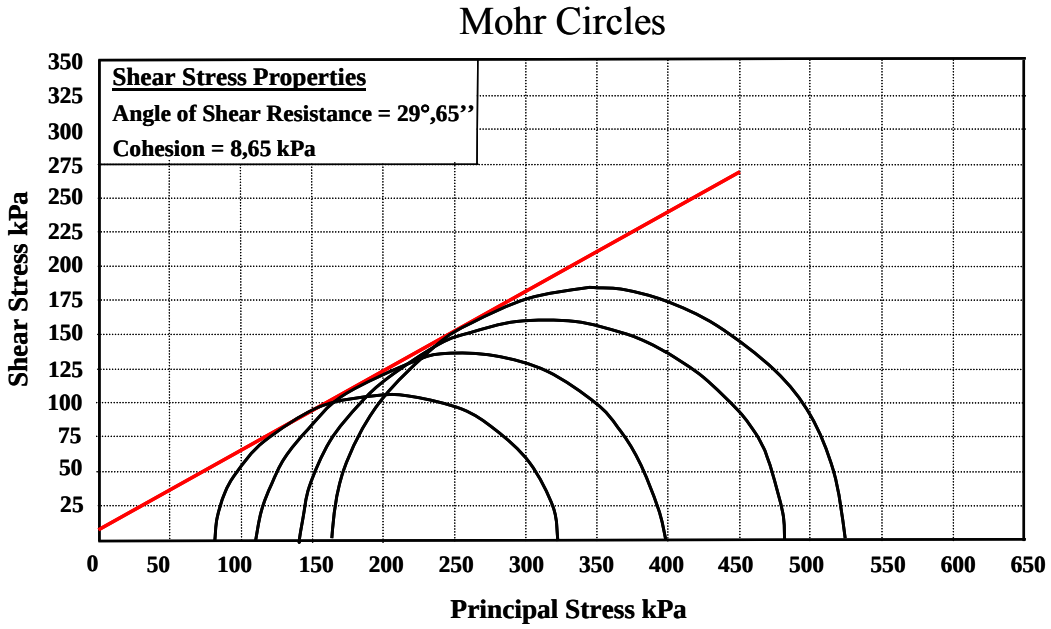

Figure 4.16. Consolidated-Undrained (CU) Triaxial Compression Test Graph

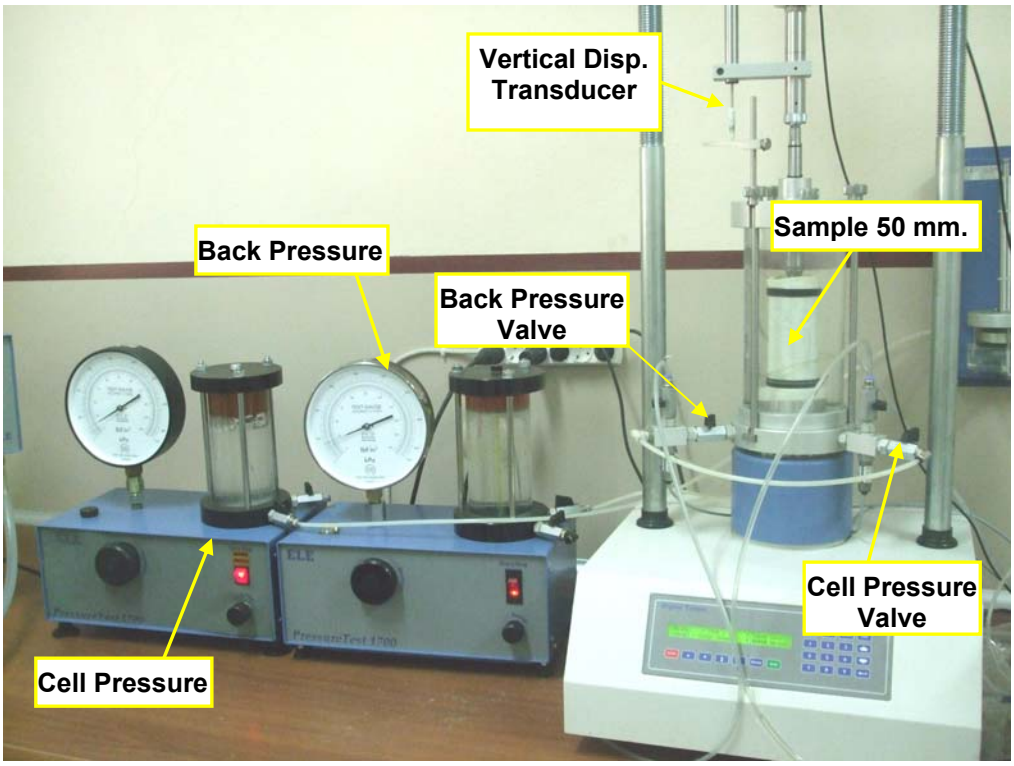

Figure 4.17. Triaxial Compression Test (TCT) Equipment

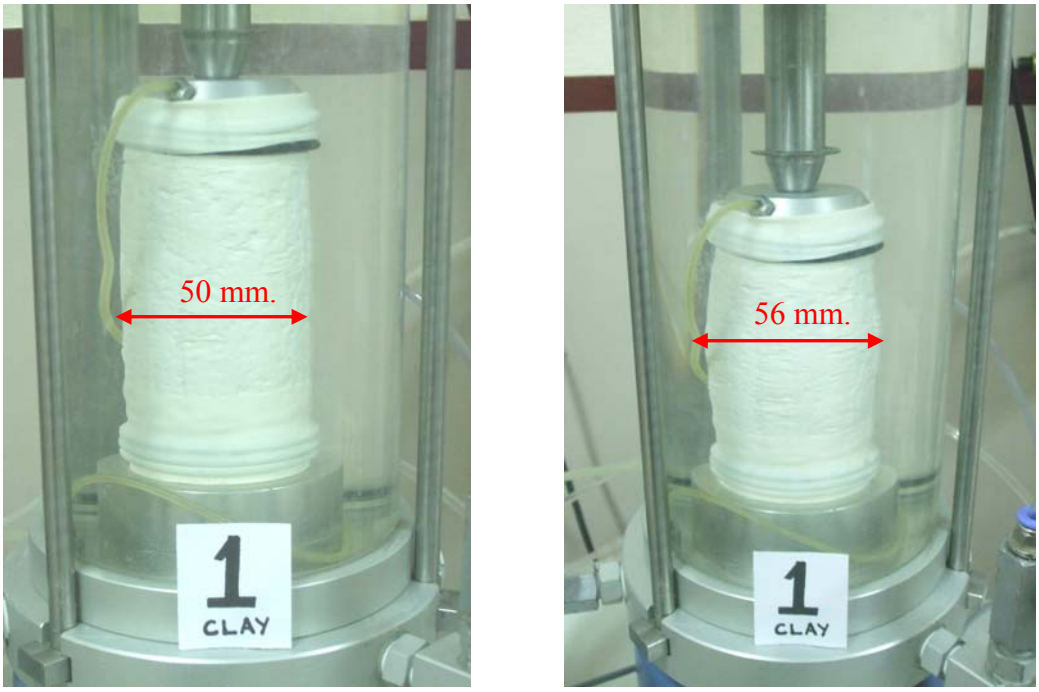

Figure 4.18. Diameter Enlargement at the Middle of the Test Samples (before and after Consolidated Undrained Triaxial Compression Test)

In summary: soil shear strength is one of the most decisive parameters for a soil sample. Without shear strength parameters; neither static calculations, nor dynamic calculations reach the solution. Assigning of the shear strength parameters can be acquired by two different methods. Direct Shear Test is simpler, inexpensive and faster. Triaxial Compression Test is more reliable and technologically newer method. Both of them were conducted for the study described in section 4.4.2 and average results of c'=9 kPa, ϕ'=32º were obtained (Table 4.2).

4.5. Permeability Test

Permeability is a measure of the ease in which water can flow through a soil mass. It is one of the most important geotechnical parameters. However, it is probably the most difficult parameter to determine.

Permeability enters all problems involving the flow of water through soils such as; seepage under dams, expulsion of water from soils under loading, drainage of subgrades, dams and backfills. The strength of a soil is often indirectly controlled by its permeability. The permeability of a soil is dependent upon:

- the size of soil grains
- the properties of pore fluids
- the void ratio of the soil
- the shapes and arrangement of pores
- the degree of saturation

In 1856, a French engineer Darcy proposed that; the flow through soils is laminar, the discharge velocity (v) is proportional to the hydraulic gradient (i), which gives the relationship known as the Darcy's law:

$$v = k\,I \tag{4.4}$$

where; the coefficient of proportionality, k, has been called as the "Darcy's coefficient of permeability", "coefficient of permeability", "permeability", or "hydraulic conductivity". Since I is dimensionless, k has the unit of a velocity. In geotechnical

engineering, *k* is commonly expressed in cm/s (although m/s is the preferred metric unit) and other possible units include m/s, m/day, and mm/hour.

A number of different methods for determining the coefficient of permeability for soils exist, including the in-situ (field) methods and the laboratory methods. In the laboratory, two common tests are generally used to determine this soil property. These two tests are the falling head permeability test and the constant head permeability test. Whichever test is to be used, depends upon the type of soil to be tested. For soils of high permeability (sands and gravels) a constant head test is used. For soils of intermediate to low permeability (clays), a falling head test is used. These tests are explained below.

4.5.1. Falling Head Permeability Test

The falling head test is different in the sense that it does not fix the total head difference across the specimen. Instead, a standpipe is connected to the inflow and the water level in this standpipe is then allowed to drop, as water flows through the specimen (Figure 4.19a-b). This will not work well for coarse-grained soils, because they are so permeable that the head drops too fast to be accurately measured. (AS1289.6.7.2-2001; ASTM D5856)

$$k = \frac{aL}{At} \ln \frac{h_0}{h_1} \tag{4.5}$$

Where,

k	Coefficient of permeability
a	Area of the burette
L	Length of soil column
A	Area of the soil column
h_0	Initial height of water
h_1	Final height of water = $h_0 - \Delta h$
t	Time required to get head drop of Δh

$$k_{20°C} = k_{T°C} \frac{\eta_{T°C}}{\eta_{20°C}} \tag{4.6}$$

Where,

$k_{T°C}$ = measured permeability at the actual water temperature in the lab

$k_{20°C}$ = permeability at the standard temperature of 20° C.

4.5.2. Constant Head Permeability Test

In the constant head test, a constant total head difference is applied to the soil specimen and the resulting quantity of seepage can then be measured. This works very well for coarse-grained soils. But for clays and silts, the quantity of seepage is much too small to be accurately measured. (AS1289.6.7.1-2001; ASTM D2434)

$$k = \frac{VL}{Aht} \tag{4.7}$$

Where,

k	Coefficient of permeability
V	Collected volume of water
L	Length of soil column (13.25 cm)
A	Area of the soil column (31.65 cm^2)
h	Head difference (34.3 cm)
t	Time required to get V volume

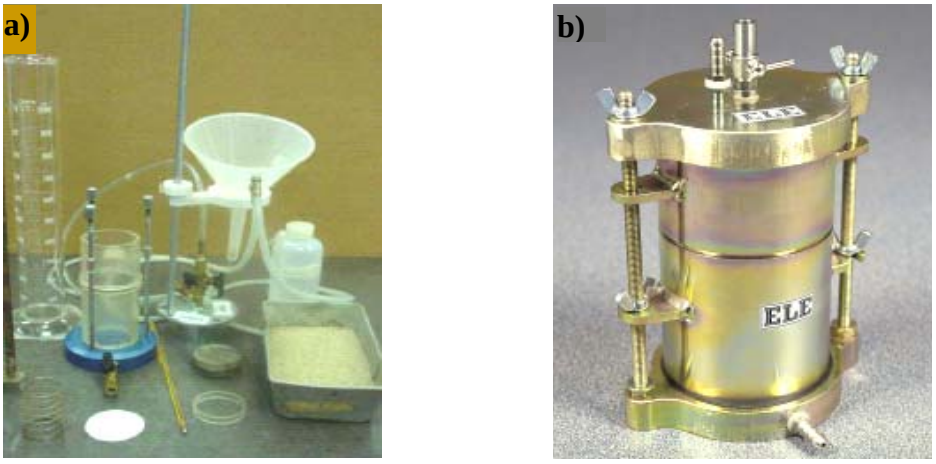

Figure 4.19. a) Falling Head Permeability Test Equipments, b) Soil Mold

Table 4.1. Soil Types, Coefficients of Permeability and Degree of Permeability

Soil	Coeff. of Perm. k (cm/sec)	Degree of Permeability
Gravel	$k>10^{-1}$	Very high
Sandy gravel, clean sand, fine sand	$10^{-1}>k>10^{-3}$	High to medium
Sand, silty sand	$10^{-3}>k>10^{-5}$	Low
Silt, silty clay	$10^{-5}>k>10^{-7}$	Very low
Clay	$k<10^{-7}$	Virtually impermeable

In summary: another important parameter of the soil is permeability, which is defined as soil particle transmission characteristics. In this thesis; falling head permeability test was performed, which is recommended for the fine grained soils. Four permeability molds were filled, then single weight and blow compacted to four different densities, in order to see the effects of density on permeability of a soil. The permeability test results graph is as shown in Figure (4.20).

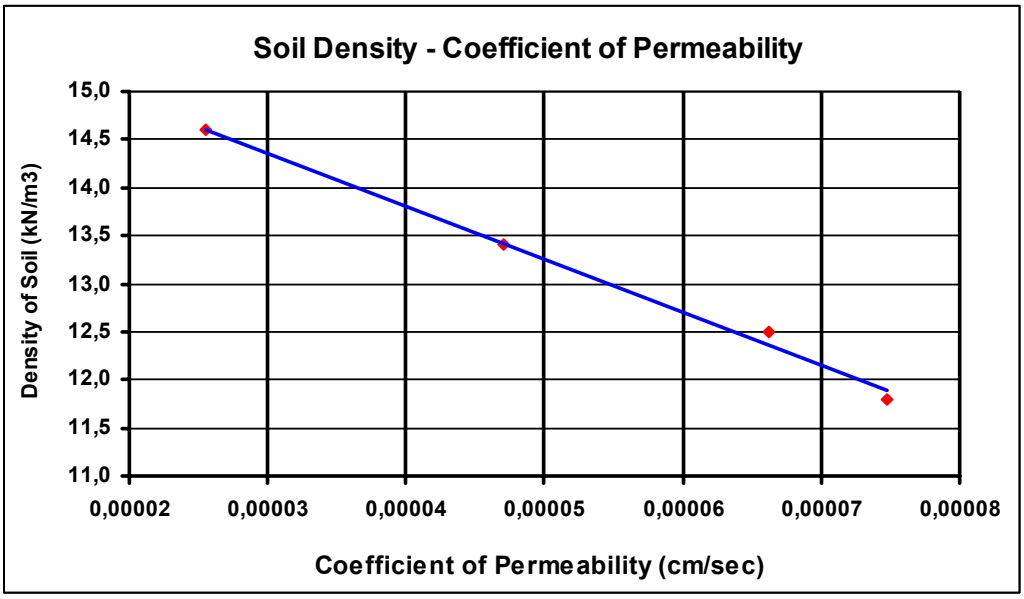

Figure 4.20. Permeability Test Results Graph at 4 Different Densities of the Tested Soil.

4.6. X-Ray Diffraction Test

Rocks, sediments and precipitates are examples of geologic materials that are composed of minerals. Numerous analytical techniques are used to characterize these materials. One of these methods is the X-ray powder diffraction (XRD), which is an instrumental technique used to identify minerals, as well as other crystalline materials.

In many geologic investigations, XRD complements other mineralogical methods, including optical light microscopy, electron microprobe microscopy and scanning electron microscopy. XRD provides the researcher with a fast and reliable tool for routine mineral identification. XRD is particularly useful for identifying fine grained minerals (e.g. clays) and mixtures or intergrowths of such minerals that may not lend themselves to analysis by any other techniques. XRD can provide additional information beyond basic identification. If the sample is a mixture, XRD data can be analyzed to determine the proportion of the different minerals present. Other information obtained can include: the degree of crystallinity of the minerals present, possible deviations of the minerals from their ideal compositions (presence of element substitutions and solid solutions), the structural state of the minerals (which can be used to deduce temperatures and/or pressures of formation) and the degree of hydration for minerals that contain water in their structure. Some mineralogical samples analyzed by the XRD are too fine grained to be identified by optical light microscopy (Figure 4.21). The XRD does not, however, provide a quantitative compositional data to be obtained by the electron microprobe or some textural and qualitative compositional data obtained by the scanning electron microscope.

First essential investigations about the XRD was developed by English physicists: Sir W.H. Bragg and his son Sir W.L. Bragg in 1913. They studied to explain why the cleavage faces of crystals appear to reflect X-ray beams at certain angles of incidence (θ). In the Bragg's Equation (4.8), the variable, *d* is the distance between atomic layers in a crystal and the variable lambda, λ is the wavelength of the incident X-ray beam, while, n is an integer. This observation is an example of X-ray wave interference, commonly known as the XRD and it was a direct evidence for the periodic atomic structure of crystals postulated for several centuries.

$$n\lambda=2d\sin\theta \qquad (4.8)$$

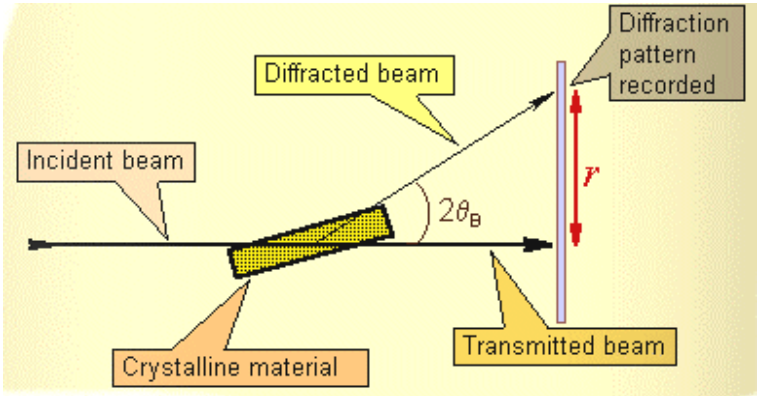

Figure 4.21. Simple representation of how the X-Ray Diffraction (XRD) system works (Source: Molecular Expressions 2009)

Numerous comprehensive data can be obtained at the end of the XRD Test such as:

- Measure the average spacing between layers or rows of atoms,
- Determine the orientation of a single crystal or grain,
- Find the crystal structure of an unknown material,
- Measure the size, shape and internal stress of small crystalline regions.

X-Ray diffraction analysis (Figure 4.22) of soil samples obtained from İzmir Institute of Technology's campus area was carried out at the Materials Research Center (MAM) Laboratory in the IYTE.

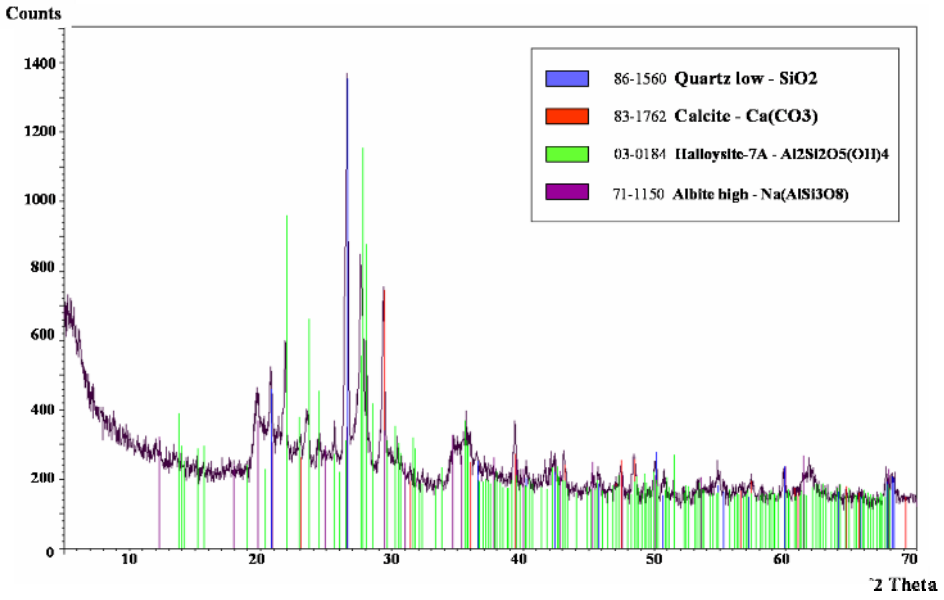

Figure 4.22. X-Ray Diffractogram of the Tested Soil Sample from the IYTE Campus.

4.7. Analysis of Scanning Electron Microscope

Scanning Electron Microscope (SEM) is a convenient and useful tool for investigation of soil particle analysis. Although the first SEM debuted in 1938 (by: Von Ardenne), with the first commercial instruments appearing around 1965. The reason of this delay, SEM was hidden in the research centers of major corporations, universities and government agencies, like the Department of Justice. The SEM, makes it possible for the quick resolution of tough analytical problems effectively, timely and economically. The SEM permits the observation of materials to be made in macro and submicron ranges.

The SEM generates high energy electrons and focuses them on a specimen. The electron beam is scanned all over the surface of the specimen, in a motion similar to a television camera to produce a rasterized digital image. Electrons are speeded up in a vacuum, until their wavelength is extremely short to the extend that it's only one hundred-thousandth of a white light. Beams of these fast-moving electrons are focused on a sample, are absorbed or scattered by the specimen and electronically processed into an image. Most electron microscopes available today can image down to about 10 angstroms-A^o, (which is 0.001 microns).

Topography: The surface features of an object or "how it looks", its texture. It provides a direct relationship between these features and materials properties.

Morphology: The shape and size of the particles making up the object. It provides a direct relationship between these structures and materials properties.

Composition: The elements and compounds that the object is composed of, as well as the relative amounts of them. It gives a direct relationship between the composition and properties of materials.

Crystallographic Information: How the atoms are arranged in the object. It gives a direct relationship between the arrangements and properties of materials.

SEM analysis was conducted at the Material Research Laboratories (MAM) of IYTE. Obtained images from the SEM analyses showing shape of the particles mostly elongated, as shown in Figures 4.23a-d.

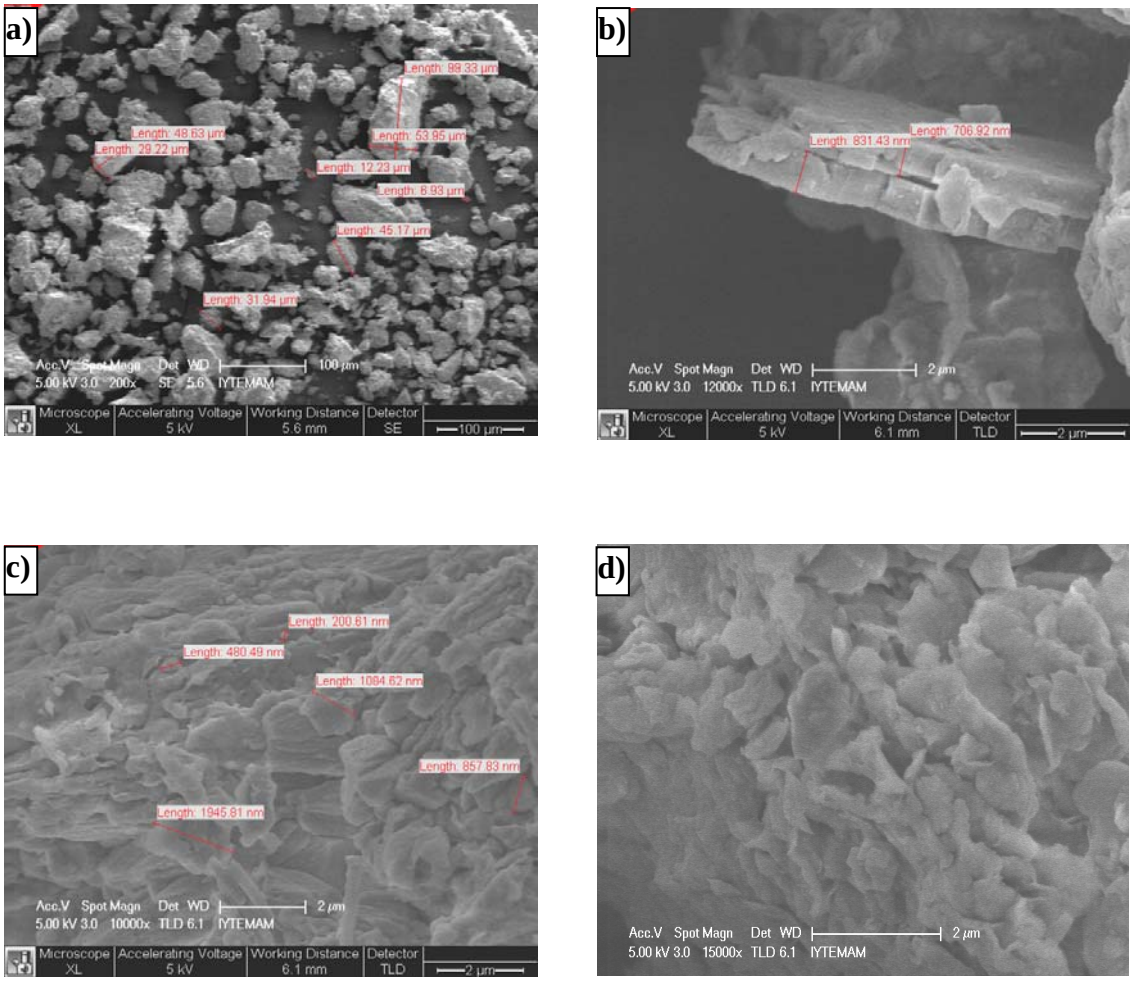

Figure 4.23. a-d: Overviews of the soil sample, for fraction smaller than 0,075mm

In summary: advancement of the technology provides, availability of various research possibilities for the soil testing in many respects. XRD (X-Ray diffraction) and SEM (Scanning Electron Microscope) are the latest technological and convenient methods. Nanomicron size particle analysis can be done by using the SEM. The additionally minerals that make up the soil sample can be determined by XRD.

4.8. Summary of the Laboratory Tests

Basic soil mechanics laboratory experiments were performed for this study and given in this thesis. In this part, completed soil mechanics tests were summarized briefly as below:

In addition to the mentioned tests, one dimensional (uniaxial) compression and relative density tests were completed for this study. Results are summarized as shown in Table 4.2.

Table 4.2. Summary of the Completed Tests Results

No	Experiment Name	Used Method	ASTM-D	Value	Unit
1	Particle Size Analysis	Dry Sieve Analysis	ASTM-D 1140-00	Look at Figure 4.2.	(%)
2	Particle Size Analysis	Wet Sieve Analysis	ASTM-D 422-63	Look at Figure 4.2	(%)
3	The Laboratory Compaction Test	Standard Proctor Method	ASTM-D 698-00	W_{opt}=22 γ_{drymax}=15,3	(%) kN/m^3
4	Specific Gravity of Soil Solids	Pycnometer Method	ASTM-D 854-02	2,61	Kg/cm^3
5	Determination of Water (Moisture) Content	Oven Dried Method	ASTM-D 2216-98	(%7) in laboratory conditions	(%)
6	Classification of Soil	USCS	ASTM-D 2487-00	CL & ML	-
7	X-Ray Radiography of Soil Samples	Phillips X'Pert Pro	ASTM-D 4452-85	Look at Figure 4.21.	(Counts)
8	Triaxial Compression Test	Consolidated Undrained (CU)	ASTM-D 4767-04	c=9 ϕ=30	kPa (°)
9	Direct Shear Test	Consolidated Drained (CD)	ASTM-D 3080-00	c=9 ϕ=34	kPa (°)
10	Liquid Limit Test	Casagrande Method	ASTM-D 4318-00	47	(%)
11	Plastic Limit Test	Hand Method	ASTM-D 4318-00	32	(%)
12	Maximum Index Density	Vibration Table Method	ASTM-D 4253-00	0,77	(%)
13	Scanning Electron Microscope (SEM)	Phillips XL-30S FEG	-	Look at Figure 4.22.	(μ)

4.9. Slope Model Preparation Procedures

Soils used for the model slope experiments were obtained from the İzmir Institute of Technology campus area. Lots of comprehensive soil mechanic experiments were done to obtain reliable information about the engineering properties of the tested soils. For the determination of the soil type, the unified soil classification system (USCS) procedures were used. Atterberg limit tests (ASTM D4318) run on the soil type used resulted in a liquid limit (LL) of 47 and a plasticity index (PI) of 15, giving PL of 32. Grain size analysis indicated that the soil had approximately 10% clay size particles by dry weight. By using plasticity chart of the USCS classification, soil is defined a ML type, low plasticity silt. The silty clay was chosen as a compromise between cohesive and cohesionless soils. Clean granular soils would produce extremely shallow failures, while cohesive clayey soils would produce much deeper slides.

4.9.1. Initial Soil Conditions

Before the testing began, lots of field research was made so as to find a convenient and preferred soil type to be tested. Soil is received from the source by an excavator. The first sieving progress was completed by using large scale sieve with dimensions of 1000mm height and 1500mm width. At the end of the first sieving, the maximum grain size of the soil was 5 mm. Afterwards, the soil was taken to the İYTE Soil Mechanics Laboratory and natural water content (w_{Cn}) was defined as 6-7 % (by weight) of the dry weight.

Another significant variable to be used in this study is the initial water content of the soil. Soil behavior is highly depend on its water content (w_c). In order to examine the effect of the water content on slope stability, two different initial water contents were taken into account.

The assessment, about which initial water content value was to be used, was depended upon the optimum moisture content of the soil, as found from the Standard Proctor Test (ASTM D 698). Although, the compaction test's curve is expected to be symmetric with respect to the optimum moisture content point, it was not due to many discrepancies in the soil characteristics. Right side of the peak point of the curve is called wet side which includes higher water contents than the optimum moisture content

having softer consistency and left side of the symmetry axis has lower water contents than the optimum with stiffer consistency. To define how these two different initial water content parameters effects the stability of soil and infiltration process, the tests are conducted at 14% (on the dry side of the optimum) and at 30% (on the wet side of the optimum) initial water contents (Figure 4.24).

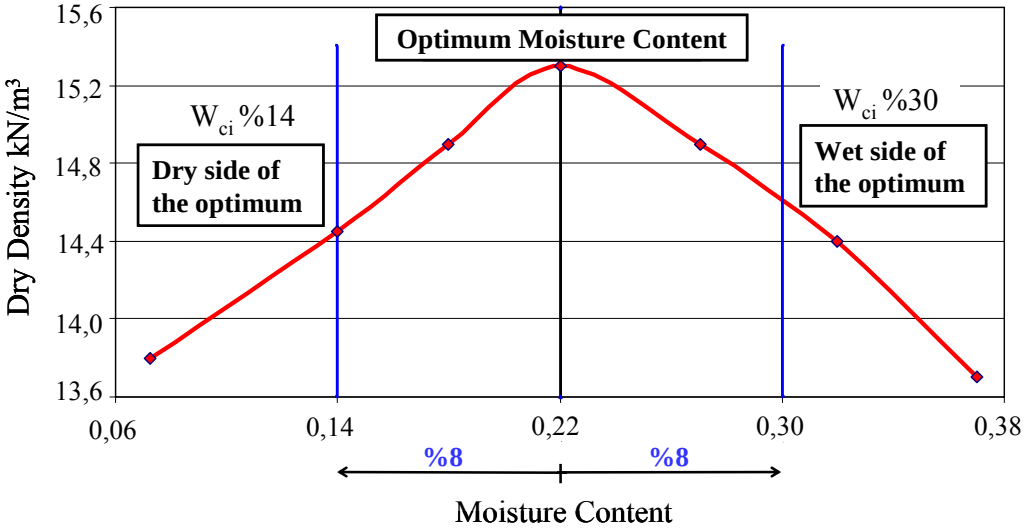

Figure 4.24. Proctor Test Result Showing Dry Density on the Wet and Dry Side of the Optimum Moisture Content

4.9.2. Compaction Procedure

Soil density is another variable affecting soil slope stability. Compaction is the process by which the soil particles are closely packed by mechanical means, thus increasing their dry density. Dry unit weight here is defined as the ratio of the weight of the soil particles to the total volume. The soils are made up of solid grains with voids filled with air and water. Compaction only decreases the air fraction. It has no affect on the solid volume and on the water content.

Shear strength, compressibility and permeability are fundamental engineering characteristics of a soil. Compaction of the soil generally increases its shear strength, decreases its compressibility and decreases its permeability (Figure 4.27). An important characteristic of the cohesive soils is that compaction process, improves soil's shear strength, while compressibility decreases. Such characteristics follow the principles stated by R.R. Proctor in 1933.

Two different soil densities are used in tests. In order to obtain a uniform and homogeneous soil mass, a specific compaction method, based on the Standard Proctor Test was used. Figure 4.25 shows Standard Proctor test details.

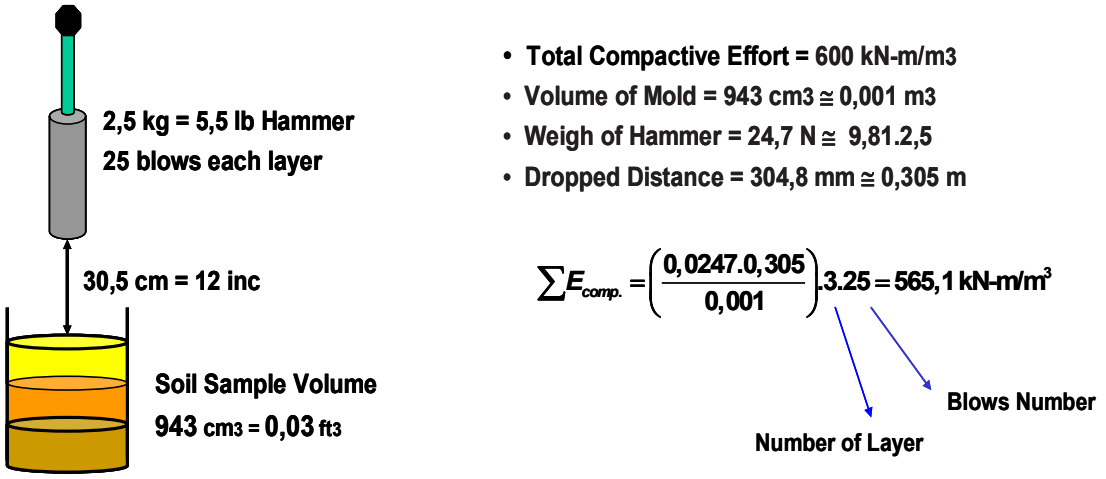

Figure 4.25. Standard Proctor Test Details

In the Standard Proctor Test, sample is subjected to a compactive effort of 12400 ft-lbf/ft3 (600 kN-m/m3). Compaction of the soil sample is achieved by using three layers, each with 25 hammer blows. To find the total compaction effort, the energy which provided from a single stroke of hammer is first calculated. As indicated in the ASTM D 698, (Standard Compaction Method) the volume of the mold is 943 cm^3, which equals to approximately 0,001 m^3. In view of this information, by using the standard proctor test's hammer, a rigid plate with dimensions of 500mm, 500mm and 20mm was used. The total volume of the soil in the container box is divided into six equal parts to obtain a uniform compression performance. Similar to the standard proctor test procedure, the soil is placed in the soil container in three layers and compacted by 25 blows per layer. Figure 4.26 shows the details of the compaction layer dimensions.

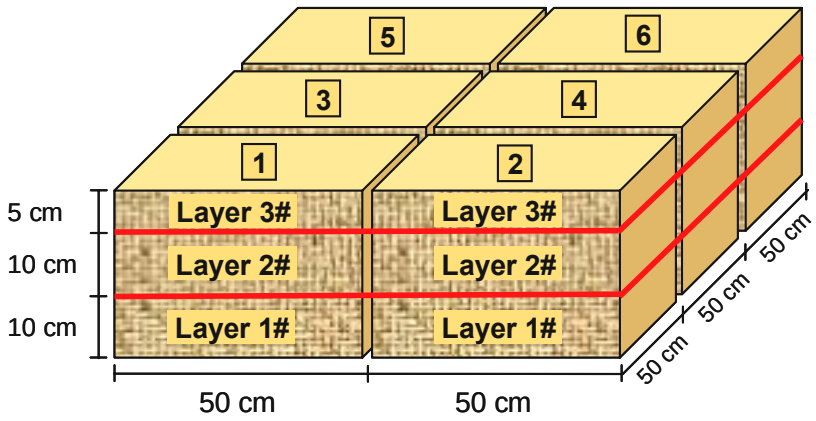

Figure 4.26. Compaction Layer Dimensions

The first layer is loaded and spread with shovel then trowel is used to provide flat surface for compression plate. Rigid plate (50x50cm) is placed on the smooth surface and compression process is started by hitting with the Standard Proctor hammer (Figure 4.28). To obtain two different soil densities, two different number of strokes of 10 and 25 blows per layer were used. Until the compression process is finished for a single soil layer, rigid plate has been replaced six times. To capture the uniformity in the experiments, it is important that the same procedure is used. The first and the second layers of each test consist of same weight of soil (2-kN). On the contrary, the third layer's weight could be different from the other two by about ± 30 kg, depending on the soil settlement and agglomeration.

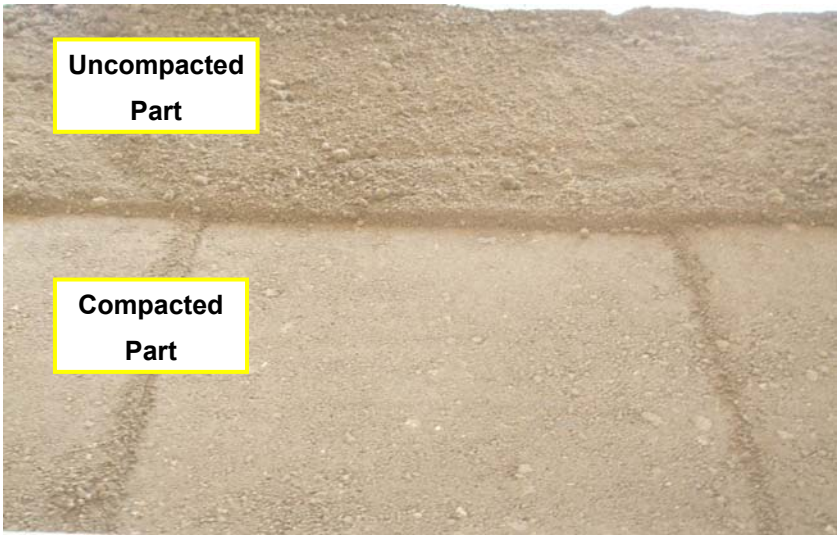

Figure 4.27. Obvious Differences between the Compacted and Uncompacted Soils

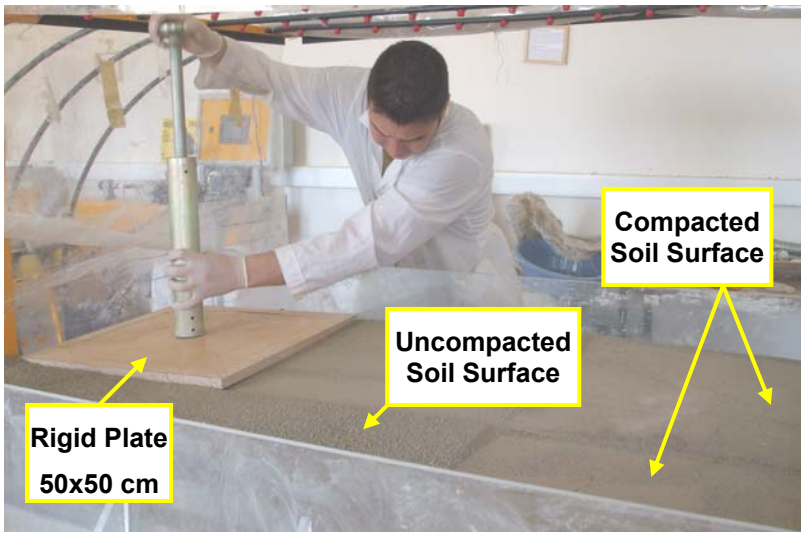

Figure 4.28. A View from the Compaction Process

4.9.3. Artificial Rainfall Process

After the slope construction process is completed, main water storage tank is filled. Runoff collector equipment and graded storage bins are placed for use. Initial water height is read from the indicator. Main water valves are opened, hoses are controlled, system is checked for any leakage and nozzles' directions are examined.

The test is completed when the amounts of pumping water reaches 400 lt. This process is complemented between 20 to 30 minutes. During the experiments, a lot of data should be noted at the same time, in order to determine soil movements such as; displacements, overturning, sliding and collapsing, while the digital camera keeps recording during the experiment.

4.9.4. Undisturbed Soil Sampling

Once the artificial rainfall process stops after using 400 lt. of total water, undisturbed soil samples are taken from the tested slope model. This undisturbed soil samples are used for the determination of the water content profile, wetting band depth and the degree of saturation profile.

Three different undisturbed samples are taken from the middle of the short side of the model slope and it should be noted that undisturbed samples are taken from the

equivalent heights. Otherwise, water contents of the samples may be incompatible with their true depths.

Figure 4.29. Deformed Soil Surface and Sampler in Place for Sampling

To minimize the side friction effect and to remove the soil in the sampler easily, exterior and interior surface of the sampler was silicone greased. Sampler can be inserted easily into soft soil by applying a driving force. Sampler is pushed upto the base of the soil container, then sampler's surrounding is excavated carefully and removed from the soil container (Figure 4.29). Sampler taken from the soil container is immediately weighted. Lost soil's depth at the surface is determined by a measurement at the top of the sampler. At the beginning of the experiment, the initial soil height is constant, which is 25 cm. But at the end of the experiment, soil height may reduce, due to lost soil by surface runoff or failure taking place. Afterwards, the Sampler is placed on the glass plate. By using sample extractor produced from wood with its diameter is equal to the internal diameter of the sampler, tested soil is cut into 3 cm high pieces of subsamples and each piece is weighted so as to define its water content and the degree of saturation. The sampler and sampler extractor is given in Figure 4.30. Afterwards, the depth vs. water content and the depth vs. the degree of saturation graphs are drawn Figure 5.26-28.

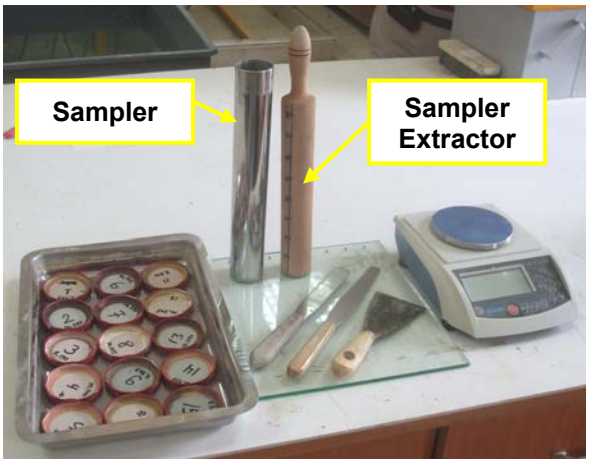

Figure 4.30. Sampling Equipment

The volume of each specimen is almost equal having 3cm heights and 4.8cm diameters, but their weight is different from each other, as a result of different water contents, depending on infiltration and wetting front band depths. The view of the 3cm high soil sample is shown in Figure 4.31. Because, at the beginning of each experiment the soil is in unsaturated condition, but with the rain water infiltration, water content and unit weight of soil will increase.

During the sampling process, the soil should be as low disturbed as possible and all these applications must be conducted as soon as possible. Otherwise, soil may lose water and inaccurate results can be obtained.

Figure 4.31. A View from how 3cm High Soil Subsample is Obtained

4.9.5. The Effect of Fine Grained Soil

Various soil characteristics may contribute to decrease in the shear strength of soils, which may result in occurrence of landslides. Soils with high clay content tend to decrease soil strength because of two primary characteristics inherent to the clay mineral. Firstly, clay particles are very small, less than 0,002 mm in size and have a large specific surface area. This large surface area 1000 times the surface area of the same mass of sand-sized particles, meaning that clays have a much greater capacity for absorbing water (Brady & Weil 2002). Surface area makes a difference in the absorption capacity of a particle, because a larger surface area means far more surface(s) to which water and other materials may adhere (Figure 4.32). Increased water holding capacity of a soil often means eventual liquefaction of the soil and movement of soil material down the slope.

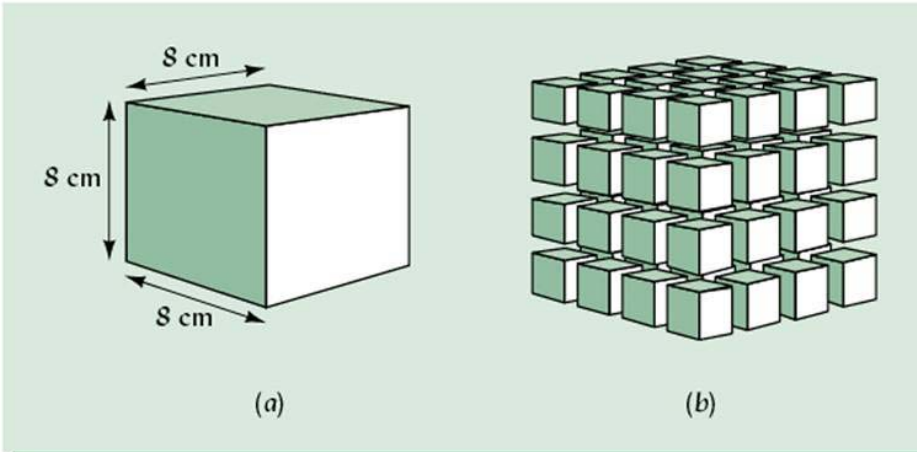

Figure 4.32. Illustration Showing Surface(s) Available for Adherence of Particles (a) with a Small Surface Area (b) vs. Large Surface Area (Source: Brady and Weil 2005)

Secondly, some clays have extensive internal surface area in the interlayers between their crystal units to which water can adhere (Brady and Weil 2005). The 2:1 silicate to clay minerals ratio is characterized by one octahedral sheet between two tetrahedral sheets (Brady and Weil 2005). Water is greatly attracted to the spaces between the layers (interlayer spaces) and adsorption of water between the crystal layers can cause layers to move apart and create extensive internal surface areas (Brady and Weil 2005, Figure 4.32). 2:1 expandable clays with interlayer spaces, including the

smectite group (e.g. the montmorillonites and the vermiculites), have abundant internal surface areas, in addition to a large external surface areas. The phenomenon of adsorption of interlayer water brings about high degrees of shrinking and swelling, plasticity, sitickiness and soil movement, as occurring in landslides. Additionally, 1:1 silicate clay minerals, such as; kaolinites, have been shown experimentally to exhibit much greater strengths than the 2:1 layer silicates, such as; illites and montmorillonites (Olson 1974).

Clay mineralogy of landslide soils is commonly studied in geotechnical investigations and the presence of expandable 2:1 silicate clays in soils on landslides is well documented (Matsukura and Mizuno 1986, Chleborad, et al. 1996, Teoman, et al. 2004, Bhandary, et al. 2005, Fall and Sarr 2007). The presence of these clays has been linked to decreases in soil strength. Shear strength values have been experimentally shown to decrease for slope materials with a high percentage (60%+) of smectite.

CHAPTER 5

EXPERIMENTAL SET-UP AND RESULTS

5.1. Introduction

Although, there have been many methods of stability analyses, almost all of them have some deficiency. Especially when the natural factors are involved, such as; rainfall infiltration, freezing, melting, numerical methods can not meet expectations. The reason of this shortcoming is that it is difficult to clarify precisely the effect of rainfall in producing shallow landslide and debris flow activity, because rainfall alone influences slope stability indirectly.

In order to overcome this uncertainty, one tool used by engineers and researchers to generate the needed data is to use modelling, which can save time and money. Because modelling provides the ability to quickly and efficiently analyze or simulate possible multiple design scenarios over long periods of time and may compare the results, the best design for a particular soil and climatic conditions can be determined.

In this chapter, development of the Slope-Water Interaction Modeling System (SWIMS) by IYTE and how the system functions is described in five parts. In the introduction part, development of the SWIMS is examined. Equipment parts of the SWIMS (water pump, water storage tank, sprinkler hoses and nozzles, soil container, infiltration bands and discharge tanks) are described in the second section. In the third part, information is given about the engineering properties of the tested soil , reasons for using the fine grained soils and the construction process of the testing slope, including the compaction procedure, precautions taken to reduce the side friction and obtaining undisturbed soil samples from SWIMS. In the fourth section, the experimental data accumulation and observations made during and after the experiments are explained. Finally in the fifth section, experimental results, graphs, discussion and conclusion are provided.

5.2. Soil -Water Interaction Modeling System

As one of the purposes of this postgraduate research study, the needed experimental equipment, soil-water interaction modeling system (SWIMS) was to be designed. This task was achieved by the Department of Civil Engineering-Geotechnical Division members and the project funding was provided under the Scientific Research Program of the IYTE. There are 5 main parts of the equipment, as described below:

5.2.1. Soil Container

Dimensions of the Soil Container part of the modeling system is a rectangular box with dimensions of 2m in length, 1.5m in width, 0.4m in height. Top view of the soil container is shown in Figure 5.1. All 4 sides are made of 8mm thick plexiglass to retain the earth pressure, while for the bottom surface 5mm thick and 100mm wide metal plates (having 50 mm wide permeable bands of very fine mesh sieving strips, placed at 100mm intervals, so that no soil, but only the percolated infiltrating water can pass thru it to the bottom tank) was used. Soil Container has been designed to have a maximum of 20 kN carrying capacity.

Lateral surface of the soil container was designed from plexiglass, enabling observations of displacement and infiltration ratio to be made during the experiment. Another important reason of using plexiglass is minimizing the friction along the sidewalls of the soil container, so that plane strain conditions are closely approximated with low friction surface along the sides of the container.

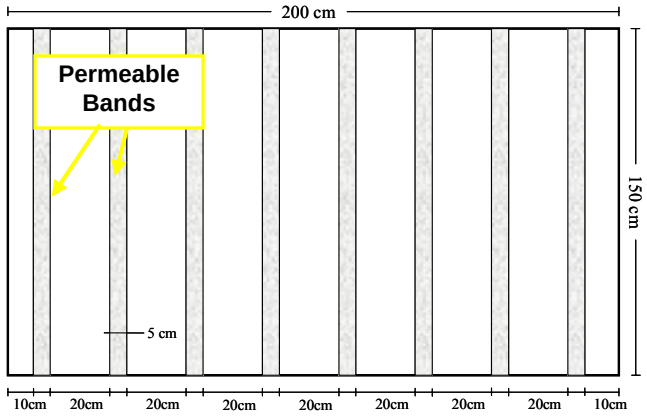

Figure 5.1. Top View of the Soil Container

Chen and Holtz (2004) evaluated a number of cases and found out that the least interface friction measured in a scaled model test came from the use of a plastic backing with layers of plastic sheeting lying overtop. An important problem of this enormously heavy system was to design a sustainable support frame, without causing any overturning or collapse. Soil container was carried by two rectangular sectioned steel box profiles with dimension of 60mm x 40mm and a wall thickness of 4 mm. In addition to these box profiles, two suplementary support elements made of stainless steel with height adjustable features are attached to the support frame. General view of the SWIMS is presented in Figure 5.2.

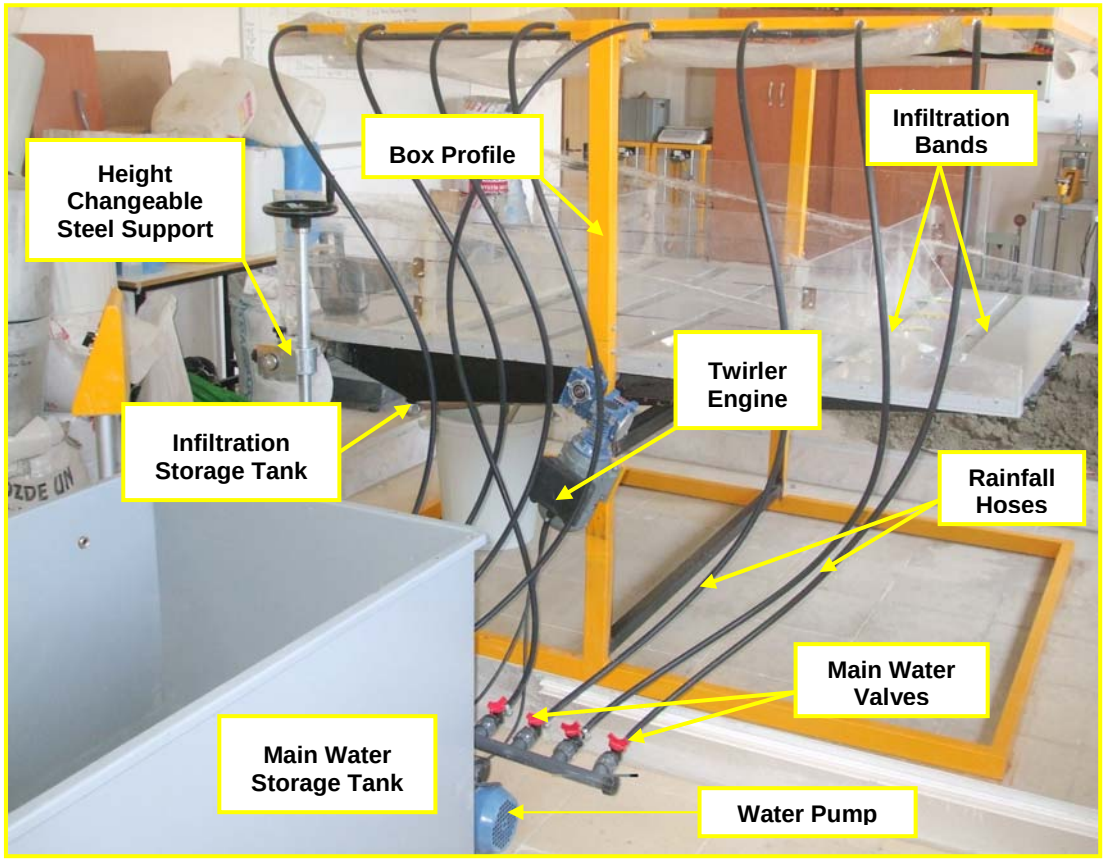

Figure 5.2. General View of the Soil Water Interaction Modeling System (SWIMS)

5.2.2. Artificial Rainwater System

Rainfall was artificially produced using a specially-designed sprinkler system. The artificial rainfall system was used to produce uniform and adjustable (intensity, duration) rainfall simulation. The artificial rainfall system consists of the main water storage tank (described below), water pump, main water supply valves, rainfall hoses and sprinklers (Figure 5.2).

5.2.2.1 Main Water Storage Tank

In order to determine the amounts of the infiltrated water to be supplied from the artificial rainwater system, a Water Storage Container (a rectangular tank made of sheet metal and can hold upto about 800 liters of water) was also manufactured to provide water supply (Figure 5.3). Thus intensity and volume of the generated rainfall through fine spray nozzles connected to the water pump and water container via rubber pipes could be measured. Infiltration water is discharged from the soil storage tank with the aid of discharge hose to the graduated plastic storage bins for volume measurement. The main water storage tank was constructed from metal plates which has a wall thickness of 3mm. Graduate indicator is used to determine the amounts of total water and consumed water during tests.

Figure 5.3. Lateral View of the Main Water Storage Tank

5.2.2.2. Water Pump

Task of the water pump (Figure 5.4) is transport water from the main storage water tank to soil container. For this job, “Best” named water pump having a model no. PR100, manufactured by the Best Science and Technology Co. was used. Capacity of the pumping was 45lt/hr. and its power rating is 1HP and 0,75 Kw. Maximum height of the water to pump is 74 m. Despite the pump’s modest capacity, it was adequate for this work.

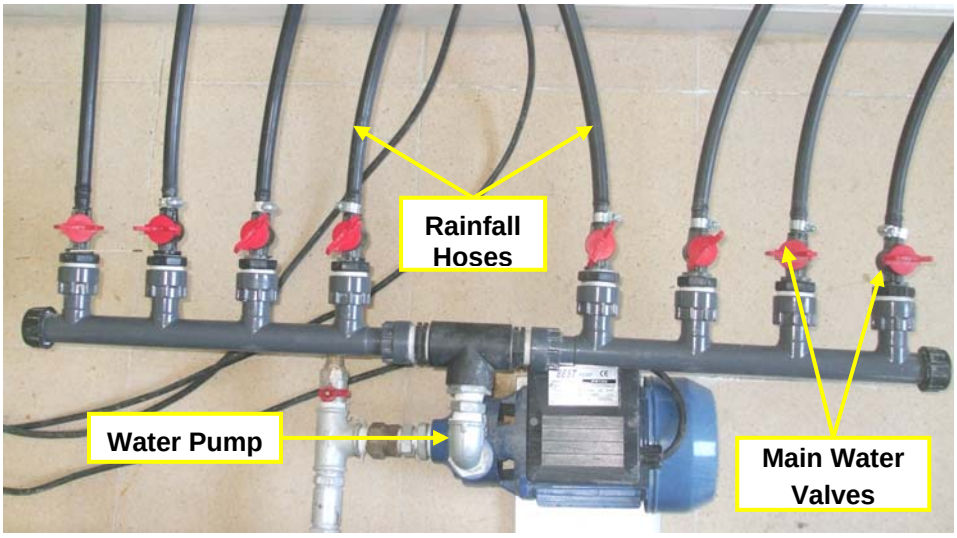

Figure 5.4. Water Pump, Main Water Valves and Rainfall Hoses

5.2.2.3. Main Water Supply Valves

To obtain equal and homogeneous intensity of rainfall, main water supply valves (Figure 5.4) were used. Before the experiment started, uniform rainfall intensity giving ability of each nozzle was controlled. If the nozzle gives nonuniform rainfall intensity, this problem was solved by using screw-valves. To prevent possible water leakage between the water pump and the valves system, junction points should be controlled. In the event of a leakage, water leak was prevented by using a teflon tape.

5.2.2.4. Rainfall Hoses and Sprinklers

The most fundamental task of the artificial rainfall system was undertaken by hoses and sprinklers. The system was constructed with 1 cm diameter PVC pipe and the simple frame to hold the sprinklers above the soil container. Sprinkler frame has a 8 rows and each row has a 12 nozzles (Figure 5.4).

5.2.3. Infiltration Bands and the Discharge System

The construction aim of the SWIMS is to investigate the effects of rainfall infiltration on slope stability as contributed by decreases in the matric suction, increases in the pore water pressures and in reducing the shear strength. As a result of these conditions, large displacements can take place and some shallow landslides can be observed.

Rainwater starts to infiltrate by effects of the gravity and the capillary forces. As the rainwater infiltrates through the soil layer and reaches to the steel bottom plate, fine-meshed percolation bands prevent soils, but let water to pass through, thus enabling rainwater to reach to the infiltration water tank, placed under the soil container. Gathered percolated water in the infiltration storage tank is discharged to the graduated plastic bins placed nearby, with the help of 2 numbers of 2m long an 30mm diameter discharge hoses. Another important part of the SWIMS is the surface runoff water discharge system, where the quantity of the surface runoff water could be masured. When the rainwater reachs to the soil surface, part of the rainfall starts to infiltrate into soil and the other part flows down the slope as the surface runoff. If the slope angle is steep, surface runoff can reach high speeds, causing great deformations on the slope surface. To determine of how much rainwater starts to flow on the slope surface, runoff collector is used. Surface water first reaches to the runoff collector and afterwards is discharged by using the discharge hoses. Amounts of runnoff water can be measured using the graduated storage bins made of plastic. Filled container and drainage equipments are shown in (Figure 5.5).

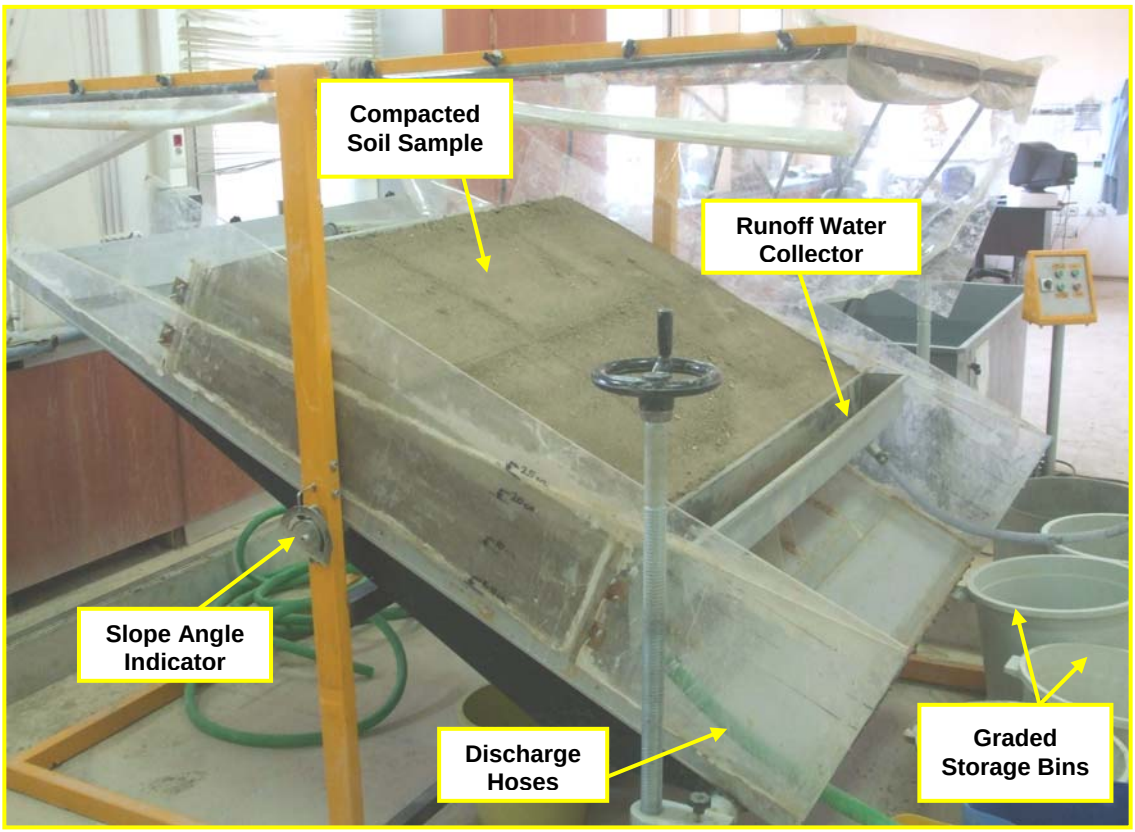

Figure 5.5. Filled Soil Container and Drainage Equipments

5.2.4. Determination of the Slope Angle

In order to investigate effects of different slope angles on the slope stability, slop angles should be measured precisely. Sloping mechanism is provided by two equipments. One of them is the twirler engine, which is a mechanical motor providing 2 HP rotation force and the other is the calibrated slope scale. Due to the great weight of the soil and its steel container, setting the soil filled container for testing is significant but difficult problem. Fixity of the slope angle is provided by the screw type stainless steel supports.

5.3. Main Experiments

A total of 12 SWIMS tests were conducted to model the failure behavior of the slopes with two different moisture contents, three different slope angles and two different soil densities.

In this study, two different types of soils were used to build the slope models. One of the main soil is fine grained cohesive soil which consists of 30% fine sand, 45% silt and 25% clay (Type 1 soil). Second one is a mixture, which consists of 90% type 1 soil and 10% coarse sand. Second soil type is created so as to inspect better the effect of the coarse material on the soil infiltration processes.

Table 5.1 summarizes the general characteristics of the model slopes. Most of these model tests were performed early in the testing program to evaluate the model device's performance and to develop suitable procedures. The following sections describe each of these tests in more detail.

Table 5.1. General Characteristics of Model Slopes

Test No	Angle of Slope	Number of Blows	Initial Water Content w_{ci}	Soil Type	Test Order
1	15º	10 blows/layer	14 %	CL - ML	1
2			30 %	CL - ML	3
3		25 blows/layer	14 %	CL - ML	2
4			30 %	CL - ML	8
5	25º	10 blows/layer	14 %	CL - ML	9
6			30 %	90%(CL-ML) + 10%(SP)	11
7		25 blows/layer	14 %	CL - ML	10
8			30 %	90%(CL-ML) + 10%(SP)	12
9	35º	10 blows/layer	14 %	CL - ML	4
10			30 %	CL - ML	5
11		25 blows/layer	14 %	CL - ML	6
12			30 %	CL - ML	7

5.3.1. Main Experiment 1

Model slope 1 was constructed on 23 March 2009, which is the first experiment of the range. Angle of the slope was 15 degrees, initial moisture content was 14% and compaction characteristic is 10 blows for each layer of soil. Type 1 soil was used to create soil model which consist of fine grained cohesive soils (ML & CL). 511 kg soil was used to construction of the soil model. Experiment was completed in approximately 25 minutes. While the 74% of the total rainfall water was flown from the surface of the slope (as Runoff), 18% has infiltrated through the soil and is collected in the infiltration tank, while 8% was absorbed by the soil. Due to the influence of the mild slope angle (15^{o}), which was not steep, surface deformation was not very large. Infiltration depths were measured at both sides of the soil container as 25 cm, which was equal to the depth of initial unsaturated soil depth.

5.3.2. Main Experiment 2

Model slope 2 was built on 13 May, 2009, which was ranked third in twelve experiments (Figure 5.6). Degree of slope angle was 15 degrees, initial water content of soil was 30% and the last variable for the number of blows per soil layer was 10. Type 1 soil was used during the construction of the slope model. 505 kg soil was used for filling the soil container which was slightly smaller than the first experiment's weight. As the 72% of the total pumped water was runoff, 21% was infiltrated through the soil, which was gathered in the infiltration tank and 7% was absorbed by the soil. Great movements or any sliding did not observe. At the end of the experiments, infiltration depths were measured 25 cm.

Figure 5.6. Front View of the Soil Slope Sample in Experiment 2

5.3.3. Main Experiment 3

Model slope 3 was constructed on 30 March 2009, which was ranked as the second one in twelve experiments (Figure 5.7). Angle of slope was 15 degrees, initial moisture content was 14% and compaction was achieved by applying 25 blows for each of 3 layers of soil. Type 1 soil was used to create a soil model, which consisted of fine grained cohesive soils (ML- CL). Totally 545 kg soils were used to construct the soil model. Experiment was completed in approximately 25 minutes. While the 79% of the total rainfall water was flown from the surface of the slope (as surface runoff), 13% was infiltrated through the soil and was collected in the infiltration tank, while the other 8% was absorbed by the soil. Due to mild slope angle (15º) under rainfall, surface deformation was not very large. Infiltration depths were measured on both sides of the soil container as 25 cm, which was equal to the depth of the initial unsaturated soil depth, before the rainfall began. When the third model slope is compared to the first two model slopes, density differences can be realized easily, because of the total compaction effort by applying 25 strokes per layer. Another important discrepancy between the third model and the first two models is runoff infiltration water relationship. While the rainfall water infiltrates hardly in well compacted soils, it can be infiltrate readily in loose soils.

Figure 5.7. Lateral View of the Soil Slope Sample in Experiment 3

5.3.4. Main Experiment 4

This was the last model of the 15 degrees slope angles and it was constructed on 4 July 2009, which ranked eighth among the twelve experiments done. The initial moisture content was 30% and the compaction input provided was 25 blows for each of 3 layers of soil. Type 1 soil was used to create soil model, which consisted of fine grained cohesive soils (ML-CL). 532 kg soil was used to construct the soil model. Experiment was completed in approximately 25 minutes. While 77% of the total rainfall water has flown on the slope surface as runoff, 14% has infiltrated through the soil into the infiltration tank and 9% was absorbed by the soil. Due to the mild slope angle (15º), surface deformation under the action of rainfall was not very large. Infiltration depths were measured on both sides of the soil container as 25 cm, which is equal to the depth of the initial unsaturated soil before rainfall started. Figures 5.8 and 5.9 show the front and side views of this experiment, respectively.

5.3.5. Main Experiment 5

Model slope 5 was constructed on 8 July 2009, which ranked ninth in twelve experiments done. For this model; 25 degrees slope angle, the initial moisture content of 14% and a compaction effort of 10 blows for each of 3 layers of soil was used. Type 1 soil was used to create a soil model consisting of fine grained cohesive soils (CL-ML). 515 kg soil was used to construct the soil model. Experiment was completed in approximately 25 minutes. While 88% of the total rainfall water has become the surface runoff, another 12% has first infiltrated into the soil, but later has been absorbed by the soil, as no water has passed through the soil to be collected in the infiltration tank. Having increased slope angle and looser soils has caused some little sliding and overturning to occur in the experiment. Infiltration depths on the right side of the soil container was measured as 19,3 cm and on the left side as 19,6 cm (Figure 5.10). These measurements also gave further evidence as to no infiltration through the soil has taken place during the experiment.

Figure 5.8. Front View of the 4th Experiment

Figure 5.9. Side View of the 4th Experiment

Figure 5.10. Infiltration Depth after the Experiment 5

5.3.6. Main Experiment 6

Model slope 6 was constructed on 22 July 2009 and ranked eleventh in the twelve experiments done. Angle of slope was 25 degrees, initial moisture content was 30% and the compaction input provided was 10 blows for each of 3 layers of soil. In this experiment six changes were made in the soil composition used. In addition to 90% of Type1 soil, which is defined as CL-ML, 10% medium sand (SP) is added. As a result of this experiment, effects of mixed soil containing 10% sand upon infiltration characteristics could be examined. A total of 562 kg soil was used to construct the soil model. Experiment was completed in approximately 25 minutes. While the 76% of the total rainfall water has flown down the slope surface as runoff, 20% has infiltrated into the soil and was collected in the infiltration tank. The remaining 4% was absorbed by the soil. At the end of the experiment, it was seen that medium sand particles made an important contribution for the rainfall water to infiltrate through the soil into the collection tank below. The reason for this behavior can be explained as the increased permeability of the mixed soil.

5.3.7. Main Experiment 7

Model slope 7 was constructed on 15 July 2009 and ranked tenth in twelve experiments done. Angle of slope was 25 degrees, the initial moisture content was 14% and the compaction provided was 25 blows for each of 3 layers of soil. Type 1 soil was used to create a soil model consisting of fine grained cohesive soils (CL-ML). Totally 527 kg soil was used to construct the soil model. Experiment was completed in approximately 25 minutes. While the 90% of the total rainfall water has discharged as surface runoff, 10% water was absorbed by the soil. Any infiltrated through the soil water into the bottom tank was not observed, probably due to the increased slope angle and dense soil state. Contrary to the previous experiments done using only type 1 soils, larger deformations and displacements on the slope surface were detected. Depth of infiltration on the right side of the soil container was measured as 18,8 cm and on the left side as 19,1 cm.

5.3.8. Main Experiment 8

This experiment was the last one of those having slope angles of 25 degrees. Model slope 8 was built on 29 July 2009 and ranked the last one in twelve experiments done. Similar to the experiment 6, some changes were also made so as to obtain the maximum amounts of infiltrated through the soil water. Moreover, the number of blows for each of 3 soil layers was changed to 10 blows from 25 blows. Thus loose soil mass was obtained, while the initial water content remained the same. Also, the same mixed proportion was for used for the soil (i.e. 90% CL-ML and 10% medium sand). Totally 552 kg soil was used to construct the soil model. Experiment was completed in approximately 25 minutes. While the 74% of the total rainfall water has become surface runoff, another 22% has infiltrated through the soil to be collected in the infiltration tank below and 4% was absorbed by the soil. Consequently, the biggest amount of infiltrated water passing through the soil was obtained so far. The infiltration depth measurements made on both sides of the soil container gave the same value of 25 cm, which was equal to the depth of initial unsaturated soil before rainfall started.

5.3.9. Main Experiment 9

New series of experiments were started on 25 May 2009. This experiment series had the steepest slopes at angles of 35 degrees, but other parameters varied from test to test. In the experiment 9, the initial moisture content was 14% and provided compaction input was 10 blows for each of 3 layers of soil. Type 1 soil was used to create a soil model consisting of fine grained cohesive soil (CL-ML). Totally 522 kg soil was used to construct the soil model. Experiment was completed in approximately 25 minutes. While the 82,5% of the total rainfall water has become surface runoff, 6% has infiltrated thru' the soil and was collected in the infiltration tank, as another 11,5% was absorbed by the soil. In this first experiment of the new series, it was obvious that the angle of slope was the main factor to trigger the slope instability, with great displacements and deformations. Another important point; surface runoff water causes the erosion, which creates a new parameter to be measured at the end of the test. Although, in all experiments, the initial soil height was equal to 25 cm, the final height of the tested soil varies under the influence of the runoff water. During the previous experiments, only

small and negligible erosion had taken place on the surface. But in experiment 9 the average final height of the soil was measured as 22,7 cm., while the infiltration depths on both sides of the soil container were measured as 25 cm and this value was equal to the depth of the initial unsaturated soil, before rainfall started.

During the new series of experiments with slope angles of 35 degrees, the SWIMS equipment was under the influence of great horizontal forces. To prevent possible collapse, additional support elements of wooden struts were used, as assembled to the SWIMS set-up (Fig.5.11).

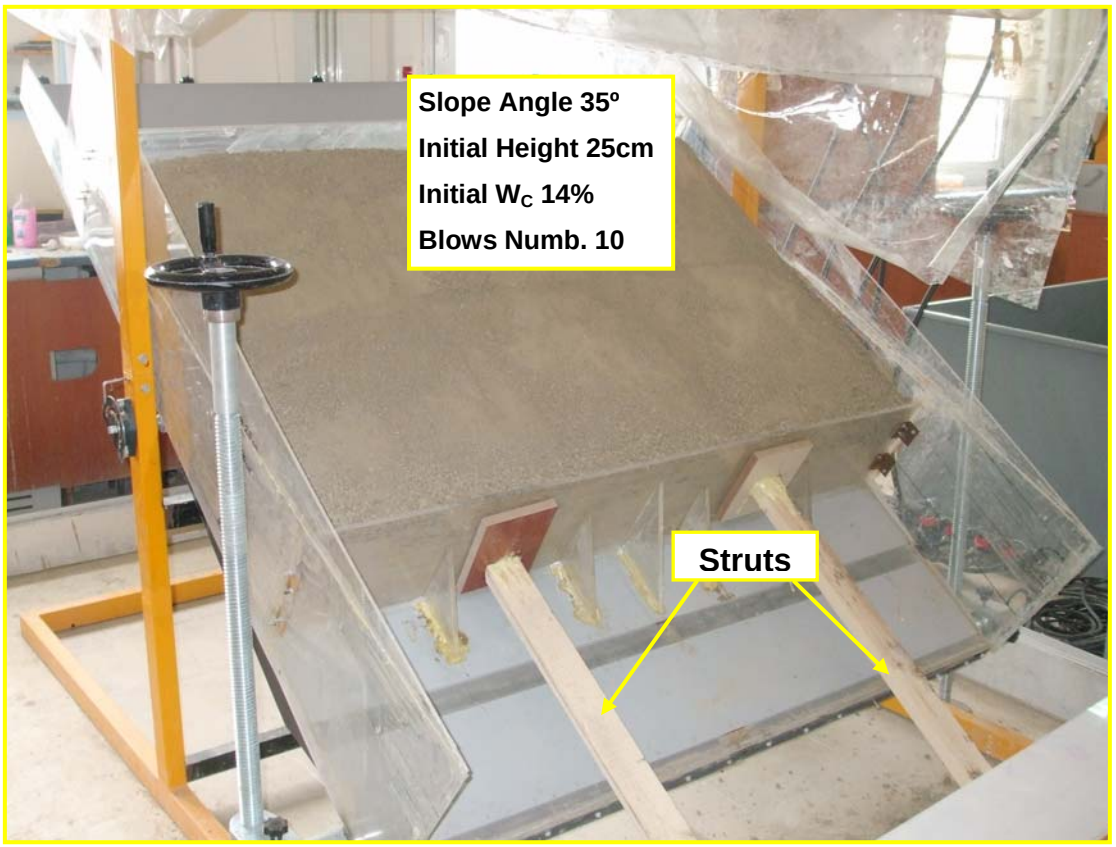

Figure 5.11. The Steepest Slope Angle and Struts (35º)

5.3.10. Main Experiment 10

Model slope 10 was constructed on 10 June 2009 and ranked fifth in twelve experiments done. Angle of slope was 35 degrees, initial moisture content was 30% and compaction effort was 10 blows for each of 3 layers of soil. Type 1 soil was used to this

create soil model, which consisted of fine grained cohesive soils (CL-ML). Totally 518 kg soil was used to construct the soil model. Experiment was completed in approximately 25 minutes. While 91% of the total rainfall has become surface runoff, other 9% was absorbed by the soil. Increased slope angle has led to decrease in infiltration depth, but has caused an increase in the erosion depth. In this experiment, the final average height of the soil was measured as 21,6 cm. This means eroded soil height was 3.4 cm. Infiltration depths were measured on both sides of the soil container as approximately 17,6 cm. Additionally, as shown in Figure 5.12, great translational mass-slide has occurred and there was a gap at the top of the slope due to slope failure, as demonstrated by a separation taking place between the back plexiglass' interior surface and the tested soil block's back end.

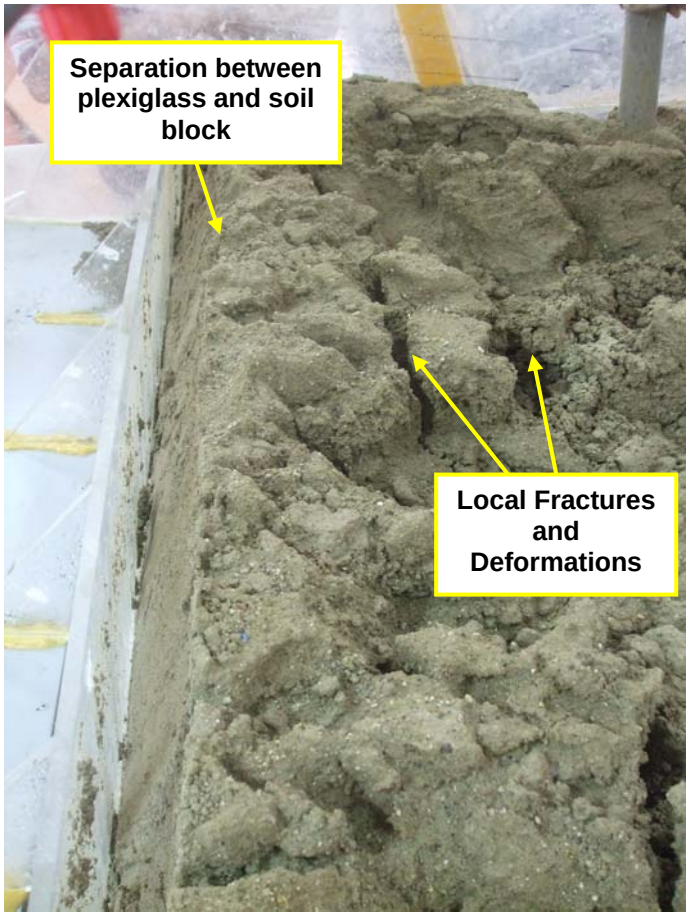

Figure 5.12. Local Failures and Collapses in Experiment 10

5.3.11. Main Experiment 11

Model slope 11 was built on 17 June 2009, which ranked sixth in twelve experiments done. Angle of slope was 35 degrees, initial moisture content was 14% and compaction characteristic was 25 blows for each of 3 layers of soil. Type 1 soil was used to create soil model, which consisted of fine grained cohesive soils (CL-ML). Totally 541 kg soil was used to construct the soil model. Experiment was completed in approximately 25 minutes. While 94% of the total rainfall has become surface runoff, other 6% was absorbed by the soil. For this experiment, the average final height of the soil was measured as 22,2cm, meaning an erosion loss of 2,8cm on the surface. Infiltration depths measured on both sides of the soil container were both approximately 18,4 cm., meaning no water has passed through the soil into the tank below. Also significant translational slidings, slope failures and collapses were observed to have occurred, similar to experiment 10.

5.3.12. Main Experiment 12

Model slope 12 was constructed on 25 June 2009 and ranked seventh in twelve experiments done. Angle of slope was 35 degrees, initial moisture content was 30% and compaction input provided was 25 blows for each of 3 layers of soil. Type 1 soil was used to create the soil model, which consisted of fine grained cohesive soils (CL-ML). A total of 517 kg soil was used to construct the soil model. Experiment was completed in approximately 25 minutes. While the 95% of the total rainfall has become surface runoff, other 5% was absorbed by the soil with no infiltrated-through water into the tank below. In this experiment, the final height of the soil was measured on average as 21,3 cm. Infiltration depths of rainfall water measured on both sides of the soil container were both approximately 17,7 cm. Additionally, in this experiment, also significant translational slidings, slope failures and collapses were Figure 5.13 observed, similar to experiments 10 and 11.

Figure 5.13. View of the Soil Slope at the end of the Experiment 12

5.4. Results of Main Experiments

As discussed comprehensively in the previous sections, twelve main experiments were performed at the İzmir Institute of Technology (IYTE)'s-Soil Mechanics Laboratory. In these twelve main experiments, there were three different soil parameters, which were the initial moisture content, soil density and the slope angles. Tests were conducted in 3 different slope angles (15°- 25°- 35°). Various records were obtained from the experiments, such as; amounts of surface runoff, infiltrated or infiltrated-through water, absorbed water, infiltration depth, eroding height. In addition to the collected data, lots of observation were also made about the failure mechanisms occurring during the experiments, such as; soil translational sliding, collapsing, overturning, soil displacements and deformations. Preparation of experimental set-up took approximately 6 months. Further, the elapsed time between the first and the last experiment was about 5 months. Finally, compiling and interpretation of the collected data took about 2 months. Following Tables (5.2), (5.3) and (5.4) summarize results of 12 completed main experiments using the SWIMS set-up.

Table (5.2) gives summary of the runoff, absorbed and infiltrated water in liter units for each experiment. The vast majority of the total rainwater flows as the surface runoff, whose volume increases proportionally to the increase in the slope angle. Another important conclusion, as can be seen from Table (5.2) is that the number of blows (for each soil layer) and infiltration amounts are in inverse relationship. As one

increases, the other one decreases. As a result of increased compaction performance, the soil failures reduce and the amount of infiltrated water decreases. In the tests with low initial water contents (ie. 14%), the amounts of infiltrated water is small or non-existent, due to soils developing big initial suctions and slower infiltration rate occurs. In the tests with high initial water contents (ie.30%), the amounts of infiltrated water is large, due to soils reach saturation quicker and the occurring infiltration rate is faster.

Table 5.2. Summary of Runoff, Absorbed and Infiltrated Water for each Experiment

No	Angle of Slope	Number of Blows	Initial W_c (%)	Total (lt.) Water Q_T	Runoff Water (lt.) Q_R	Absorbed Water (lt.) Q_M	Infiltrated Water (lt.) Q_i
1	15°	10 blows	14	400	295,4	32,60	72
2	15°	10 blows	30	400	286,96	25,49	87,55
3	15°	25 blows	14	400	315,2	32,4	52,4
4	15°	25 blows	30	400	307	36	57
5	25°	10 blows	14	400	353	47	0
6*	25°	10 blows	30	400	302	18	80
7	25°	25 blows	14	400	361	39	0
8*	15°	10 blows	30	400	294,5	16,8	80,7
9	35°	10 blows	14	400	330	46	24
10	35°	10 blows	30	400	364	36	0
11	35°	25 blows	14	400	376	24	0
12	35°	25 blows	30	400	382	18	0

(*): Soil sample consist of 90% CL-ML and 10% SP

Table (5.3) gives the total weight of soils tested in the main experiments, including the density of soil and the date of experiments. The weight of soil directly relevant to compaction effort. The weight of soils ranged between 5,05 kN which equals to 505 kg. and 5,62 kN equals to 562 kg. The date of experiments was planned at the beginning of the thesis, because the amounts of soil used in 12 experiments were a lot. Thus in order to control the initial water content precisely, soil materials was first air-dried and then re-used again in another experiment. For example; for the %14 initial water content, soil material was used and then soil material was left to dry, whose water content was checked at frequent intervals. When the soil reached to the desired water content (eg.±1 %), the soil was ready to use in another experiment.

Table 5.3. Summary of Weight of Soil, Density of Soil and Date of Experiments

No	Angle of Slope	Number of Blows	Initial W_c (%)	Weight of Soil (kN)	Volume of Soil (m^3)	Density of Soil (kN/m^3)	Soil Type
1	15°	10 blows	14	5,11	0,375	13,60	CL - ML
2	15°	10 blows	30	5,05	0,375	13,40	CL - ML
3	15°	25 blows	14	5,45	0,375	14,50	CL - ML
4	15°	25 blows	30	5,32	0,375	14,20	CL - ML
5	25°	10 blows	14	5,15	0,375	13,70	CL - ML
6*	25°	10 blows	30	5,62	0,375	15,00	90%(CL-ML) + 10%(SP)
7	25°	25 blows	14	5,27	0,375	14,10	CL - ML
8*	15°	10 blows	30	5,52	0,375	14,70	90%(CL-ML) + 10%(SP)
9	35°	10 blows	14	5,22	0,375	13,90	CL - ML
10	35°	10 blows	30	5,18	0,375	13,80	CL - ML
11	35°	25 blows	14	5,41	0,375	14,40	CL - ML
12	35°	25 blows	30	5,17	0,375	13,80	CL - ML

(*): Soil sample consist of 90% CL-ML and 10% SP

Depth of infiltration and erosion vary depending on many parameters. Indeed, one of the most important parameters is the slope angle. It was observed in the experiments that; as the slope angle increases, the depth of erosion increases, due to faster flowing surface runoff. In addition to this; there is the effect of gravity force, which is more effective to encourage vertical infiltration for milder (ie.near horizontal) slopes, provided that surface cover is non-existent. Another important point; is the compaction effort. Denser the soil is, surface erosion, permeability and infiltration tend to decrease. (in unsaturated compacted cohesive clays, matric suction and capillary forces between the clay particles may further decrease rainwater infiltration and soil permeability). Also, rainfall intensity and rainfall duration are other important factors, affecting the slope stability, the infiltration and erosion depths. All these are observations made during the tests with limited applied rainfall volume of 400 litres and in 20-30 minutes.

Table 5.4. Summary of Infiltration Depth and Erosion Depth for Each Experiment

No	Angle of Slope	Number of Blows	Initial W_c (%)	Maximum Infiltration Depth (cm)	Maximum Erosion Depth (cm)	Deformation Group
1	15°	10 blows	14	25	1,6	2
2	15°	10 blows	30	25	1,4	1
3	15°	25 blows	14	25	1,3	1
4	15°	25 blows	30	25	1,2	1
5	25°	10 blows	14	19,4	2,0	2
6*	25°	10 blows	30	25	2,1	2
7	25°	25 blows	14	18,9	1,9	2
8*	15°	10 blows	30	25	1,5	1
9	35°	10 blows	14	25	3,7	3
10	35°	10 blows	30	17,6	3,4	3
11	35°	25 blows	14	18,4	2,8	3
12	35°	25 blows	30	17,7	2,6	3

(*): Soil sample consist of 90% CL-ML and 10% SP

During this study, in addition to the quantitative observations, the qualitative observations have also been done. As a result of the completed experiments, deformations and displacements were defined in three different groups. The first group consisted of those showing comparatively small displacements and deformations, such as; small cracks near the crest of the slope. The second group contained those showing relatively large displacements, deeper erosions and even some overturning, which took place at various points. The third group involves those showing big fractures, eroded soil surfaces, completely instable and translationally failed or slided slopes with soil top end and soil container completely separated from each other.

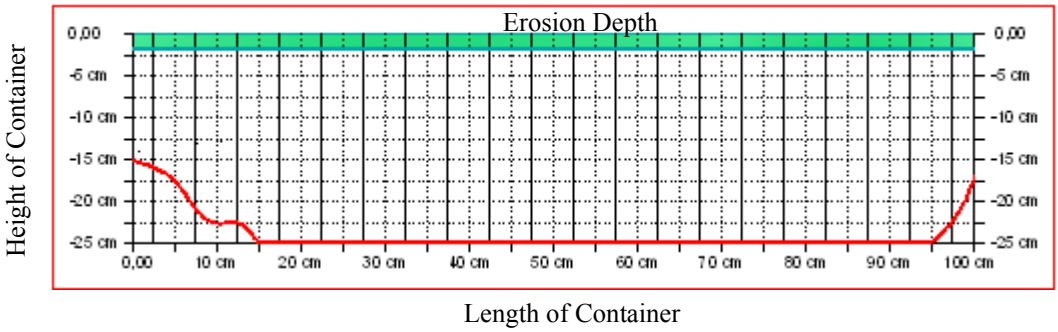

Figure 5.14. Lateral Profile View of the Infiltration Process and Erosion Depth for Main Experiment 1 (w_{ic}=14%, α_{as}=15°, number of blows=10)

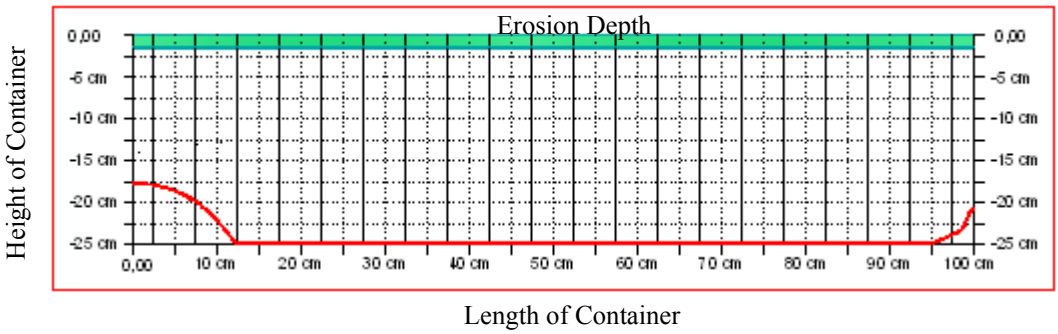

Figure 5.15. Lateral Profile View of the Infiltration Process and Erosion Depth for Main Experiment 2 (w_{ic}=30%, α_{as}=15°, number of blows=10)

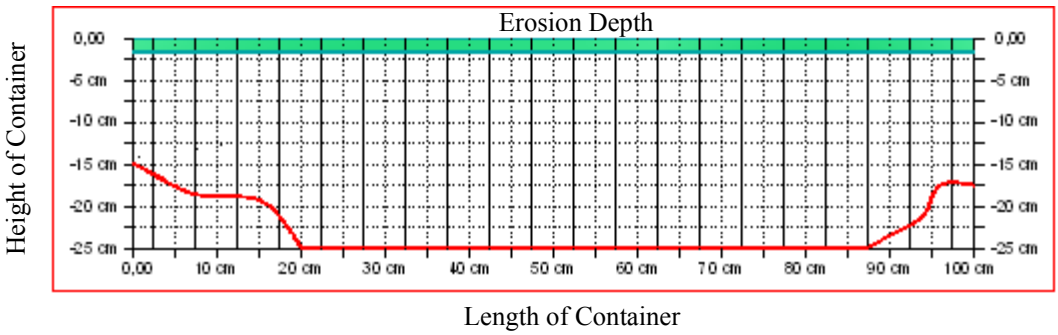

Figure 5.16. Lateral Profile View of the Infiltration Process and Erosion Depth for Main Experiment 3 (w_{ic}=14%, α_{as}=15°, number of blows=25)

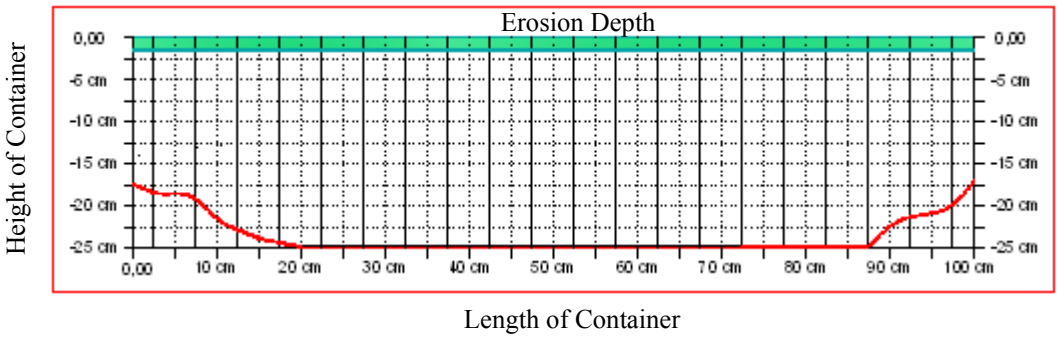

Figure 5.17. Lateral Profile View of the Infiltration Process and Erosion Depth for Main Experiment 4 (w_{ic}=30%, α_{as}=15°, number of blows=25)

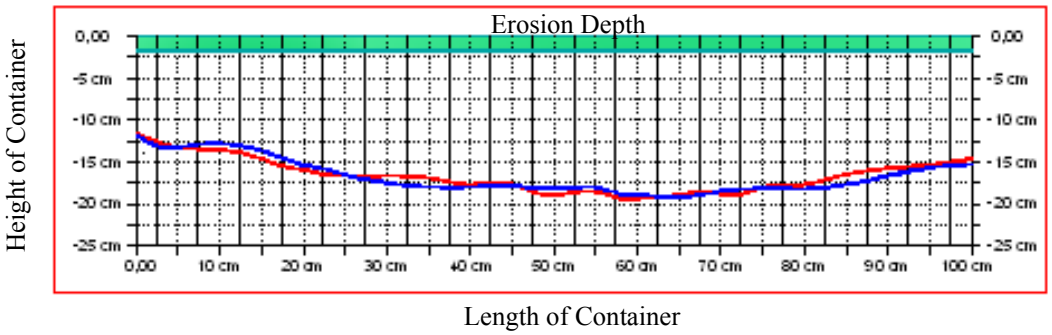

Figure 5.18. Lateral Profile View of the Infiltration Process and Erosion Depth for Main Experiment 5 (w_{ic}=14%, α_{as}=25°, number of blows=10)

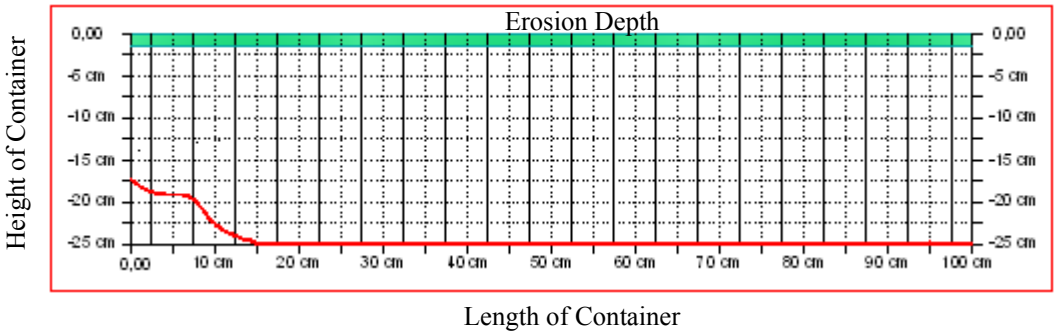

Figure 5.19. Lateral Profile View of the Infiltration Process and Erosion Depth for Main Experiment 6 (w_{ic}=30%, α_{as}=25°, number of blows=10)

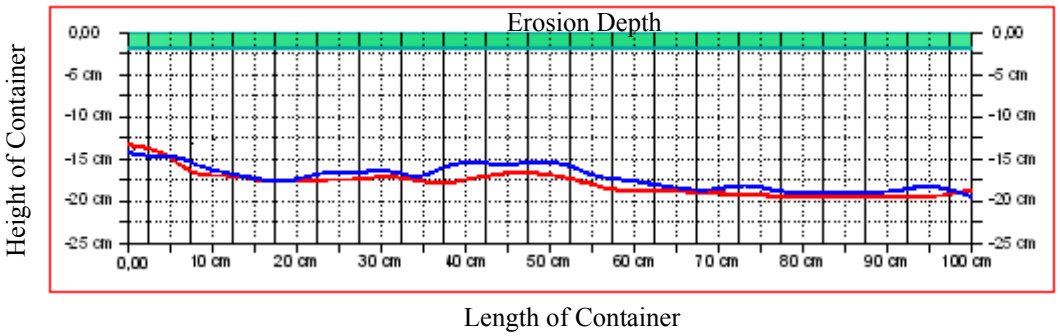

Figure 5.20. Lateral Profile View of the Infiltration Process and Erosion Depth for Main Experiment 7 (w_{ic}=14%, α_{as}=25°, number of blows=25)

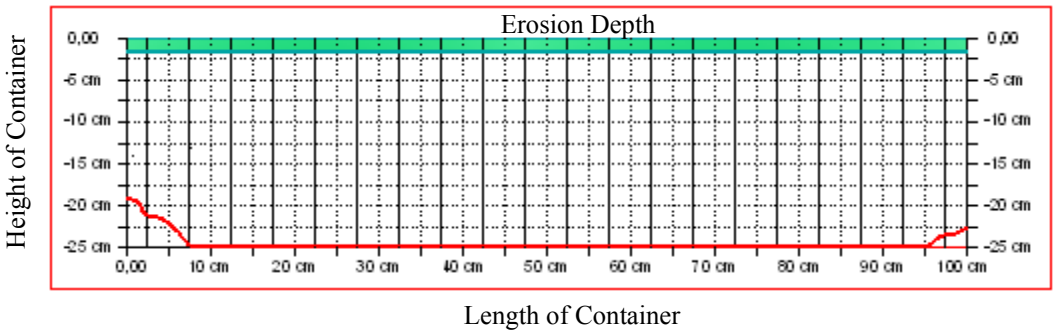

Figure 5.21. Lateral Profile View of the Infiltration Process and Erosion Depth for Main Experiment 8 (w_{ic}=30%, α_{as}=15°, number of blows=10)

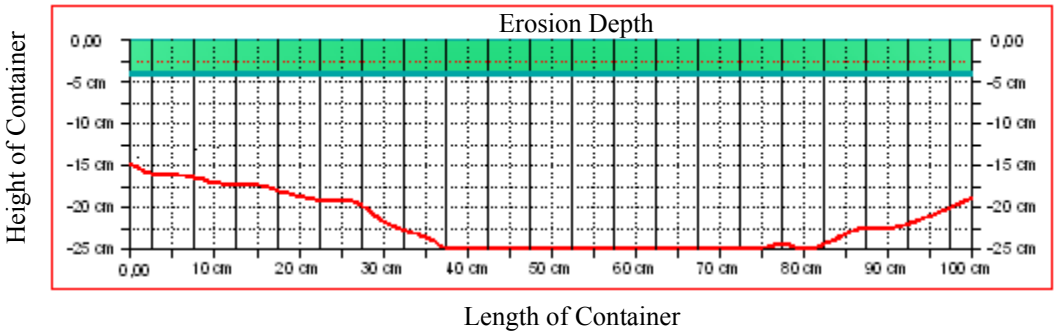

Figure 5.22. Lateral Profile View of the Infiltration Process and Erosion Depth for Main Experiment 9 (w_{ic}=14%, α_{as}=35°, number of blows=10)

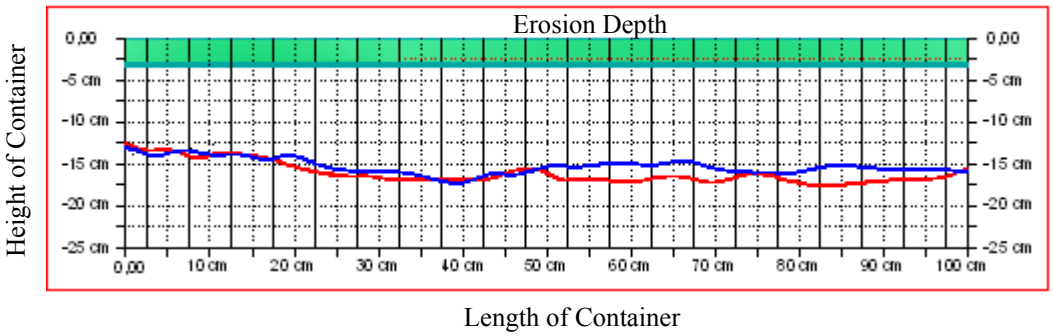

Figure 5.23. Lateral Profile View of the Infiltration Process and Erosion Depth for Main Experiment 10 (w_{ic}=30%, α_{as}=35°, number of blows=10)

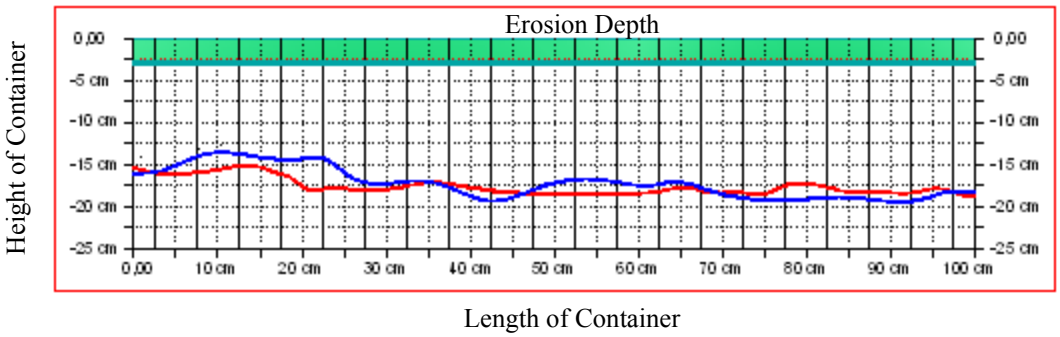

Figure 5.24. Lateral Profile View of the Infiltration Process and Erosion Depth for Main Experiment 11 (w_{ic}=14%, α_{as}=35°, number of blows=25)

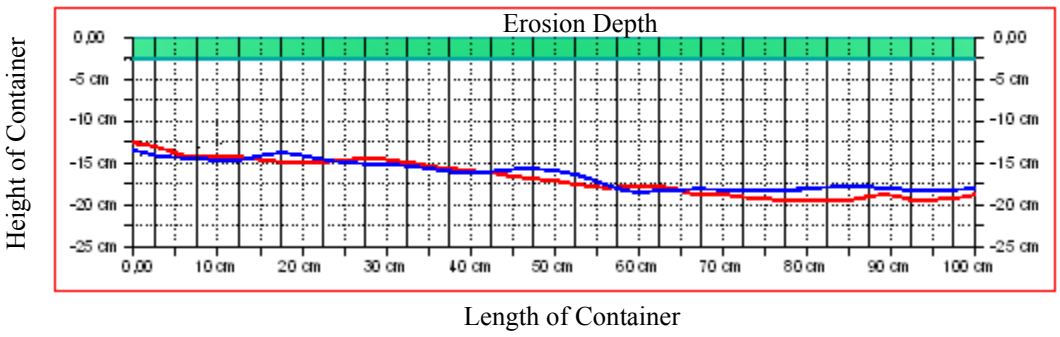

Figure 5.25. Lateral Profile View of the Infiltration Process and Erosion Depth for Main Experiment 12 (w_{ic}=30%, α_{as}=35°, number of blows=25)

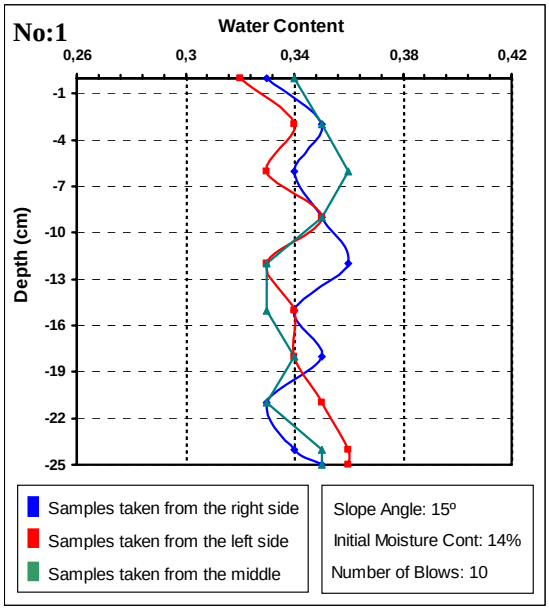

(a) Experiment No:1

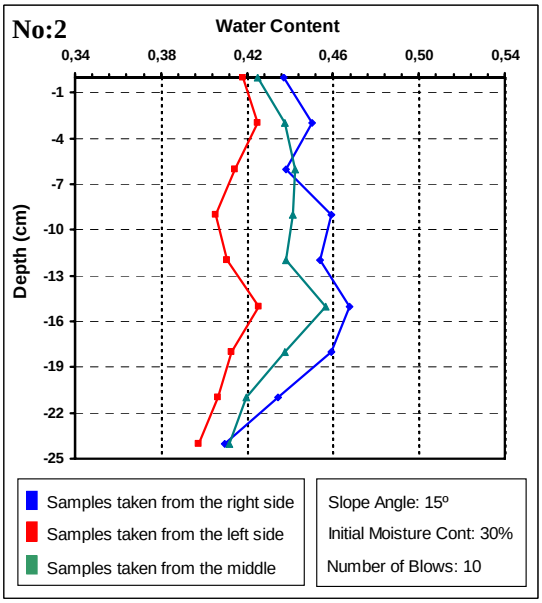

(b) Experiment No:2

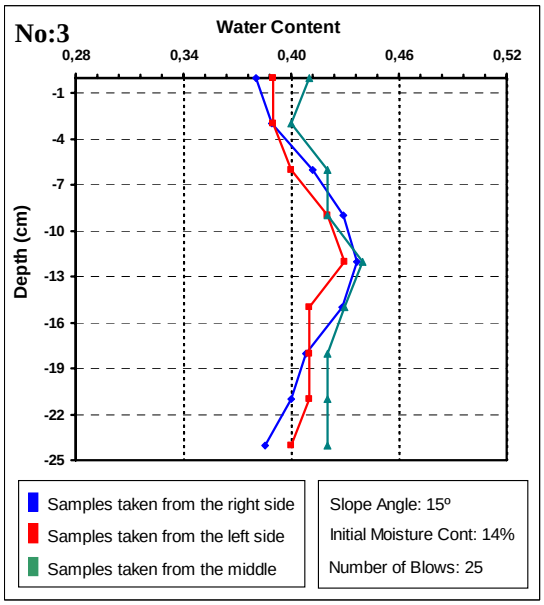

(c) Experiment No:3

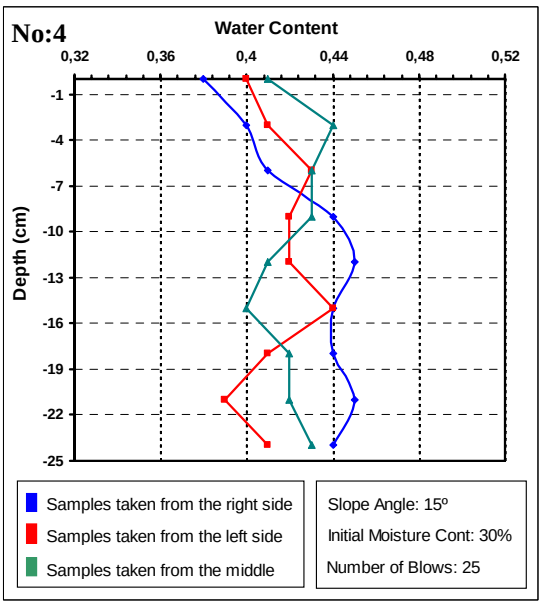

(d) Experiment No:4

Figure 5.26. The First Group of 15°, Infiltration Depth Water Content Graphs (a-d)

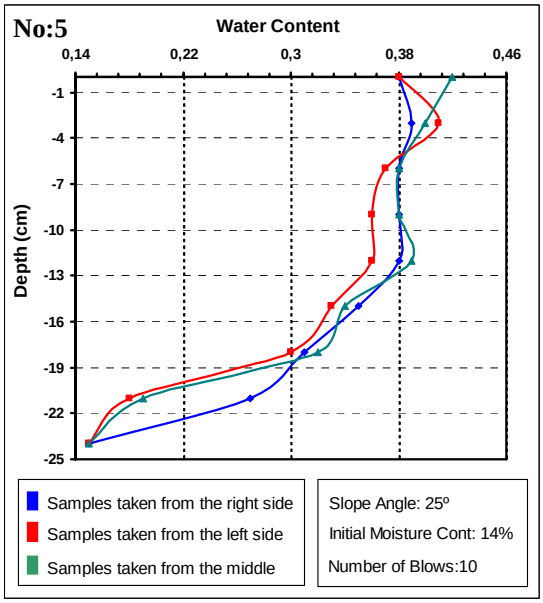

(a) Experiment No:5

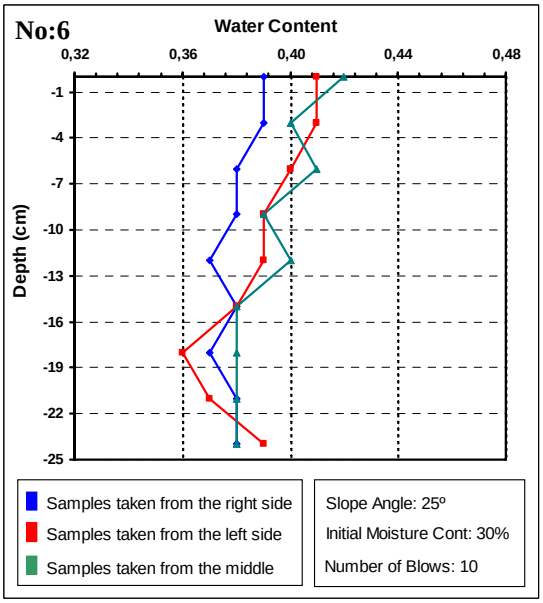

(b) Experiment No:6

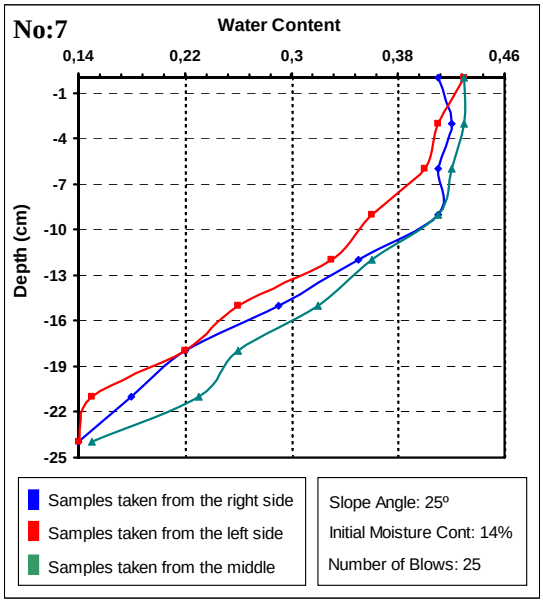

(c) Experiment No:7

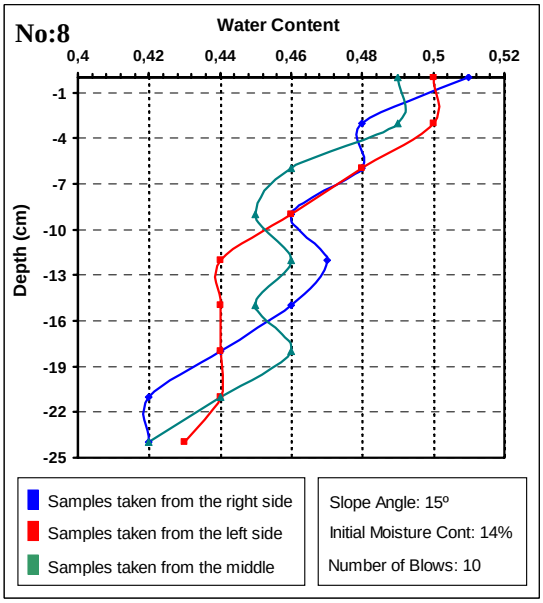

(d) Experiment No:8

Figure 5.27. The Second Group of 25°, Infiltration Depth Water Content Graphs (a-d)

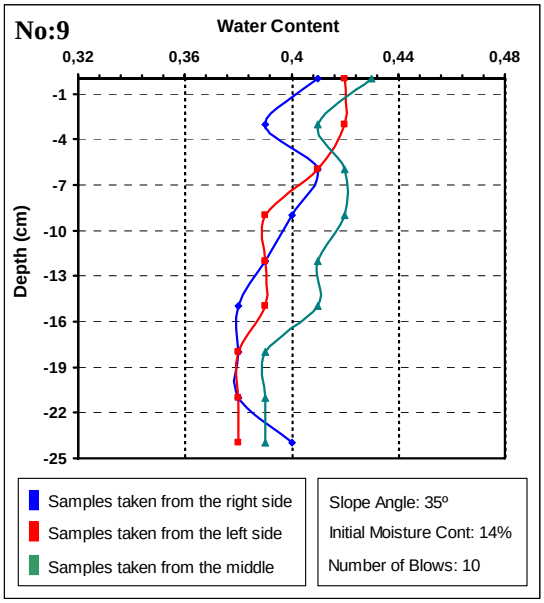

(a) Experiment No:9

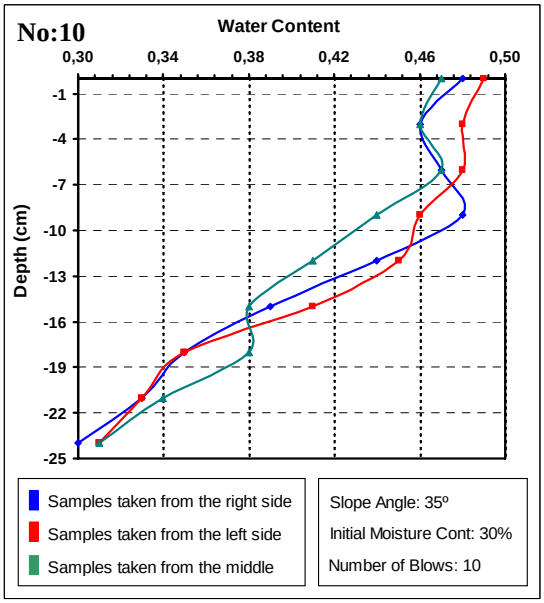

(b) Experiment No:10

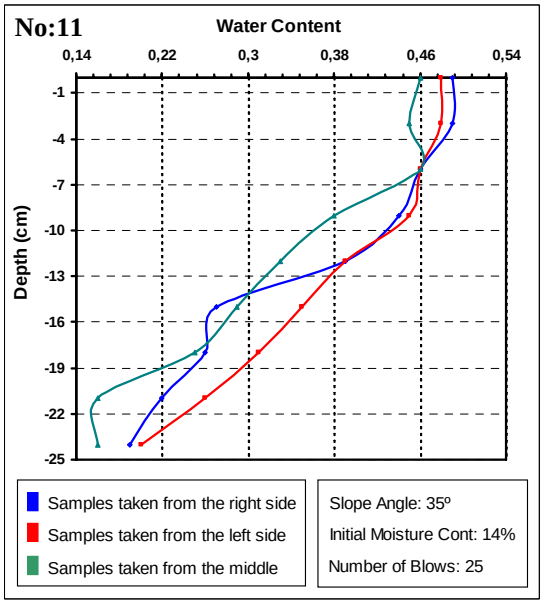

(c) Experiment No:11

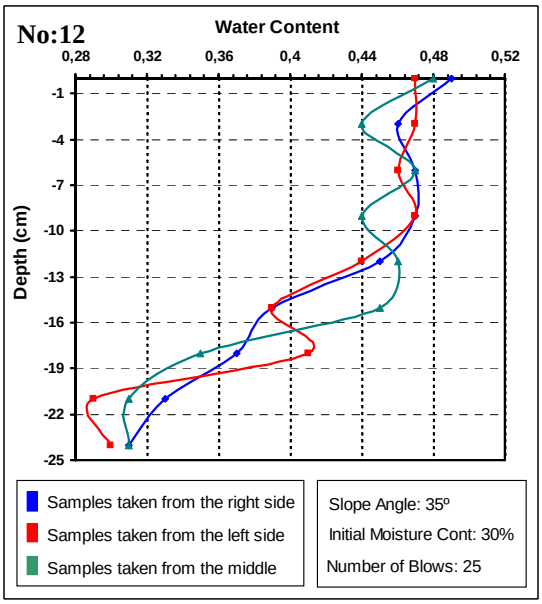

(d) Experiment No:12

Figure 5.28. The Third Group of 35°, Infiltration Depth Water Content Graphs (a-d)

Conclusion and summary of these graphs and figures are given in Chapter 7.

CHAPTER 6

ANALYSIS OF SLOPE MODELS

6.1. Introduction

The primary purpose of any slope stability analysis in most engineering applications is to design safely and economically excavations, embankments, earth dams and natural slopes. In each of these structures, the greatest economy may be derived by altering the slope dimensions, which may reduce the factor of safety (FOS). The design of these structures is governed by the minimum factor of safety allowed by the designer. It is thus necessary to have the best possible estimate of the factor of safety.

In the assessment of slopes, engineers primarily use factor of safety values to determine how close or how far slopes are from failure. Conventional limit-equilibrium techniques are the most commonly-used analysis methods. These methods include the Ordinary method of slices, Bishop's modified method, Force Equilibrium methods, Janbu's generalized procedure of slices, Morgenstern and Price's method and Spencer's method. These methods, in general, require the soil mass to be divided into slices. The directions of the forces acting on each slice in the slope are assumed. This assumption has a key role in distinguishing one limit equilibrium method from another. Limit equilibrium methods require that a continuous surface passes the soil mass. This surface is essential in calculating the minimum FOS against sliding or shear failure. Before the calculation of slope stability in these methods, some assumptions (for example; the side forces and their directions) have to be given out artificially, in order to build the equations of equilibrium.

With the recent advancements in technology, some significant low cost computing and memory resources became available to the geotechnical engineer and this has led the Finite Element Method (FEM) a powerful, viable alternative to solve slope stability problems. The Shear Strength Reduction (SSR) technique (Dawson, et al. 1999, Griffith and Lane 1999, Hammah, et al. 2004) enables the FEM to calculate the

factors of safety for slopes. The method enjoys several advantages, including the ability to predict stresses and deformations of support elements, such as; piles, anchors and geotextiles at failure.

6.2. The Finite Element Method

The finite element method (FEM) is a numerical method that can be used to solve problems in many engineering applications. The finite element method is useful for problems involving complicated geometries, loadings and material properties, where analytical mathematical solutions are not possible to obtain. These analytical problems generally require solution of ordinary or partial differential equations that are not easily computed. The use of numerical methods (such as; FEM) is often necessary to obtain acceptable solutions (Logan 2002).

FEM has been widely accepted as a technique to analyse geotechnical problems. The method can utilize elastic-plastic constitutive laws that can capture the non-linearity of soils and the development of pore pressure under various loading conditions. To approximate the non-linear stress-strain curves, incremental and iterative techniques are used to compute the stresses and strains in each element. Individual finite elements can be visualized as small pieces of a structure. The first step of a finite element analysis is to divide the actual geometry of a structure using a collection of discrete portions, called “finite elements”. Elements are connected at points, called “nodes”. The collection of the nodes and finite elements is called the “mesh”. The number and the type of the elements need to be carefully chosen to effectively approximate the variables, over the region of interest. The governing equations for each finite element are determined and assembled to analyze the behavior of the solid body (Cook, et al. 2003), which is subjected to external loads and boundary conditions.

The governing equation for the discritized domain can be written as:

$$[K].\{r\} = \{R\} \tag{6.1}$$

[K] = global stiffness matrix

{r} = global displacement vector

{R}= global load vector

In this study, the constitutive model used for soils was the Mohr-Coulomb criteria with non-associative plastic flow (Griffiths and Lane 1999). Therefore, the resulting [K] matrix is non-symmetric (Abaqus 2006), and the equations solved by using a non-symmetric solver (Abaqus 2006).

In this thesis, the soil was modeled as a homogeneous, two-dimensional, plane-strain medium. It was assumed that the soil properties do not depend on temperature. In description of the material properties of soil, non-associated Mohr-Coulomb plasticity model is used. The soil model included six parameters;

ϕ': Friction Angle (degree)
c' : Cohesion
ψ : Dilation angle (degree)
ν : Poisson's ratio
E : Young's modulus (kN/m^2)
γ : Unit weight (kN/m^3)

The relationship between the dilation angle ψ, and the friction angle ϕ', determines whether the soil dilates or compacts, when subjected to plastic deformation (Fenton 1990). If the ratio of dilation angle to the friction angle exceeds 1.0 ($\psi/\phi' > 1.0$), then only compaction occurs. Otherwise initial compaction is followed by dilation (Fenton 1990). Dilation is a measure of how much volume change takes place, when the material undergoes shearing (Griffiths and Lane 1999). For a Mohr-Coulomb material, dilation is an angle that generally varies between zero and the friction angle. If Ψ=ϕ', the plastic flow occurs according to "associative flow rule". If, Ψ=0, then the plasticity corresponds to a "non-associated flow rule" (Griffiths and Lane 1999). Previous studies on soil dilatancy were mostly concentrated on the theoretical analysis of the dilation angle and its influence on soil shear strength (Chen, et al. 2003). Very few actual test data of dilation angles were reported (Chen, et al. 2003). In this study, the volume change in soil during the failure was not considered. Therefore, dilation angle, ψ, was taken as zero. Poisson's ratio, ν, and Young's ratio, E, are the elastic parameters of the soil. Although, these parameters have a significant influence on the computed deformations prior to failure, they have very little influence on the predictions of factor of safety of slopes (Griffiths and Lane 1999).

The most important parameters which could be obtained from triaxial and direct shear tests in the finite element analysis of slope stability analysis are: friction angle (ϕ'), cohesion (c), unit weight (γ), and geometry of the model (Griffiths and Lane 1999). Different values of these parameters were used in the problems solved in this research.

6.2.1. PLAXIS Finite Element Program

PLAXIS is a finite element software for soil and rock that has been used by geotechnical engineers and researchers for more than two decades. The software was first developed by The Technical University of Delft in 1987 to analyze soft soils of the low lands of Holland (Brinkgreve and Vermeer 2001). The software then was extended to cover all aspects and applications of geotechnical engineering simulations using a userfriendly interface with the power of finite element. The first version of PLAXIS was commercially available in 1998. Different soil models are incorporated in PLAXIS with a versatile library of structural elements. The automated mesh generation tool in the program makes the creation of soil models easy and practical, since 6-node as well as 15-node triangular elements are available. The program uses the Mohr-Coulomb (M-C) method to calculate the factors of safety of slopes.

The computer program is applicable to many geotechnical problems, including stability analyses and steady-state groundwater flow calculations. This software contains several FE models and four main sub-routines. These sub-routines are inputs, calculations, outputs and curve plots. The FOS versus displacement is plotted from the curve plots' sub-routine. The slope models are analyzed by the input sub-routine. Material properties including the shear strength parameters are given as input and is defined for a specific soil layer. A plain strain model of 6 nodded triangular elements was selected to be used to generate the finite element mesh. Moreover, a M-C material model was utilized for the stability analyses. The selected M-C model is based on the elastic-perfectly plastic theory of soil mechanics. Accordingly, both elastic parameters (E, ν) and plastic parameters (c', ϕ', Ψ) are utilized in the model. Similarly, in addition to the yield function (f), the model has incorporated a plastic potential function (g), where the dilatancy angle (Ψ) is associated with the plastic behaviour of soils. The formulation of the M-C model consists of six yield functions and six plastic functions. One of each function is given below for demonstration purposes (PLAXIS 2008) as:

$$f_1 = \frac{1}{2}(\sigma_2^{'} - \sigma_3^{'}) + \frac{1}{2}(\sigma_2^{'} + \sigma_3^{'})sin\phi - c.cos\phi \leq 0 \tag{6.2}$$

$$g_1 = \frac{1}{2}(\sigma_2^{'} - \sigma_3^{'}) + \frac{1}{2}(\sigma_2^{'} + \sigma_3^{'})sin\psi \tag{6.3}$$

The terms are defined under the list of symbols, at the beginning of the thesis.

6.2.1.1. Computation of the Factor of Safety (FOS)

FOS was computed by using the 'c-ϕ reduction' procedure. According to PLAXIS V9 (2008), this approach involves in successively reducing the soil strength parameters c' and tanϕ' until the failure occurs. The strength parameters are automatically reduced, until the final calculation results-in a fully developed failure mechanism. Further, by lowering the strength incrementally, a soil body is identified to fail, after a certain strength reduction occurs (Nordal and Glaamen 2004). In this way, PLAXIS computes the FOS as the ratio of the available shear strength to the strength at failure by summing up the incremental multiplier (M_{sf}) as defined by;

$$FOS = \frac{available\ shear\ strength}{shear\ strength\ at\ failure} = value\ of\ \sum M_{sf}\ at\ failure \tag{6.4}$$

Table 6.1 gives the significance of FOS for design (Liu and Evett 2005).

Table 6.1. Significance of the Factor of Safety, FOS for Design

Safety Factor	Significance
Less than 1,0	Unsafe
1,0 – 1,2	Questionable safety
1,3 – 1,4	Satisfactory for cuts, fills, questionable for dams
1,5 – 1,75	Safe for dams

6.2.1.2. The Shear Strength Reduction Technique

The Shear Strength Reduction Technique (SSR) is a new method used in the FEM to obtain FOS of earth slopes. The FEM was first applied to geotechnical engineering in 1966 (Rocscience 2004). In the mid 1970s, slope stability analyses started appearing in the literature. According to the SSR method, soil shear strength is reduced to bring a soil slope to the verge of failure (Duncan and Wright 1996). In the FEM, such a state is detected by the inability to reach equilibrium. In the SSR method, it is assumed that the slope materials have elasto-plastic behavior. The material strength is reduced, until failure occurs. The main advantages of the SSR are as follows: (1) The critical failure surface is found automatically from the application of gravity loads and/or the reduction of the shear strength; (2) It requires no assumption to be made on the interslice shear force distribution; (3) It is applicable to many complex conditions and can give information on stresses, movements and pore water pressures. One of the main disadvantages of the SSR is the long solution time required to develop the computer model and to perform the analyses. With the development of some computer hardware and software, 2D SSR can now be performed within the reasonable time span suitable for routine analysis and design.

6.2.1.3. Mathematical Details of Triangular Elements

The soil body (slope) was modeled by using 6-noded quadratic triangular plane strain (CPE6) elements. A quadratic triangle has side nodes, in addition to corner nodes, as shown in Figure (6.1). For the stress analysis, nodal unknowns (degree of freedoms) are u_i and v_i at each node and defined as;
i=1, 2,…, 6, can be expressed as (Cook, et al. 2003):

$$u = N_1U_1 + N_2U_2 + ... + N_6U_6 \tag{6.5}$$

$$v = N_1V_1 + N_2V_2 + ... + N_6V_6 \tag{6.6}$$

where,

u_i, v_i represent the nodal displacements in the x- and y- directions

N_i, represents interpolation function.

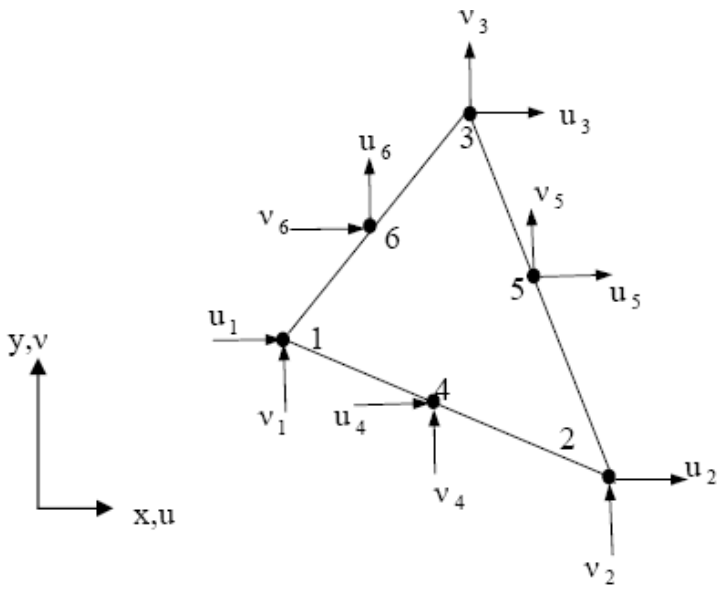

Figure 6.1. Quadratic Triangle
(Source: Cook, et al. 2003)

Element strains can be expressed in terms of displacements as (Cook, et al. 2003);

$$\varepsilon_x = \frac{\delta u}{\delta x} \tag{6.7}$$

$$\varepsilon_y = \frac{\delta v}{\delta y} \tag{6.8}$$

$$\gamma_{xy} = \frac{\delta u}{\delta y} + \frac{\delta v}{\delta x} \tag{6.9}$$

6.2.1.4. Advantages of Plaxis in Simulating Model Slopes

The advantages of using the advanced FE program such as: PLAXIS are as follows;

(1) Horizontal and vertical displacements of the whole model slope are calculated.

(2) No predetermined/distinct failure surface is required.

(3) Progressive failure and distributed deviatoric deformations are somewhat captured.

(4) Dynamic responses and seismic deformations are calculated simultaneously.

6.2.2. Soil Models

The numerical modeling is going to be carried out by means of the finite-element method, as it allows modeling of complicated nonlinear soil behavior and various interface conditions with different geometries and soil properties.

6.2.2.1. The Mohr-Coulomb Model

The elastic-plastic Mohr-Coulomb (M-C) model involves six input parameters, i.e. E and ν for soil elasticity; ϕ, γ and c for plasticity and Ψ as an angle of dilatancy. This Mohr-Coulomb model represents a "first order" approximation of soil or rock behaviour. It is recommended to use this model as a first analysis of the problem considered. For each layer, one estimates a constant average stiffness. Due to this constant stiffness, computations tend to be very fast and one obtains a first impression of deformations. Besides the five model parameters mentioned above, initial soil conditions play an essential role in most soil deformation problems. Initial horizontal soil stress has to be generated by selecting a proper K_0-value.

6.2.2.2. The Hardening-Soil Model

The Hardening-Soil (HS) model represents a much more advanced model than the Mohr-Coulomb (M-C) model. As for the M-C model, limiting states of stress are described by means of the friction angle, ϕ, the cohesion, c, and the dilatancy angle, Ψ. Soil stiffness is described much more accurately, by using three different input stiffnesses; the triaxial loading stiffness, E_{50}, the triaxial unloading stiffness, E_{ur} and the oedometer loading stiffness, E_{oed}. As average values for various soil types, we have $E_{ur} \approx 3\ E_{50}$ and $E_{oed} \approx E_{50}$. But note that; both very soft and very stiff soils tend to give other ratios of E_{oed} / E_{50}.

In contrast to the Mohr-Coulomb model, the Hardening-Soil model also accounts for stress-dependency of stiffness moduli. This means that all stiffness, increase with pressure. Hence, all three input stiffnesses, related to a reference stress, are usually taken as 100 kPa (1 bar).

6.2.2.3. Soft-Soil-Creep Model

The above Hardening-Soil model is suitable for all soils, but it does not account for viscous effects (i.e. creep and stress relaxion). In fact, all soils exhibit some creep and primary compression and thus followed by a certain amount of secondary compression.

The latter is the most dominant aspect of the soft soils (e.g. normally consolidated clays, silts and peat) and in such soils to account for the viscous effects, a model under the name of Soft-Soil Creep (SSC) model could be implemented.

6.3. Slope Models and Soil Characteristics

In this section of the thesis, similar slope models, constructed and tested in the laboratory conditions, are analysed. Three different slope angles (α) are used for the analyses, which are 15, 25, and 35 degrees. Scale factor ratio, between the laboratory model and the analysis model is assumed to be:1/10. Therefore, the slope surface length was accepted as 10m. for each slope model (as the Laboratory test slope's surface length is 1m.). Slope heights vary, depending on the slope angle. Considered slope dimensions for the FEM analyses are as follows;

- Slope Model 1: α=15º (Figure 6.2)
- Slope Model 2: α=25º (Figure 6.3)
- Slope Model 3: α=35º (Figure 6.4)

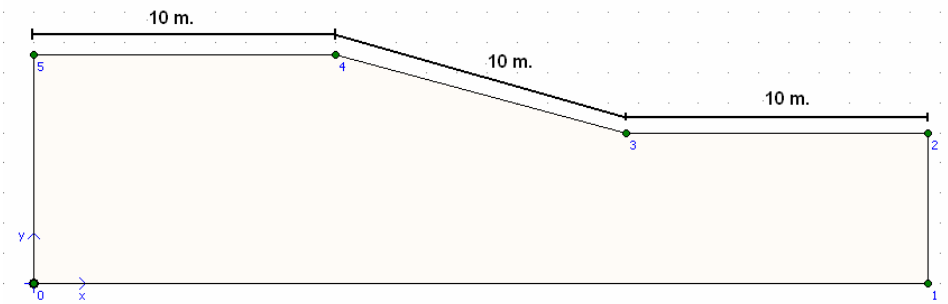

Figure 6.2. Slope Model 1 (α=15º)

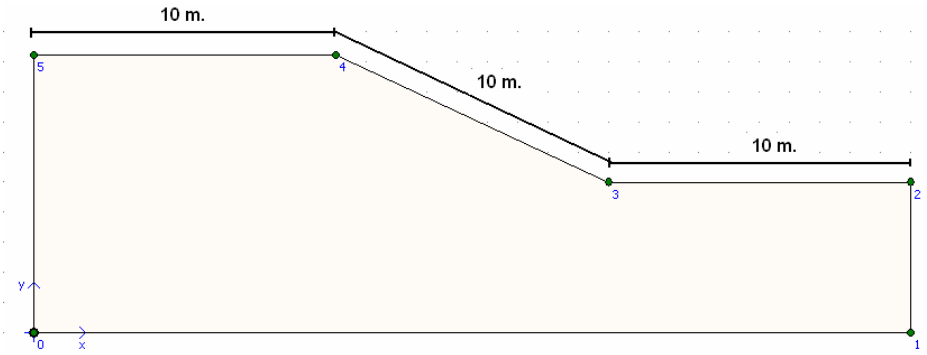

Figure 6.3 Slope Model 2 (α=25º)

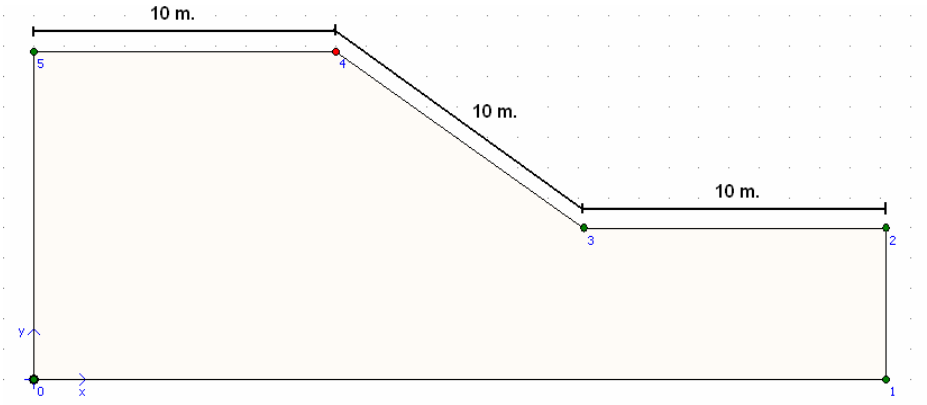

Figure 6.4. Slope Model 3 (α=35º)

After the slope geometry was created, parametric values which belong to the tested soil type were entered into the FE program. These soil parameters were obtained from the previously done laboratory tests at the IYTE - Soil Mechanics Laboratory (Chapter 4). In addition to such completed tests, some assumptions were made such as Young Modulus (E), which was approximated as: 10,000 kPa and the Poisson Ratio (ν), which was assumed as: 0,30. Other necessary parameters, such as; the angle of (effective) friction and (effective) cohesion were taken from the results of the performed CU triaxial and direct shear tests. Analyses were conducted for the state conditions and the soil water transient behaviors were considered as “drained” conditions.

Table 6.2 Summary of Soil Parameters used in FEM

Parameter	**Symbol**	**Value**	**Unit**
Friction Angle (eff.)	ϕ	32	(°)
Cohesion (eff.)	c	9	(kPa)
Poisson's Ratio	ν	0,30	(-)
Young Modulus	E	10,000	(kPa)
Dilatancy Angle	ψ	0	(°)

6.4. Phases of Slope Model Analysis

Step 1 Mesh Generation: After determining the slope model's shape, material properties are defined for model slope. Global coarseness section of the Plaxis program which exist under the "Mesh" menu enables the user to use different mesh sizes. The mesh sizes range from very coarse to very fine. Smaller mesh sizes provide more comprehensive work. Afterwards, to obtain detailed and reliable analysis, fine generated mesh coarseness is selected. Figures (6.5), (6.6) and (6.7) represent the generated model slope.

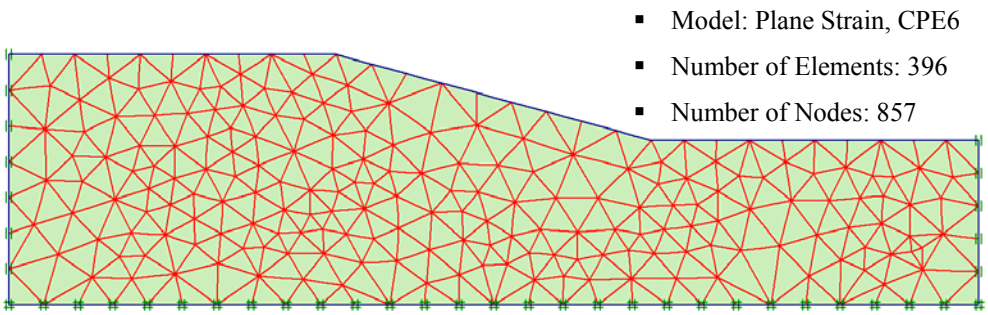

Figure 6.5. Fine Generated Slope Model 1 (α=15°)

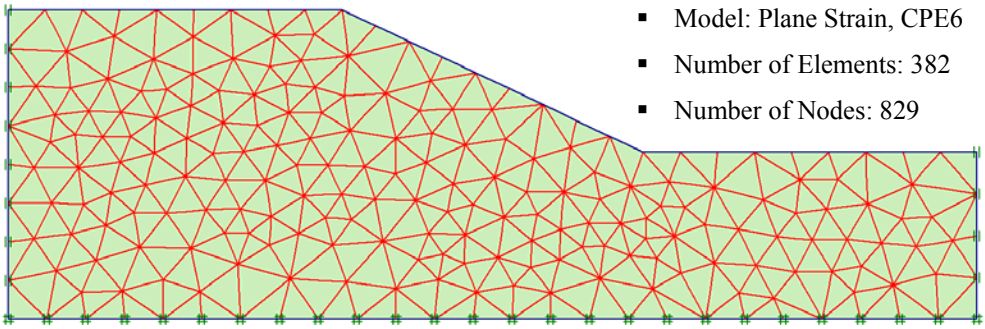

Figure 6.6. Fine Generated Slope Model 2 (α=25°)

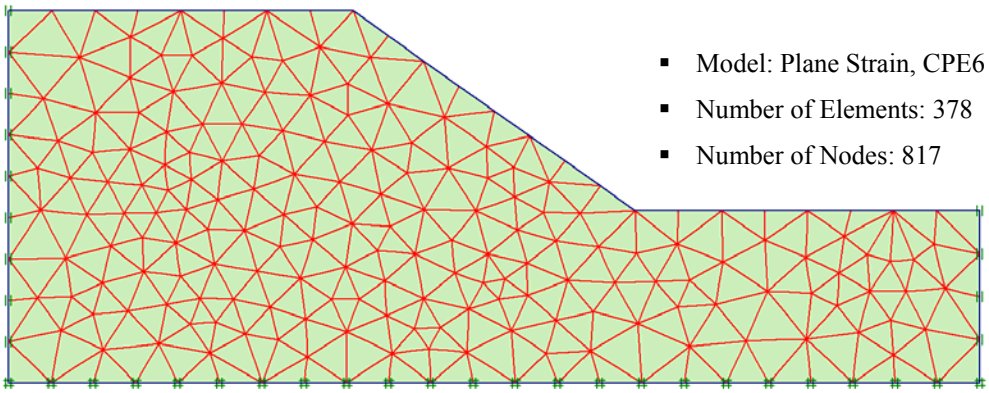

Figure 6.7. Fine Generated Slope Model 3 (α=35°)

Step 2 Determination of Initial Conditions: This step provides information about the location of the ground water table (GWT) level, specification for the closed boundary or phreatic level etc. GWT level was defined as being the entire slope surface and then processing of the water pressure generation is completed. Figures (6.8), (6.9) and (6.10) represent the generated water pressures of the model slopes.

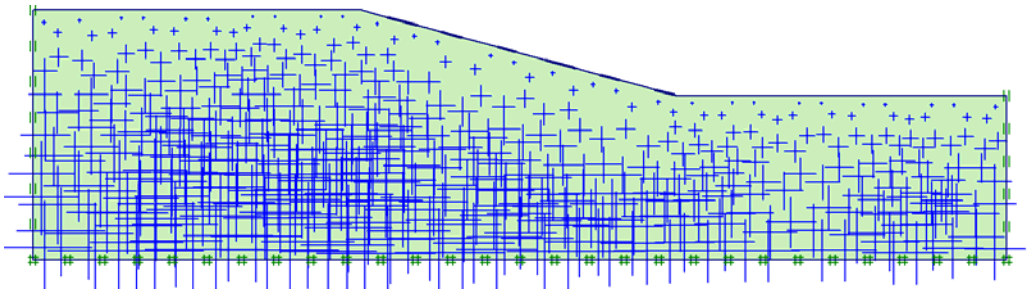

Figure 6.8 Slope Model 1: Distribution of the generated water pressure (α=15°)

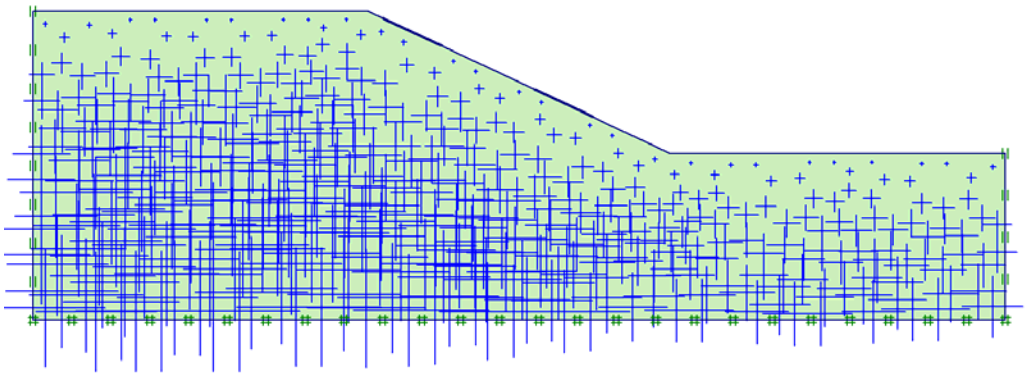

Figure 6.9 Slope Model 2: Distribution of the generated water pressure (α=25°)

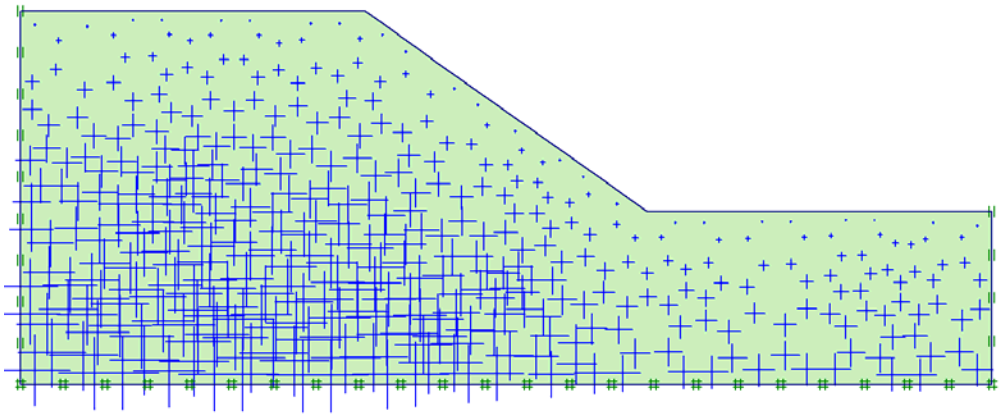

Figure 6.10 Slope Model 3: Distribution of the generated water pressure (α=35°)

Step 3 Calculations: Calculation part is the final stage, which may use various calculation methods for different soil models. In this study, Shear Strength Reduction (SSR) method is used in order to determine the minimum factor of safety for the defined slope model. SSR method, basically depended upon the Mohr-Coulomb (M-C) soil model parameters (c': cohesion and ϕ': internal friction angle, both in effective stress terms). SSR method works as follows; firstly, soil strength parameters are determined and then the FE program calculates the existing soil strength. Thereafter, program decreases the values of the soil shear strength parameters automatically, while at the same time it continues to calculate the FOS, until it is smaller than 1. When the FOS is smaller than 1, the slope is accepted as collapsed. Figures 6.11, 6.12 and 6.14 represent the FEM generated deformed shapes of the model slopes tested in the IYTE laboratory.

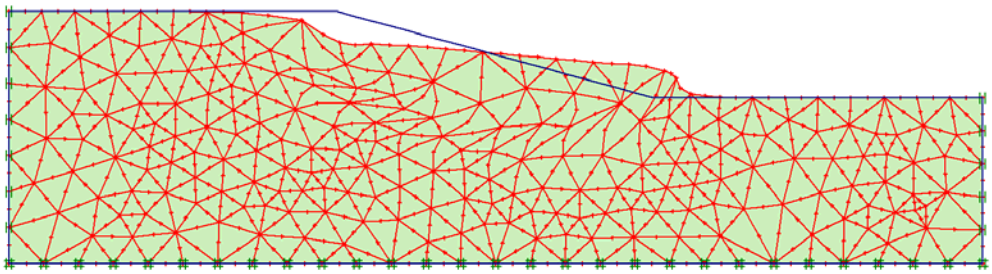

Figure 6.11 Deformed Shape of the Model Slope 1, after the Failure (α=15°)

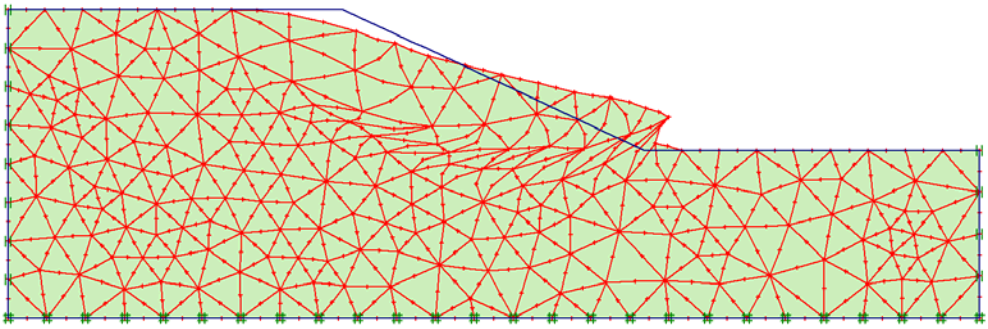

Figure 6.12 Deformed Shape of the Model Slope 2, after the Failure (α=25°)

As a result, three slope analyses were conducted, the first (15º) and the second (25º) slope models are more durable than the third one (35º), because at the beginning of the third analysis, slope model has collapsed to indicate failure (Figure 6.13). In other words, before the shear strength reduction has been reduced by program, the initial factor of safety is smaller than 1. For this reason, determination of the FOS was not completed for the defined third soil model.

This condition gives an opportunity to examine the effect an existing ground water table (GWT) on slope stability. When the same slope model was analyzed with no GWT existing in the slope, existing at the bottom of the slope), factor of safety was found as: 1,97.

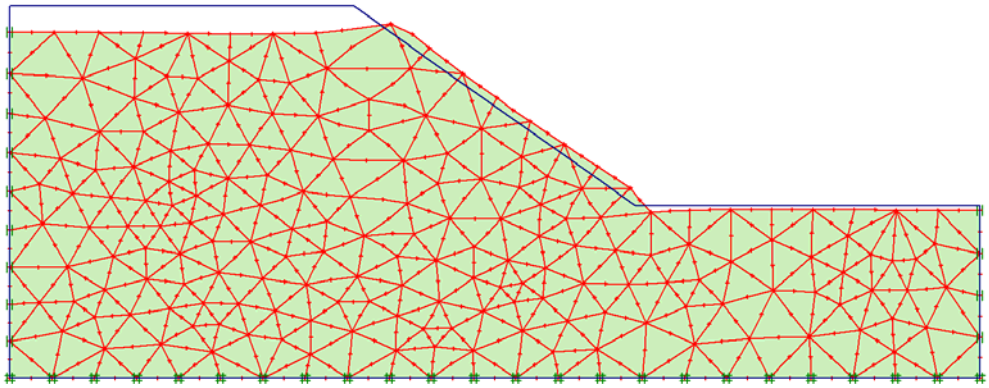

Figure 6.13 Incomplete Model Slope, where the final deformed shape after failure could not be obtained (α=35º)

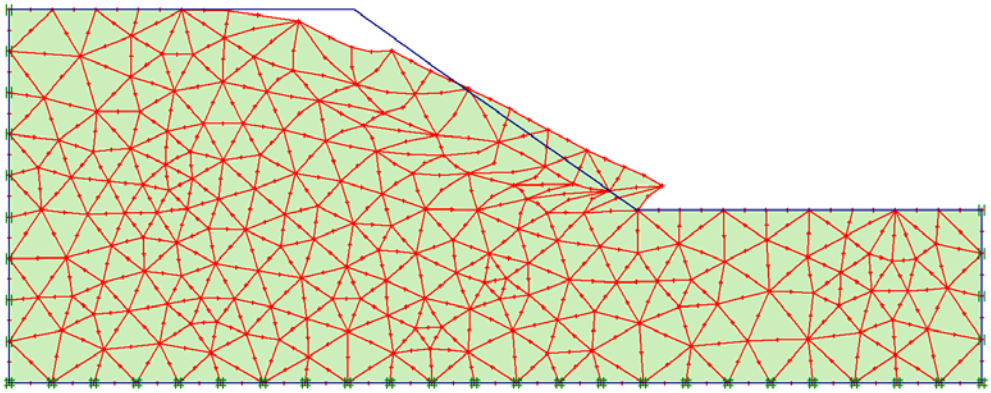

Figure 6.14 Deformed Shape of the Model Slope 3 after the failure, where no GWT exists in the slope, but it exists at the bottom of the slope (α=35°)

Step 4 Evaluation of Analyses Results: After the analysis process is completed, Plaxis enables the user to see results in graphics, tables and figures. Potential slip surfaces, determined by the FE program can be seen as "deformations", under the main menu. Hence, Figures: (6.15) and (6.16) represent the potential slip surfaces. In addition to these, the values of the factors of safety can be reached for the tested model slopes under the view menu. Factor of safety value obtained for the first model slope was 2,902, for the second model slope was 1,610. On the contrary, factor of safety for third model slope was not obtained, because the slope model failed, before the analysis process was completed.

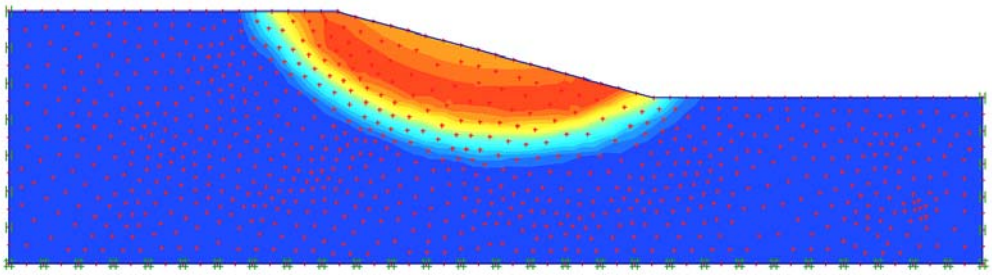

Figure 6.15 Potential Slip Surface for Model Slope (α=15°)

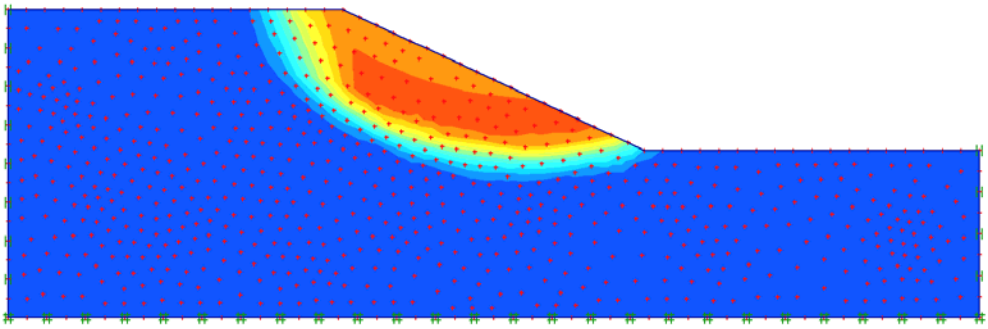

Figure 6.16 Potential Slip Surface for Model Slope (α=25°)

Table 6.3. Summary of the model slope analyses' results with respect to slope angle

Model Type	**Factor of Safety**
15º Model slope, GWT is at the GS of the slope	2,902
25º Model slope, GWT is at the GS of the slope	1,610
35º Model slope, GWT Non-existing in the slope	1,970

** GWT: Ground Water Table

** GS: Ground Surface

In addition to static slope stability analysis by using Plaxis V9, examining for the effects of rainwater infiltration on slope stability, several Plaxflow analysis was performed. At the end of the analysis results active pore water pressure, excess pore water pressure, saturation-depth values are obtained which are seen below in figures (6.17), (6.18).

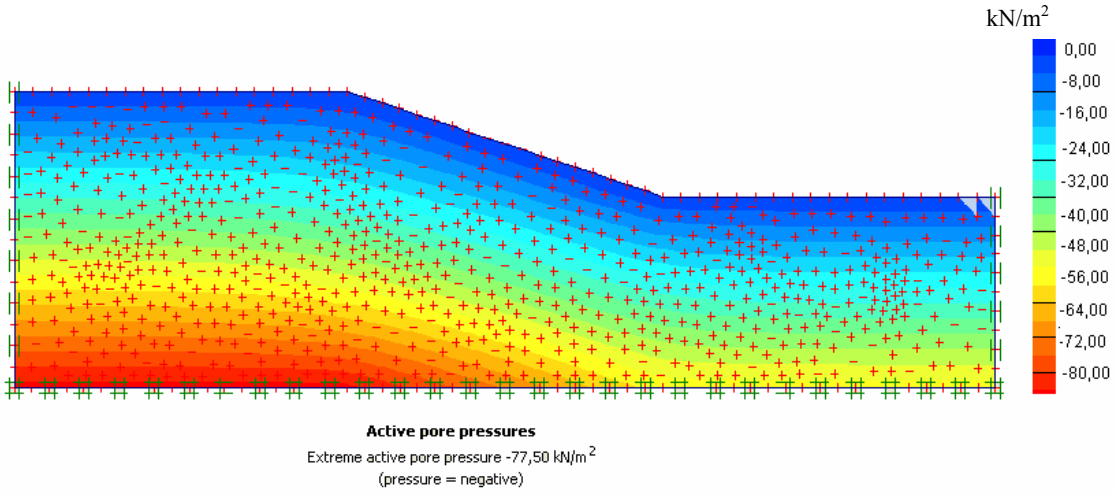

Figure 6.17. Active Pore Water Pressures for Model Slope 1 (α=15°)

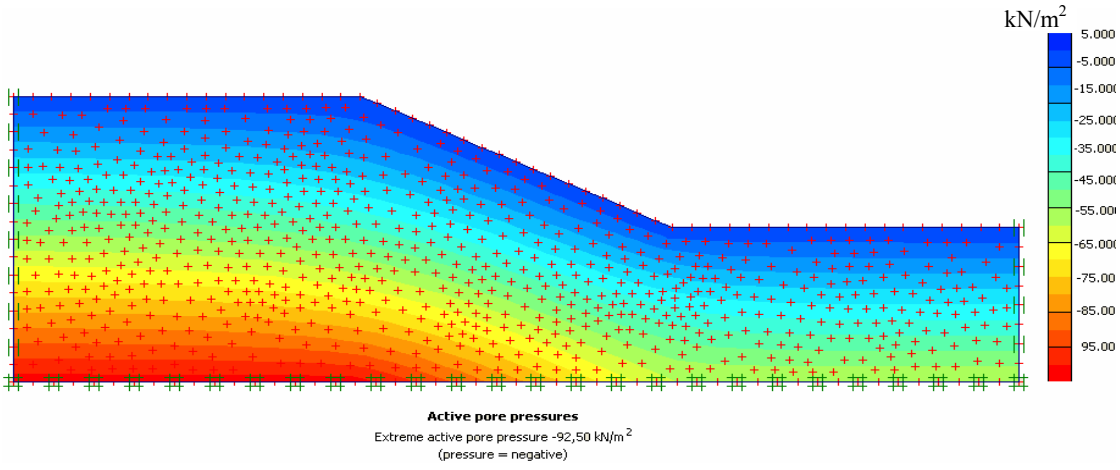

Figure 6.18. Active Pore Water Pressures for Model Slope 2 (α=25°)

6.5. Evaluation of the Tests Results

Model slope laboratory test results and slope stability analysis results are combined in Table (6.4) below including soil types, initial water contents, proctor maximum dry density results, factors of safety obtained from Plaxis V9 and degrees of relative compaction which are calculated as:

$$\text{Relative Compaction } (\%) = \frac{\gamma_{dry\ \text{model}}}{\gamma_{dry\ \text{maximum}}} \tag{6.10}$$

where;

$\gamma_{drymodel}$: Dry density of the soil in the model tested

$\gamma_{drymaximum}$: Maximum dry density of the soil from the proctor test (ASTM D698)

Table 6.4. Overall Summary of the Tests Results

No	Soil Type	Wc_i (%)	γ_{drymax} (kN/m^3)	$\gamma_{Model\ (wci)}$ (kN/m^3)	γ_{Model} (kN/m^3)	Degree of $R_{comp.}$(%)	FOS	α (º)
1	CL-ML	0,14	15,30	13,60	11,93	77,97	2,87	15
2	CL-ML	0,30	15,30	13,40	10,31	67,37	2,65	
3	CL-ML	0,14	15,30	14,50	12,72	83,13	2,92	
4	CL-ML	0,30	15,30	14,20	10,92	71,39	2,73	
5	CL-ML	0,14	15,30	13,70	12,02	78,55	1,59	25
6	CL-ML (%90), SP (%10)	0,30	15,30	15,00	11,54	75,41	1,55	
7	CL-ML	0,14	15,30	14,10	12,37	80,84	1,61	
8	CL-ML (%90), SP (%10)	0,30	15,30	14,70	11,31	73,91	1,53	
9	CL-ML	0,14	15,30	13,90	12,19	79,69	< 1	35
10	CL-ML	0,30	15,30	13,80	10,62	69,38	< 1	
11	CL-ML	0,14	15,30	14,40	12,63	82,56	< 1	
12	CL-ML	0,30	15,30	13,80	10,62	69,38	< 1	

Figures 6.19 and 6.20 present the change of FOS with degree of relative compaction, respectively for α=15º and 25º slope angles.

It is noted that all 35º slope models have failed and their Plaxis V9 results gave FOS less than one which could not be plotted.

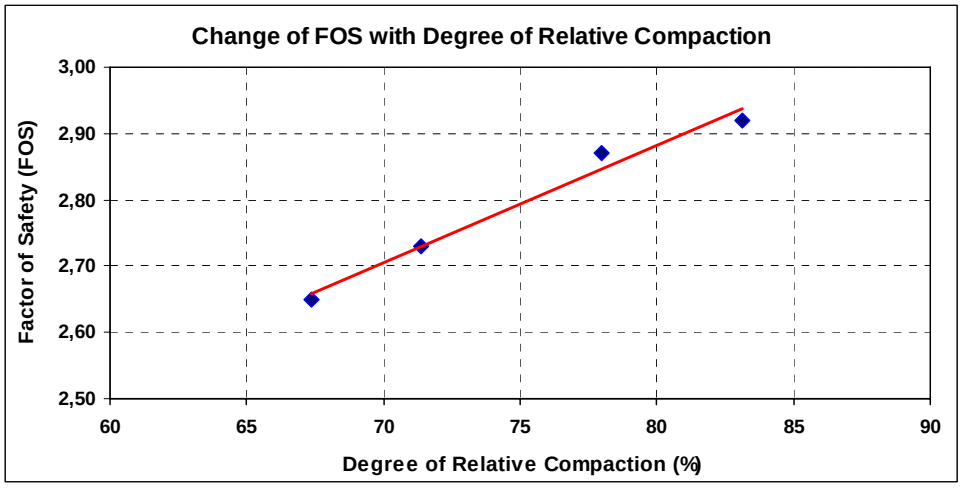

Figure 6.19. Variation of FOS with Degree of Relative Compaction (α=15º)

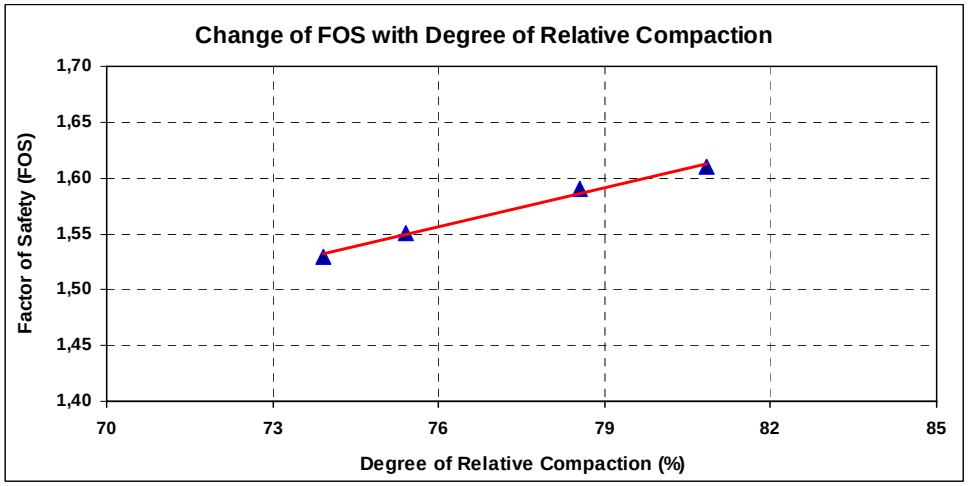

Figure 6.20. Variation of FOS with Degree of Relative Compaction (α=25º)

Figure 6.21 shows the change of FOS with Slope Angle, respectively for α=15º, 25º and 35º.

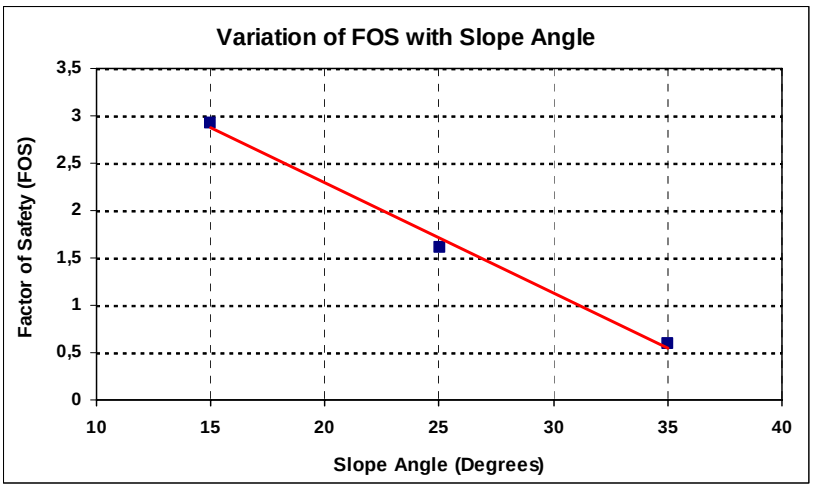

Figure 6.21. Variation of FOS with Slope Angle

6.5.1. Comparison of Laboratory and Lumb's Equation Results

Wetting band theory developed by Lumb (1975) considers only vertical infiltration and no lateral infiltration. Also, this theory takes into account constant intensity and short duration (for few hours) rainfall. Whereas, rainfall intensity may vary and rainfall duration may last long hours. Comparison shows that Lumb's equation underestimates wetting band depths observed from the model slope tests (Table 5.4). Differences between Lumb's equation results and observed values are bigger if the soil is unsaturated during infiltration process effects. Thus, Lumb's equation is more suitable to be used for the fully saturated soils (S=1).

CHAPTER 7

SUMMARY, CONCLUSIONS AND RECOMMENDATIONS FOR FUTURE STUDIES

7.1. Thesis Summary

Slope stability is a significant subject of geotechnical engineering. Slope failures triggered by rainfall are causing considerable damage and loss of life every year throughout the world. The objective of this research study has been to develop and applicate a small-scale physical slope model (SWIMS) in laboratory conditions. SWIMS was designed by the Department of Civil Engineering-Geotechnical Division members and the project funding was provided under the BAP (Scientific Research Project) program of the İzmir Institute of Technology (İYTE).

In Chapter 2, general information about traditional slope stability methods and slope stability affecting factors were given. Also, different types of mass movements were described, such as; topples, falls, slides, flows, and creeping.

In Chapter 3, information was provided about the rainfall infiltration process into uncovered soil slopes and infiltration affecting factors. Further, relevance between the shallow landslides (mostly occurring within the top 3-4 meters of the soil profile, where the groundwater table was at deeper depths) and the rainfall infiltration process was established, considering saturated and unsaturated soil slopes

In order to obtain some detailed information about specific type soil behaviour, a number of laboratory experiments were conducted on selected 2 kinds of soils, as described and summarized in Chapter 4. Soil parameters obtained from the laboratory tests were later used in the slope stability analyses performed.

In Chapter 5, description and results were given about the twelve main slope model experiments done in laboratory conditions. Although, a great number of parameters (variables) affect occurrence of the shallow landslides triggered by rainwater infiltration, in this study only three of them were used. These variables were; the initial

water content, the density of soil used and the slope angle. The main slope model experiments were examined in three different slope angle groups (15º, 25º, 35º) with each having different soil properties. There were 10 experiments by using type-1 (CL-ML) soil. Then in order to investigate the effects of having more pervious soil on slope drainage characteristics, soil type was slightly changed by adding 10% medium sand to the type-1 soil mixture and the test procedure was repeated in the other 2 tests (main experiments: No.6, No.8). Also, video recordings were made during the experiments, so as to better observe deformations, failures and mass slidings occured at the tested model slopes. Additionally lots of numerical data obtained from the tests, relating various variables in slope stability, such as; the total amount of rainfall, surface runoff, absorbed and infiltrated water. From the transparent sides of the soil container, observations were made about the progress of the wetting-band, including initial and final measurements for depths of infiltrated and infiltrated-throuh rainwater and surface erosion, occurring due to runoff water. As soon as the artificial rainfall stopped, an undisturbed soil sample was taken from the slope model by using a 50mm. diameter thin-walled stainless steel sampler. After undisturbed soil sample was extracted, it was sub-divided into 3cm high pieces and its water content was determined.

Chapter 6 presented slope stability analyses results (FOS) of the 12 tested slope models that were done by using the Plaxis V9 2D program, which utilized the finite element method (FEM), in which the strength reduction technique was considered. Slope Model Slope experimental results were compared with the FEM results, including the deformation shape and the most critical potential failure surfaces.

In Chapter 7, a brief summary of results, conclusions and recommendations for future studies were given.

7.2. Conclusions

It is understood as a results of the conducted experiments that the following factors affect slope stability:

1. Slope Angle: Steeper the slope is uncovered soil slope instability under rainfall infiltration tends to increase (Figure 6.21). Comparison of the two slope model results having the same soil features but different slope angles show that; in mild slopes (at angles of 15º) rainfall infiltration into uncovered soil slope may cause

only small deformations, thin cracks and little risk for slope instability (though slope surface remains stable, if properly compacted. Otherwise it could be covered by an impermeable barrier to reduce risk). But in steep slopes (at angles of 35º), a steady rainfall infiltration into an uncovered soil slope may cause great deformations, deeper erosion depths with an high risk for slope instability/failures to occur (slope surface is in unstable condition, even if it is properly compacted and hence it should definitely be covered by an impermeable barrier to reduce risk). For soils on the dry side of their optimum moisture content (ie. for so called "semi-dry" soils), another important parameter is the

2. Density of the soil: This directly affects the infiltration process and thus the stability of slopes in such soils. Hence in such "semi-dry" soils, the denser the soil is, bigger the matric-suctions (the negative pore water pressures) and this state provides higher shear strength for the soil mass, meaning less risk for slope instability. If such soil has loose density, the soil initially absorbs more rainfall water gradually upto a stage, when water phase becomes continuous and by permeability process water infiltrates through the soil layer. In "semi-wet" soils, infiltrated rainwater percolates through the soil more easily and faster (Egeli 1981, Egeli 1992).
3. Relative Compaction also directly affects slope stability. If relative compaction increases FOS increases too for 15º and 25º slope angles (Figures 6.20 and 6.21). On the other hand for 35º slope angle, both slope model and FOS fail irrespective of the degree of relative compaction.
4. Initial Moisture Content of Soil: Experiments done in this study showed after comparing the two slope models having the same initial water contents and the slope angles that the denser soil slope had less infiltration and erosion depths than the looser soil slopes, which had deeper erosion and infiltration depths. The bigger the initial moisture content value is, the more permeable soil becomes, because of the ease to reach higher saturation degrees, when rainfall water can infiltrate throuh the soil more easily, compared to smaller initial water contents.
5. Analyses' Results: These were compared with the results of the main slope model experiments done in the laboratory conditions. For the analyses, a commercial finite element program, Plaxis V9 2D was used for the soil stability analyses and Plaxflow module was used to assess the effect of infiltration on

slope stability. The finite element program divides soil mass into mesh. A finer mesh provides means of a more sensitive analysis to be done. In this study, the strength reduction technique (SSR) was used to determine the factors of safety. Shear strength parameters are reduced step by step by SSR technique until the slope model fails. The first slope model analysis made for the 15º slope angle, gave the FOS=2,92 and the total incremental displacements are comparatively smaller than the those of the 25º and 35º slope angles. In the second slope model (25º slope angle), factor of safety result obtained was 1,610. The last defined slope model which has the steepest slope angle has failed (i.e.FOS<1) at the end of the test. The last slope model's analysis was repeated for the same geometry and material properties, but inactive infiltration effect condition (non existing rainfall water on the slope surface), the FOS was found as 1,97.

6. Comparison of the observed infiltration depths with the wetting band thicknesses obtained from the Lumb's equation shows that Lumb's equation underestimates wetting band depths. Discrepancy increases with rainfall infiltration taking places in unsaturated soil conditions, increased rainfall intensity and prolonged rainfall conditions.

7.3. Recommendations for Future Studies

In this thesis, several research topics were investigated as below:

1. In order to extend this study and achieve reliable data some digital measuring equipment should be included, such as; negative pore water pressure sensors (tensiometers), excess pore water pressure transducer, infiltrometer etc.
2. To determine various slope angles easily, more powerful hydraulic jacks should be assembled.
3. Sprinkler system can be equipped with digital apparatus.
4. Smaller nozzles should be used in the sprinkler system, giving smaller rainfall quantity and in spray form, rather than the large drops. Reduced rainfall intensity will extend the rainfall duration, which is typically and mostly lasts for 1-2 days, which will bring a more realistic slope model.

5. Effect of different parameters on slope stability (initial moisture content, soil density, angle of slope, rainfall intensity, rainfall duration, different soil types, and different slope geometries) can be studied.
6. Compaction process can be done using a single rigid plate covering the whole soil slope model surfaces (rather than dividing it into six equal areas) to eliminate side friction between the areas and to obtain more uniform soil densities.
7. Another concept for the semi-wet slopes (by disregarding the suction effects in the semi-dry slopes, in which soils exist on the dry side of the optimum water content) worth studying in future is to assess the failure risk of a particular existing slope during an approaching severe rainfall (with a predicted rainfall intensity and its duration) though a computable dimensionless number, called Slope Drainage Index (SDI) defined as;

$$\text{SDI} = \frac{\text{Infiltrated } (\text{or drained}) \text{ through water } + \text{ Surface Runoff}}{\text{Total Rainfall Water}} \tag{7.1}$$

or,

$$\text{SDI} = \frac{\text{Total Rainfall Water - Absorbed Water}}{\text{Total Rainfall Water}} \tag{7.2}$$

SDI could be obtained as a dimensionless number varying between 0 and 1, where values above 0.5 may denote good drained slopes (failure risks are low) and values below 0.5 may indicate poor drained slopes (failure risks are high). SDI is workable, provided that the surface runoff term is not a major part of the total rainfall discharge. If it is, then its computation may be unrealistic, as no infiltration water could be obtained.

SDI could not be assessed in this current study, as the constantly kept single rainfall intensity used could not be varied in time, due to time constraints of the study. Thus, the effects of the slower rainfall intensity on the results obtained could not be studied. This has led to the most of the rainfall applied to the slopes to be discharged as surface runoff with almost no infiltrated water to occur. This indicated that the selected single rainfall intensity used was very high, while it should have been a much smaller

value, to have slower water infiltration rate into the soils and that would in turn lead to more time for water to be drained through the soils. SDI would have been more realistically computable then.

REFERENCES

ABAQUS version 6.6. 2006. ABAQUS user's manual. Hibbitt, Karlson & Sorensen, Inc., Pawtucket, RI.

Abramson, L. W., Lee, T. S, Sharma, S. and Boyce, G. M. 2002. Slope Stability and Stabilization Methods. *John Wiley and Sons, Inc., New-York*, New-York.

Adams, BA, Wulfsohn, D, and Fredlund. 1996. DG: Air volume change measurement in unsaturated soil testing using a digital pressure-volume controller, *Geotech. Test. J.*, December, 1996, Vol. 19, No. 4.

Affendi, A. A. and Faisal, A. 1994. Field measurement of soil suction. *Proceeding of 13th International Conference on Soil Mechanical and Foundation Engineering*. New Delhi, India, 1012-1016.

Alexander, D. 1993. Natural Disaster. *London, University College Library Press*.

Alonso, E. E., Lloret, A., Gens, A. and Yang, D. Q. 1995. Experimental behavior of highly expansive double structure clay. *Proc. Of 1st intenational conference on saturated soils*, Paris, Vol. 1, 11-18.

Anderson, M.G and Richards, K.S. 1987. Slope Stability; *Geotechnical Engineering and Geomorphology*. Chichester, John Wiley and Sons.

Aniya, M., 1985. Contemporary erosion rate by landsliding in Amahata River basin, Japan. *Zeitschrift für Geomorphologie, Neue Folge* 39, 301–314.

ASTM. 2005. Standard test method for particle-size analysis of soils, *American Society for Testing and Materials.* Designation 04.08: D422

ASTM. 2005. Standard test methods for laboratory compaction characteristics of soil using standart effort 12400 ft-lbf/ft^3 (600 kN-m/m^3), *American Society for Testing and Materials.* Designation 04.08: D698

ASTM. 2005. Standard test methods for specific gravity of soil solids by water pycnometer, *American Society for Testing and Materials.* Designation 04.08: D854

ASTM. 2005. Standard test methods for amount of material in soils finer than No.200 (75-m) sieve, *American Society for Testing and Materials.* Designation 04.08: D1140

ASTM. 2005. Standard test methods for laboratory compaction characteristics of soil using modified effort 56000 ft-lbf/ft^3 (2700 kN-m/m^3), *American Society for Testing and Materials.* Designation 04.08: D1557

ASTM. 2005. Standard test methods for laboratory determination of water (moisture) content of soil and rock by mass, *American Society for Testing and Materials.* Designation 04.08: D2216

ASTM. 2005. Standard test method for permeability of granular soils (constant head), *American Society for Testing and Materials.* Designation 04.08: D2234

ASTM. 2005. Standard practice for classification of soils for engineering purposes (Unified Soil Classification System), *American Society for Testing and Materials.* Designation 04.08: D2487

ASTM. 2005. Standard test method for direct shear test of soils under consolidated drained conditions, *American Society for Testing and Materials.* Designation 04.08: D3080

ASTM. 2005. Standard test method for maximum index density and unit weight of soils using a vibratory table, *American Society for Testing and Materials.* Designation 04.08: D4253

ASTM. 2005. Standard test methods for liquid limit, plastic limit and plasticity index of soils, *American Society for Testing and Materials.* Designation 04.08: D4318

ASTM. 2005. Standard practice for X-Ray radiography of soil samples, *American Society for Testing and Materials.* Designation 04.08: D4452

ASTM. 2005. Standard test method for consolidated undrained triaxial compression test for cohesive soils, *American Society for Testing and Materials.* Designation 04.08: D4767

Baker, R. and Garber, M. 1978. Theoretical analysis of the stability of slopes. *Geotechnique*, 28(4), 395-411.

Bao, C. G. and Liu, T. H. 1988. Some properties of shear strength on Nanyang Expansive clay. *Proc. of the International Conference on ngineering Problems of Regional Soils. International Academic Publishers*, 543-546.

Bao, C.G., Gong, B. and Zhan, L. 1998. Properties of Unsaturated Soils and Slope Stability of Expansive Soil. *Keynote Lecture, 2nd Int. Conf. on Unsaturated Soils*. Beijing, China.

Benda, L.E., Cundy, T.W., 1990. Predicting deposition of debris flows in mountain channels. *Canadian Geotechnical Journal*. 27, 409–417.

Bhandary, Netra P., Yatabe, Ryuichi and Shuzo Takata. 2005. Clay minerals contributing to creeping displacement of fracture zone landslides in Japan in Landslides: Risk Analysis and Sustainable Disaster Management, edited by Kyoji Sassa, Hiroshi Fukuoka, Fawu Wang and Gonghui Wang, 219-223. Berlin: Springer.

Bishop, A. W. 1955. The use of the slip circle in the stability analysis of slopes. *Geotechnique* 5(1), 7-17.

Blong, R. J. And Dunkerley, D. L. 1976. Landslides in the Rozarback area, New South Wales, Australia. *Geogr. Ann*. 58(A), 179-192.

Bottero, A., Negre, R., Pastor, J., and Turgeman, S. 1980. Finite element method and limit analysis theory for soil mechanics problems. *Computer Methods in Applied Mechanics and Engineering*, 22, 131-149.

Bouwer, H 1964. Unsaturated flow in groundwater hydraulics. ASCE *Journal of the Hydraulic division*, HY5, pp121-144.

Brady, Nyle C. and Ray R. Weil. 2005. The Nature and Properties of Soils, Thirteenth Edition. Upper Saddle River, *NJ: Prentice Hall*.

Brand, E. W., Premchitt, J. and Phillipson, H. B. 1984. Relationship between rainfall and landslides in Hong Kong. *Proc. 4th Int. Symp. Landslides*, Toronto, Vol. 1, 377-384.

Brinkgreve, R.B.J., Vermeer, P.A. 2001. "Plaxis 3D Tunnel", *Balkema Publishers*, Tokyo.

Bryant, E.A. 1991. Natural Hazards. Cambridge. *Cambridge University Press*.

Campbell, D. A. 1951. Types of Erosion Prevalent in New Zealand. *Association International d'Hydrologie Scientifique, Assemblee Generale de Bruxelles*. Tome II.

Campbell, R. H. 1975. Soil slips, debris flows, and rainstorms in the Santa Monica Mountains and vicinity, southern California. *U.S. Geological Survey Professional Paper* 851, 51 p.

Chen, J., Yin, J. H. and Lee, C. F. 2003b. Upper bound limit analysis of slope stability using rigid finite elements and nonlinear programming. *Canadian Geotechnical Journal*, 40, 742-752.

Chen, S. Y. 1996. Relationship between stress-strain model of soils and growing process of landslides. *Rock and soil mechanics* (in Chinese) 17(39), 21-26.

Chen S. Y. 1997. A method of stability analysis taken effect of infiltration and evaporation into consideration for soil slopes. *Rock and soil mechanics* (in Chinese) 18(2), 8-12.

Chen, W. F. 1975. Limit analysis and Soil Plasticity. *Elsevier Scientific Publishing Co*., New York.

Chen, W. F. and Giger, M. W. 1971. Limit analysis of stability of slopes. *Journal of the Soil Mechanics and Foundations Division*, 97(!), 19-26.

Chen, Z. Y., Mi, H. L., Zhang, F. M. and Wang, X. G. 2003a. Asimplified method for 3D slope stability analysis. *Candian Geotechnical Journal*, 40, 675-683.

Cheng, Y. M., Zhao, Z. H., and Wang, J. A. 2008. Realization of Pan Jiazheng's extremum principle with optimization methods. Chinese *Journal of Rock Mechanics and Engineering,* 27(4), 782-788 (in Chinese).

Cheyo, D.R. 1999. Geohazard Around the Michesi and Zomba Areas. *in the Proceedings of the Symposium on Natural Geological Hazards in Southern Malawi*, Zomba, 27th – 28th July.

Chipili, E. and Mshali, R. 1989. A Report on Nyambilo Landslide – Nsanje District, Zomba. *Geological Survey Department*.

Chleborad, Alan F., Diehl, Sharon F., and Susan H. Cannon. 1996. Geotechnical properties of selected materials from the Slumgullion Landslide in The Slumgullion Earth Flow: A Large-scale Natural Laboratory*, U.S. Geological Survey Bulletin 2130*, edited by D.J. Varnes and W.Z. Savage, 35-39. Denver, CO: U.S. Geological Survey.

Cho, G. C. and Santamarina, J. C. 2001. Unsaturated particulate materials - Particle-level studies. *Journal of Geotechnical and Geoenvironmental Engineering*, ASCE, 127, No. 1, 84-96.

Coch K.C. 1995. Geohazards: Natural and Human. *New Jersery, Prentice Hall Inc*

Collins, B. D., and Znidarcic, D. 2004. Stability Analyses of Rainfall Induced Landslides. *Journal of Geotechnical and Geoenvironmental Engineering*, ASCE, 130(4), 362-372.

Cornforth, D. H. 2005. Landslides in Practice: Investigation, Analysis and Remedial/Preventative Options in Soils. *John Wiley & Sons, Inc*.

Crozier M.J. 1973. Techniques for the Morphometric Analysis of Landslips. *Zeitschrift fur Geomrphologie.* 17 (1), 78 - 101.

Crozier M.J. 1984. Field Assessment of Slope Instability in D Brunsden and D Prior (eds), *Slope Instability, New York, John Wiley and Sons.*

Dai, F.C and Lee, C.F 2001. Frequency-volume relation and prediction of rainfallinduced landslides. *Engineering Geology*, vol 59, pp 253-266.

D'Andrea, R. 2001. Hydraulic conductivity of soils from grain-size; New models Discussion. *Journal of Geotechnical and Geoenvironmental Engineering*. 127(10):899.

Das, B. 1994. Principles of Geotechnical Engineering. Boston: PWS Publishing Company.

Dawson, E. M., Roth, W.H. and Drescher, A. 1999. Slope Stability Analysis by Strength Reduction. *Geotechnique*, Vol. 49, No. 6, pp. 835-840.

Dietrich, W.E., Dunne, T., 1978. Sediment budget for a small catchment in mountainous terrain. *Zeitschrift für Geomorphologie Neue Folge* Supplementbände 29, 191–206.

Donald, I. and Chen, Z. Y. 1997. Slope stability analysis by the upper bound approach: fundamentals and methods. *Canadian Geotechnical Journal*, 34, 853-862.

Drucker, D. C. and Prager, W. 1952. Soil mechanics and plastic analysis or limit design. Quarterly of Applied Mathematics, 10, 157-165.

Du, R. H. 1991. Study of landslide and debris flow at Three Gorges Reservoir Area, Yangtze River. Chengdu. *Sichuan Press of Science and Technology (in Chinese)* 1991, 33-36.

Duncan, J.M. and Wright, S.G. 2005. Soil Strength and Slope Stabilty. *John Wiley & Sons, Inc*., pp. 199.

Egeli, İ. 1981. Pore Pressures and Volume Changes in Undrained Unsaturated Clays. Ph.D. Thesis submitted to Imperial College of Science and Technology-ICST (Univ.of London) Civil Engineering Dept.-Soil Mechanics, London, U.K.

Egeli, İ. 1992. Some Tests for Studying Volume Change and Pore Water Pressure Behaviour of Unsaturated Clays on the Wet Side of Optimum Water Content. In Proceedings of the 45th Canadian Geotechnical Conference. 26-28 October 1992, Royal York Hotel, Toronto-Ontario, Canada. Vol. I1-1~1-10. (Proceedings of International Conferences).

Fall, M. and A.M. Sarr. 2007. Geotechnical characterization of expansive soils and their implications in ground movements in Dakar. *Bulletin of Engineering Geology and the Environment* 66: 279-288.

Fellenius, W. 1936. Calculation of stability of earth dams. *Transactions,* 2nd Congress Large Dams 4, 445 p. Washington, D. C.

Fisher, R. V. 1971. Features of coarse-grained, high concentrations fluids and their deposits. *Journal of Sedimentary Petrology 41, 916-927.*

Fleureau, J. M., Kheirbek-Soud, S and Taibi, S. 1995. Experimental aspects and modeling of the behavior of soils with a negative pressure. *Proc. of 1st international conference on unsaturated soils*, Paris, Vol.1, 57-62.

Fourie, A. B., Rowe, D. and Blight, G. E. 1999. The effect of infiltration on the stability of the slopes of a dry ash dump. *Geotechnique*, 49(1), 1-13.

Fredlund, D. G. 1995. The scope of unsaturated soil mechanics: An overview. *Proc. Of 1st international conference on unsaturated soils*, Paris, Vol. 1, 1155-1177.

Fredlund, D.G. and Krahn, J. 1976. Comparison of slope stability methods of analysis. *Canadian Geotechnical Journal*. Vol. 14. p. 429-439.

Fredlund, D.G., Krahn, J. and Pufahl, D. E. 1981. The Relationship between Limit Equilibrium Slope Stability Methods. *ISSMFE, Stockholm*, Sweden.

Fredlund, D.G., Morgenstern, N.R. & Widger, R.A. 1978. The shear strength of unsaturated soils. *Canadian Geotechnical Journal*, vol 15, No3 pp 313-321.

Fredlund, D. G. and Rahardjo, H. 1993. Soil mechanics for unsaturated soil mechanics. *Wiley Inter Science*, New York.

Fredlund, D. G. and Xing, A. 1994. Equations for the Soil-Water Characteristic Curve. *Canadian Geotechical Journal*. 31: 521–532.

Gasmo, J. M., Hritzuk, K. J., Rahardjo, H. and Leong, E. C. 1999. Instrumenttation of an unsaturated residual soil slope. *Geotechnical testing Journal*, 22, No. 2 p. 128-137.

Gasmo, J. M., Rahardjo, H., Leong, E. C. 2000. Infiltration effects on stability of a residual soil slope. *Computers and Geotechnics*, 26, 145-165.

Geiger, S.L., and Durnford, D.S. 2000. Infiltration in Homogeneous Sands and a Mechanistic Model of Unstable Flow. *Soil Science Society of America Journal*. 64: 460-469.

Glass, R.J., Steenhuis, T.S., and Parlange, J.Y. 1989. Wetting Front Instability, Experimental Determination of Relationships between System Parameters and Two Dimensional Unstable Flow Field Behavior in Initially Dry Porous Media. *Water Resource Research*. 25: 1195-1207.

Gondwe, P. C. and Govati C.C. 1991. The Stability status of Mishesi Mountain. U*npublished report, Zomba, Geological Survey Department*.

Green, W.H. and Ampt, G.A. 1911. Studies on Soil Physics I. The Flow of Air and Water through Soils. *Journal of Agricultural Research*. 4: 1-24.

Griffiths, D.V., and Lane P.A. 1999. Slope Stability Analysis by Finite Elements. *Geotechnique*, Vol. 49, No. 3, pp. 387-403.

Haan, C.T., B.J. Barfield, and J.C. Hayes. 1994. Infiltration. Design Hydrology and Sedimentology for Small Catchments, *Academic Press*, New York, USA, p. 54-67.

Hammah, R.E., Curran, J.H., Yacoub T., Corkum, B. 2004. Stability Analysis of Rock Slopes using the Finite Element Method. *EUROCK 2004 & 53rd Geomechanics Colloquium. Schubert* (ed.)

Hillel, D.1980. Foundantals of Soil Physics. New York, *Academic Press*.

Hillel, Daniel. 1982. Infiltration and surface runoff. *Introduction to Soil Physics*. pp211.

Hollingswoth, R. and Kovacs, G. S. 1981. Soil slumps and debris flows, prediction and protection. *Bulletin of Association of Engineering Geologists* 18, 17-28.

Huang, L. J. and Lin, X. S. 2002. Study on landslide related to rainfall. *Journal of Xiangtan Normal University* (in Chinese, Natural Science Edution) 24, 55-62.

Hutchinson, J.N.1978. A Geotechnical Classification of Landslides. *London, Imperial College*, London.

Hutchinson, J. N. and Bhandari, R. K. 1971. Undrained loading, a fundamental mechanism of mudflows and other mass movements. *Geotechnique* 21, 353-358.

Istok, J. O. and Harward, M. E. 1983. Clay mineralogy in relation to landscape instability in the Cost Range of Oregon. *Soil Science Society of America Journal* 46, 1326-1331.

Iverson, R. M. 2000. Landslide triggering by rain infiltration. *Water Resources Research* 36(7), 1897-1910.

Iverson, R. M. and Major, J. J. 1986. Ground seepage vectors and the potential for hillslope failure and debris flow mobilization. *Water Resources Research* 22(11), 1543-1548.

Izbichki R. J. 1981. Limit plasticity approach to slope stability problems. *Journal of the Geotechnical Engineering Division*, 107(2), 228-233.

Jong, G. D. J. D. 1980. Application of the calculus of variations to the vertical cut off in cohesive frictionless soil. *Geotechnique*, 30(1), 1-16.

Johnson, A.M. and Rodine, J.R. 1986. Slope Instability**.** New york**,** *John Wiley and Sons Ltd.*

Johnson, K. A. and Sitar, N. 1990. Hydrologic conditions leading to debris-flow initiation. *Can. Geotech. J*., 27, No. 6, 789-801.

Karal, K. 1977a. Application of energy method. *Journal of the Geotechnical Engineering Division,* 103(5), 381-397.

Karal, K. 1977b. Energy method for soil stability analyses. *Journal of the Geotechnical Engineering Division*, 103(5), 431-445.

Kim, J., Park, S. and Jeong, S. 2006. Effect of Wetting Front Suction Loss on Stability of Unsaturated Soil Slopes. *Unsaturated Soils, Seepage, and Environmental Geotechnics*, ASCE. 148: 70-77.

Kim, J., Salgado, R., and Lee, J. 2002. Stability analysis of complex soil slopes using limit analysis. *Journal of Geotechnical and Geoenvironmental engineering*, ASCE, 128(7), 546-557.

Kirkby, M.J., 1987. General models of long-term slope evolution through mass movement. In: Anderson, M.G., Richards, K.S. (Eds.), *Slope Stability. Wiley, Chicester*, pp. 359–379.

Knapen, J. Kitutu, M. Poesen, J. Brengelmans, W. Deckers, J. and Muwanga, A. 2006. Landslides in Densely Populated County at the Foot Slopes of Mount Elgon (Uganda): Characteristics and Causal Factors. *Geomorphology* 73, 149–165.

Krahn, J. 2003. The 2001 Rr.m. Hardly Lecture: the limits of limit equilibrium analyses. *Canadian Geotechnical Journal*, 40(3), 643-660.

Lan, H. X., Wu, F. Q., Zhou, C. H. et al. 2003. Rainfall-induced landslide hazard spatial analysis and prediction using GIS. *Chinese Science Bulletin* 48(7), 703-708.

Lan, H. X., Wu, F. Q., Zhou, C. H. et al. 2003. Rainfall-induced landslide hazard spatial analysis and prediction using GIS. *Chinese Science Bulletin* 48(7), 703-708.

Leong, E. C., Low, B. K. and Rahardjo, H. 1999. Suction profiles and stability of residual slopes. *Proceedings of Slope Stability Engineering*, edited by Yagi, Yamagami and Jiang, Balkema, 387-392.

Li, X. H. and Lin, H. and Chen, X. Q. et al. 2001. GIS aided study and numerical simulation of initiation mechanism of landslide due to precipitation. *Journal of Engineering Geology* (in Chinese) 33(8), 133-140.

Lim, T. T., Rahardjo, H., Chang, M. F. and Fredlund, D. G. 1996. Effect of rainfall on matric suction in a residual soil slope. *Canadian Geotech. J.*, 33, 2, 618-628.

Liu, Y., Bierck, B.R., Selker, J.S., Steenhuis, T.S. and Parlange, J.Y. 1993. High Density

Logan, D. L.(2002). A first course in the finite element method 3rd Ed. Wadsworth Group, USA.

Loukidis, D., Bandini, P., and Salgado, R. 2003. Stability of seismically loaded slopes using limit analysis. *Geotechnique*, 53(5), 463-479.

Ludman, A. and Koch, N.I. 1982. Physical Geology, London. *McGraw-Hill Book Company*.

Lumb, P. B. 1962. The Properties of Decomposed Granite. *Geo- technique*. 12: 226-243.

Lumb, P.B. 1975. Slope Failures in Hong Kong. *Quarterly Journal of Eng.Geol*., Geological Society of London,8: :31-65, UK.

Matsui, T. and San, K. C. 1992. Finite element slope stability analysis by shear strength reduction technique. *Soils and Foundations*, 32(1), 59-70.

Matsukura, Yukinori and Keiji Mizuno. 1986. The influence of weathering on the geotechnical properties and slope angles of mudstone in the Mineoka earthslide area, Japan. *Earth Surface Processes and Landforms* 11(3): 263-273.

Mein, R.G. and Farrell, D.A. 1974. Determination of Wetting front Suction in the Green-Ampt Equation. *Soil Science Society of America, Proceeding*. 38: 872-876.

Michalowski, R. L. 1995. Slope stability analysis: a kinematical approach. *Geotechnique*, 45(2), 283-293.

Morgenstern, N. R. And Price, V. E. 1965. The analysis of stability of general slip surfaces. *Geotechnique* 15(1), 77-93.

Morgenstern, N. R. and Price, V. E. 1965. The analysis of stability of general slip surfaces. *Geotechnique* 15(1), 77-93.

Morris, P. H., Graham, J. And Williams, D. J. 1992. Cracking in drying soils. *Canadian Geotechnical Journal,* 29, 263-277.

Msilimba, G.G. 2002. Landslides Geohazard Assessment of the Vunguvungu/Banga Catchment Area in Rumphi District. *MSc. Environmental Science Thesis*, Unpublished, Zomba, University of Malawi.

Msilimba, G.G. and Holmes, P.J. 2005. A Landslide Hazard Assessment and Vulnerability Appraisal Procedure; Vunguvungu/Banga Catchment, Northern Malawi. *Natural Hazards* 34, 199 - 216.

Ng, C. W. W., Chen, S. Y. and Pang, Y. W. 1999. Parametric study of effect of rain infiltration of unsaturated slopes. *Rock and Soil Mechanics*, Vol. 20, No. 1, 1-14 (In Chinese).

Ng, C. W. W. and Shi, Q. 1998. A numerical investigation of the stability of unsaturated soil slopes subjected to transient seepage. *Computers and Geotechnics*, Vol. 22, No. 1, 1-28.

Olson, Roy E. 1974. Shearing Strengths of Kaolinite, Illite and Montmorillonite. *Journal of Geotechnical Engineering Division*, 100(GT11): 1215-1229.

Olson, Roy E. 1974. Shearing Strengths of Kaolinite, Illite and Montmorillonite. *Journal of Geotechnical Engineering Division*, 100(GT11): 1215-1229.

Pan, J. L., Goh, A. T. C., Wong, K. S., and Selby, A. R. 2002. Three-dimensional analysis of single pile response to lateral soil movements. *International Journal for Numerical and Analytical Methods in Geomechanics*, 26(8), 747-758.

Pickering, K. and Owen, L.A. 1997. An Introduction to Global Environmental Issues. 2nd ed., 317-318.

Pierson, T. C. 1980. Piezometric response to rainstorms in forested hillslope drainage depressions. *Journal of Hydrology* (New Zealand) 19, 1-10.

Plafker, G., and Ericksen, G.E. 1978. Nevados Huascarán avalanches, Peru. in Voight, B., ed., *Rockslides and avalanches*. Amstedam, Elsevier, 277-314.

Poschinger, A. Cheyo, D. and Mwenelupembe, J. 1998. Geohazards in the Michesi and Zomba Mountain Areas in Malawi. *Technical Cooperation Report* No. 96. 20915.5, Zomba, Geological Survey.

Pradel, D. and Raad, G. 1993. Effect of Permeability on Surficial Stability of Homogeneous Slopes. *Journal of Geotechnical Engineering*, ASCE. 119(2): 315-332.

Premchitt, J., Brand, E. E., Chen, P. Y. M. 1994. Rain-induced landslides in Hong Kong, 1972-1992. *Asia Engineer* 1994, 43-51.

Rahardjo, H., Leong, E. C. and Rezaur, R. B. 2003. Instrumented slopes for the study of rainfall-induced slope failures. *Geotechnical engineering*, Swets and Zeitlinger, Liesse, 307-312.

R.J. (eds). *Landslides: Analysis and Control, Transportation Research Board Special Report* 176, National Academy of Sciences, Washington, D.C.

Rocscience. 2004. A New Era in Slope Stability Analysis: Shear Strength Reduction Finite Element Technique, Article.

Schwab, G.O., D.D. Fangmeier, W.J. Elliot, and R.K. Frevert. 1993. *Other factors. Soil and Water Conservation Engineering*. pp51.

Scott, R. C. 1972. The geomorphic significance of debris avalanching in the Appalachian Blue Ridge Mountains. *Ph. D. thesis, Athens, University of Georgia*. 124 p.

Selby, M.J., 1993. Hillslope Materials and Processes, Second Edition. *Oxford University Press*, Oxford.

Skaggs, R. W. 1980. Methods for design and evaluation of drainage-water management systems for soils with high water tables. *Drainmod Reference Report*.

Smith, K. 1996. Environmental Hazards; Assessing Risk and Reducing Disaster, London, Routledge.

Spencer, E. 1967. A method of analysis of the stability of embankments assuming parallel inter-slice forces. *Geotechnique* 17, 11-26.

Starkel, L. 1979. The role of extreme meteorological events in the shaping of mountain relief. *Geograph. Polonica* 41, 13-20.

Sun, H. W., Wong, H.N., and Ho, K. K. S. 1998. Analysisi of infiltration in unsaturated ground. Slope Engineering in Hong Kong: *Proceedings of the Annual Seminar on Slope Engineering in Hong Kong*, Hong Kong, 101-109.

Swanston, D. N. 1974. Slope stability problems associated with timber harvesting in mountainous regions of the western United States. *U.S. Department of Agriculture Forest Service General Technical Report* PNW-21, Portland, Oregon, 14 p.

Takahashi, T. 1991. Debris Flow, Rotterdam, A.A. Balkema.

Tarantino, A. and Bosco, G. 2000. Role of soil suction in understanding the triggering mechanisms of flow slides associated to rainfall. *Second International Conference on debris-flow hazards mitigation*, 16-18 August, 2000, Taipei, Taiwan 81-88. A.A. Balkema, Rotterdam.

Teoman, M.B., Topal, T. and N.S. Işik. 2004. Assessment of slope stability in Ankara clay: a case study along E90 highway. *Environmental Geology* 45: 963-977.

Tohari, T., Nishigaki, M., and Komatsu, M. 2000. Laboratory experiments on initiation of rainfall induced slope failure with moisture content measurements, *GeoEng2000* (CD), EG0543. PDF, 2000.11.

Tsaparas, I., Rahardjo, H., Toll, D. G. and Leong, E. C. 2000. Controlling Parameters for Rainfall-Induced Landslides. *Computers and Geotechnics*. 29: 1-27.

Tsaparas, I., Rahardjo, H., Toll, D. G., and Leong, E. C. 2003. Inflitration Characteristics Of Two Instrumented Residual Soil Slopes. *Canadian Geotechnical Journal*. 40: 1012-1032.

X-Ray and Tensiometer Measurements in Rapidly Changing Preferential Flow Fields. *Soil Science Society of America Journal*. 57: 1188-1192.

Xie, S. Y. and Xu, W. Y. 1999. Mechanism of landslide induced precipitation. *J. Wuhan Univ. of Hydr. And Elec. Eng*. (in Chinese) 32(1), 21-23.

Varnes, D.J. 1978. Slope Movement and Types and Process; In Schuster, R.L. and Krizek,

Vanapalli, S.K., Fredlund, D.G., Pufahl, D.E., Clifton, A.W., 1996. Model for the prediction of shear strength with respect to soil suction. *Canadian Geotechnical Journal* 33, 379–392.

Vanapalli, S. K. 1994. Simple test procedure and their interpretation in evaluating the shear strength of an unsaturated soil. *PhD thesis*, University of Saskatchewan, Saskatoon, Canada.

Wang, Z., Tuli, A. and Jury,W.A. 2003. Unstable Flow during Redistribution in Homogeneous Soil. *Vadose Zone Journal*. 2: 52-60.

Wroth, C. P. And Houlsby, G. T. 1985. Soil mechanics: property characterization and analysis procedure. *Proc. 11th ICSMFE*, San Francisco, Vol.1,1-55.

Wilson, R.C. and Dietrich, W. E. 1987. The contribution of bedrock groundwater flow to storm runoff and high pore pressure development in hollows, in Erosion and Sedimentation in the Pacific Rim. *Int. Assoc. Hyd. Sci. Pub*. 165, 49-60.

Williams, G. P. and Guy, H. P. 1973. Erosional and depositional aspects of Hurricane Camille in Virginia, 1969. *U.S. Geological Survey Professional Paper* 804. 80 p.

Youngs, E.G 1957. Moisture profiles during vertical infiltration. *Soil Science*, volume 84, (July-Dec), pp283-290.

Zhan, T. L. T. and Ng, C. W. W. 2004. Analytical analysis of rainfall infiltration mechanism in unsaturated soils. *International Journal of Geomechanics*, 4, 273–284.

Zhang, X. 1999. Slope stability analysis based on the rigid finite element method. *Geotechnique*, 49(5), 585-593.

Zhang, J., Jiao, J. J. and Yang, J. 2000. In situ rainfall infiltration studies at a hillside in Hubei Province, China. *Engineering Geology*, Vol. 57, 31-38.

Zoruba, Q. and Mencl, V. 1969. Landslides and their Control, Developments in Geotechnical Engineering. Czechoslovakia Academy of Sciences, Prague 2.